Intrinsic and extrinsic mechanisms involved in treatment resistance and progression of bladder and prostate cancers

Doctoral thesis
to obtain a doctorate (PhD)
from the Faculty of Medicine
of the University of Bonn

Sana Hosni
from Damascus, Syria
2025

Written with authorization of

the Faculty of Medicine of the University of Bonn

First reviewer: Univ.-Prof. Dr. med. Manuel Ritter

Second reviewer: Univ.-Prof. Dr. med. Sven Perner

Day of oral examination: 19.02.2025

From the Department of Urology and Pediatric Urology

Table of Contents

List of abbreviations

ADSC	adipose-derived stem cells
ADT	androgen deprivation therapy
AKT	protein kinase B
AR-V7	androgen receptor variant 7
AR-Vs	androgen receptor variants
BCa	bladder cancer
CAFs	cancer-associated fibroblasts
CDCP1	CUB domain containing protein 1
CM	conditioned media
CRPC	castration-resistant prostate cancer
DPP4	dipeptidyl peptidase 4
EGFR	epidermal growth factor receptor
ERK1/2	extracellular signal-regulated kinase 1 and 2
FDA	food and drug administration
FGFR	fibroblast growth factor receptor
HER3	human epidermal growth factor 3
HR	homologous recombination
MEK1	mitogen-activated protein kinase/ERK kinase
MIBC	muscle invasive BCa

MMP3	matrix metallopeptidase 3
NMIBC	non-muscle invasive BCa
NRG1	neuregulin 1
PARP	poly ADP-ribose polymerase
PCa	prostate cancer
PDGFRA	platelet-derived growth factor receptor-A
PI3K	phosphatidylinositol 3-kinase
PLCγ	phospholipase C Gamma
STAT	signal Transducers and Activators of Transcription
TACC3	transforming Acidic Coiled-Coil Containing Protein 3
TCGA	the cancer genome atlas
TKI	tyrosine kinase inhibitors
TMA	tissue microarray
TME	tumor microenvironment
UC	urothelial cancer

1. Abstract

Prostate cancer (PCa) and urothelial cancer (UC) are the most commonly diagnosed urological cancers. Advanced PCa and UC are significant causes of cancer-related deaths. Effective treatment of advanced PCa and UC remains an unmet medical need due to emerging resistance. Therefore, a deeper understanding of resistance mechanisms in advanced cancers is of utmost importance. Resistance could be intrinsic, emerging from the cancer cell itself, or extrinsic, conferred by surrounding non-transformed cells in the tumor microenvironment (TME). This doctoral thesis is based on three publications entitled: 1) “Androgen Receptor Splice Variants Contribute to the Upregulation of DNA Repair in Prostate Cancer”; 2) “CDCP1 Expression Is Frequently Increased in Aggressive Urothelial Carcinoma and Promotes Urothelial Tumor Progression”; 3) “Adipocyte Precursor-Derived NRG1 Promotes Resistance to FGFR Inhibition in Urothelial Carcinoma”. In the first publication, androgen receptor splice variants (AR-Vs) were shown to be increased in advanced PCa compared to primary PCa. AR-Vs in PCa clinical samples were positively associated with increased DNA repair activity. LNCaP cells overexpressing AR-V7 were used as an *in-vitro* model and confirmed the findings in clinical data. In the second publication, CDCP1 expression was correlated with advanced UC stages and reduced overall survival in two UC patient cohorts. Murine bladder organoids overexpressing CDCP1, and a human BCa cell line, SCaBER, knocked-out of CDCP1 revealed the role of CDCP1 in promoting growth and migration. In the third publication, neuregulin 1 (NRG1) secreted from adipocyte precursor cell lines was shown to confer paracrine resistance to erdafitinib in FGFR-dependent bladder and lung cancer cell lines. Conditioned media from adipocyte precursors was found to activate the human epidermal growth factor 3 (HER3) pathway. Pertuzumab, an FDA-approved antibody that inhibits HER2/HER3 dimerization, was shown to reverse the resistance conferred by NRG1 against erdafitinib *in-vitro* and *in-vivo*. Conditioned media from UC-derived cancer-associated fibroblasts (CAFs) corroborated the resistance mechanism against erdafitinib. These studied mechanisms of resistance could pave the way to novel therapeutic strategies aiming at maximizing treatment efficacy and patient survival.

2. Introduction and aims with references

2.1 Prostate cancer: stages and treatment options

Prostate cancer (PCa) is the most common cancer in men worldwide, with a yearly increasing incidence (James et al., 2024; Siegel et al., 2023). PCa ranges from low-risk disease that requires surveillance or localized therapy, to high-risk disease associated with high morbidity (Parker et al., 2020). Since the majority of PCa tumors are androgen receptor (AR) dependent, the first-line therapy of high-risk PCa is hormonal therapy, also known as androgen-deprivation therapy (ADT), which aims at reducing androgen production (Harris et al., 2009). Although most PCa tumors initially respond to ADT, around 20% of PCa patients eventually progress under ADT, which is known as castration-resistant prostate cancer (CRPC) (Aurilio et al., 2020; Kirby et al., 2011). CRPC treatment options are variable, including ADT, nonsteroidal antiandrogens, chemotherapy, irradiation, and poly ADP-ribose polymerase (PARP) inhibitors (Cai et al., 2023). PARP-mediated DNA repair is an alternative mechanism that is used upon impairment of homologous recombination (HR) DNA repair, most commonly by mutations in BRCA1 and BRCA2 genes (Kanev et al., 2024). PARP positively regulates AR signaling, which may explain the synergy between PARP inhibition and ADT (Li et al., 2017; Schiewer et al., 2012). Similarly, inhibition of AR signaling has been shown to inhibit HR DNA damage response, which sensitizes PCa to PAPR inhibitors and irradiation (Asim et al., 2017; Yin et al., 2017). Based on this, few clinical trials testing the combination of PARP inhibitors and ADT have been conducted on CRPC patients regardless of HR gene status, showing conflicting results (Clarke et al., 2018, 2022; Hussain et al., 2018).

2.1.1 AR splice variants in PCa

The full-length AR is comprised of four domains (NH_2-terminal domain, DNA-binding domain, hinge, ligand-binding domain) encoded by eight exons (Kanayama et al., 2021). The expression of truncated AR splice variants (AR-Vs) lacking one or more exons emerges as a resistance mechanism against antiandrogens, and is very common in CRPC (Antonarakis et

al., 2014). AR-Vs lacking the ligand-binding domain are of significant clinical relevance, due to their constitutive activity and resistance to most antiandrogens in current clinical use (Hu et al., 2009; Watson et al., 2010). AR-V7 is the most-well studied AR-V, and has been shown to confer a castration-resistant phenotype in PCa cell lines (Cao et al., 2014; Li et al., 2013). Moreover, AR-V7 has been associated with poorer prognosis and overall survival in CRCP patients (Antonarakis et al., 2014; Sharp et al., 2018).

2.2 Bladder cancer classification

Bladder cancer (BCa), the most common type of urothelial cancer (UC), occurs with around a four-fold higher incidence in men than in women in most countries (Doshi et al., 2023; Zhang, 2013). Bladder cancer is classified based on the degree of invasion into the bladder wall into non-muscle invasive BCa (NMIBC) and muscle invasive BCa (MIBC). NMIBC and MIBC have different molecular drivers, prognoses, and risks of invasion (Tran et al., 2021). Around 70% of BCa cases are diagnosed as NMIBC, with a high 5-year survival rate but also a high recurrence rate (Berdik, 2017). MIBC is the more aggressive disease, and can be subclassified into six molecular classes based on transcriptomic profiling: luminal papillary, luminal nonspecific, luminal unstable, stroma-rich, basal/squamous, and neuroendocrine-like (Kamoun et al., 2020). Treatment of BCa is dependent on the risk and subtype of the disease, and may include surgery, chemotherapy, immunotherapy, and/or targeted therapies (Cathomas et al., 2022).

2.3 CDCP1

CUB domain containing protein 1 (CDCP1), also known as CD318 or Trask, is a transmembrane glycoprotein that acts as a substrate for Src tyrosine kinase (He et al., 2010; Wright et al., 2016). Binding of phosphorylated CDCP1 to Src kinase activates downstream signaling pathways, such as protein kinase B (AKT) and Mitogen-activated protein kinase/ERK kinase (MEK)/ extracellular signal-regulated kinase 1 and 2 (ERK1/2) (Alajati et al., 2020; Steelman et al., 2011). Early studies investigating the function of CDCP1 have found it to be activated during epithelial cell detachment (Spassov et al., 2009), and its

activation promotes cell survival in detached lung cancer cells (Uekita et al., 2007). CDCP1 activation has also been associated with reduced cell-matrix adhesion (Bhatt et al., 2005), and increased cell migration and metastasis (Benes et al., 2012; Deryugina et al., 2009; Uekita et al., 2008). CDCP1 upregulation and association with aggressiveness has been reported in several epithelial cancers including colon, pancreatic, lung, prostate, and breast cancers (Alajati et al., 2015; Miyazawa et al., 2010; Perry et al., 2007; Scherl-Mostageer et al., 2001; Wong et al., 2009).

2.4 FGFRs as molecular drivers and therapeutic targets in cancer

The fibroblast growth factor receptor (FGFR) family of tyrosine kinase receptors comprises four FGFR genes encoding four canonical receptors (FGFR1-4) (Hughes, 1997). FGFR binding to its ligand, a fibroblast growth factor (FGF), induces receptor dimerization, auto-phosphorylation, and activation of downstream signaling pathways (Goetz and Mohammadi, 2013). Depending on the recruitment of specific adaptor molecules, FGFRs can activate four major signaling pathways: Ras-Raf-MEK-ERK, phosphatidylinositol 3-kinase (PI3K)-AKT, Phospholipase C Gamma (PLCγ), and Signal Transducers and Activators of Transcription (STAT) (Ornitz and Itoh, 2015).

FGFRs play important physiological roles in embryonic development and adult tissue homeostasis by regulating cell survival, proliferation, migration, and differentiation (Turner and Grose, 2010; Xie et al., 2020). However, aberrant FGFR expression is also a common molecular driver of many disorders including cancer. FGFR aberrations may be found in the form of amplifications, mutations, and translocations (Helsten et al., 2016). FGFR1 amplifications are the most common FGFR aberrations, frequently found in squamous lung cancer. Analysis of diverse cancers has shown that urothelial cancer has the highest frequency of FGFR1-4 aberrations, with FGFR3 mutations being the most common (Helsten et al., 2016). Indeed, more than half of low-grade BCa patients harbor FGFR3 mutations (Gust et al., 2013; Tomlinson et al., 2007; van Rhijn et al., 2003). Moreover, FGFR3 is one of the seven key cancer genes used in the consensus classification of MIBC, and is found to be mutant in around 40% of luminal papillary MIBC (Kamoun et al., 2020; Robertson et al.,

2017). Since most of FGFR3 mutations are gain-of-function mutations, several FGFR3 inhibitors have been developed and tested for UC therapy (Ascione et al., 2023).

Clinical trials testing pan tyrosine kinase inhibitors (TKIs) on UC patients have shown minimal efficacy and adverse events in a large fraction of patients, leading to treatment discontinuation or dose reduction (Hahn et al., 2016; Milowsky et al., 2013; Necchi et al., 2023). The modest clinical benefit from pan TKIs supported the use of selective TKIs targeting FGFRs. Erdafitinib (JNJ-42756493) is a small molecule that selectively binds to and inhibits FGFR1-4 phosphorylation and signaling, with negligible activity to other tyrosine kinase receptors (Karkera et al., 2017; Perera et al., 2017). Erdafitinib is the first selective FGFR inhibitor approved by the Food and Drug administration (FDA), for treating locally advanced and metastatic UC with FGFR2/3 alterations. Clinical trials on Erdafitinib have shown around 40% overall response rate and acceptable toxicity, supporting its clinical use (Loriot et al., 2023, 2019). However, most patients develop resistance within few months after treatment onset.

2.5 Aims

Emerging resistance remains the most critical challenge in cancer treatment that contributes to metastasis and death (Garraway and Jänne, 2012). Considering the resistance to antiandrogens in AR-V-expressing CRPC (Cao et al., 2014; Li et al., 2013), it may plausible to investigate the effects of AR-Vs' expression on pathways targeted by drugs used in combination with ADT. Few studies have shown that AR-Vs promote DNA repair *in-vitro* (Luo et al., 2022; Yin et al., 2017), which may explain the lack of added benefit of ADT combination with radiotherapy in metastatic PCa patients (Boevé et al., 2019; Lee et al., 2024), and with PARP inhibitors in patients with wildtype DNA repair status (Hussain et al., 2018). In the first paper (Tolkach et al., 2022), we aimed to evaluate the expression of AR-Vs in clinical PCa samples at varying stages of the disease, and to investigate the effect of AR-V expression on AR target genes and DNA repair genes.

Despite the implementation of novel therapies for the treatment of advanced UC, only a minority of patients are cured, emphasizing the need to explore potential drug targets. Although CDCP1 role as an oncogene is well established in many epithelial cancers, its role in UC has been not been characterized. In the second paper (Saponaro et al., 2023), we aimed to evaluate CDCP1 expression in two large BCa tissue microarray (TMA) cohorts, and to functionally investigate the role of CDCP1 in promoting BCa growth and migration *ex-vivo* and *in-vitro*.

Although a considerable fraction of patients respond to Erdafitinib, the progression free survival remains short (around five months) (Loriot et al., 2023, 2019). This suggests the rapid development of resistance, and highlights the importance of investigating targetable resistance mechanisms. Multiple intrinsic mechanisms of resistance to FGFR inhibitors have been suggested. The emergence of “gatekeeper” mutations in the kinase domain of FGFRs, which hinder drug binding to this domain, has been described as a common resistance mechanism to FGFR inhibitors (Sohl et al., 2015; Zheng et al., 2022). Another reported resistance mechanism is the activation of other “bypass” signaling pathways, most commonly the PI3K-AKT pathway (Cowell et al., 2017; Datta et al., 2017; Wang et al., 2017). However, resistance mechanisms to Erdafitinib remain poorly characterized. To date, only two studies have investigated alterations in tumor tissue and circulating tumor DNA pre- and post-treatment. Samples from patients progressing on Erdafitinib were found to harbor FGFR mutations and/or alterations in the PI3K-AKT pathway (Facchinetti et al., 2023; Guercio et al., 2022).

Most of the studies on resistance to FGFR inhibition did not explore potential extrinsic mechanisms of resistance, conferred by the tumor microenvironment (TME). The TME consists of non-transformed cells surrounding the tumor, including immune cells, endothelial cells, and stromal cells (Zhang et al., 2024). Since most FGFR2/3 dependent UC tumors have poor immune infiltration (Sweis et al., 2016), it is compelling to investigate the effect of the stromal compartment on drug response in these tumors. Multiple stromal cell types are found in the TME, such as cancer-associated fibroblasts (CAFs), adipocytes, osteocytes, and chondrocytes (Atiya et al., 2020). Adipose-derived stem cells (ADSCs) are multipotent stem

cells of the adipose tissue, that can differentiate into adipocytes, chondrocytes, and osteocytes (Tsuji, 2014). ADSCs have been implicated in promoting proliferation and chemotherapy resistance in breast, bladder, and pancreatic cancer cell lines (Fajka-Boja et al., 2020; Lu et al., 2017; Maj et al., 2018; Miyazaki et al., 2021). Moreover, the positive correlation between obesity, associated with higher frequency of ADSCs, and cancer risk and aggressiveness is well-established (Bunnell et al., 2022; Saha et al., 2023). Considering the profuse adipose tissue surrounding BCa tumors (Cheng et al., 2009; Philip et al., 2000), we aimed to investigate the role of secreted factors from ADSCs and 3T3-L1 pre-adipocytes on the response of FGFR-dependent BCa and lung cancer cells to Erdafitinib in the third paper (Hosni et al., 2024).

2.6 References

Alajati, A., D'Ambrosio, M., Troiani, M., Mosole, S., Pellegrini, L., Chen, J., Revandkar, A., Bolis, M., Theurillat, J.-P., Guccini, I., Losa, M., Calcinotto, A., De Bernardis, G., Pasquini, E., D'Antuono, R., Sharp, A., Figueiredo, I., Nava Rodrigues, D., Welti, J., Gil, V., Yuan, W., Vlajnic, T., Bubendorf, L., Chiorino, G., Gnetti, L., Torrano, V., Carracedo, A., Camplese, L., Hirabayashi, S., Canato, E., Pasut, G., Montopoli, M., Rüschoff, J.H., Wild, P., Moch, H., De Bono, J., Alimonti, A., 2020. CDCP1 overexpression drives prostate cancer progression and can be targeted in vivo. J. Clin. Invest. 130, 2435–2450. https://doi.org/10.1172/JCI131133

Alajati, A., Guccini, I., Pinton, S., Garcia-Escudero, R., Bernasocchi, T., Sarti, M., Montani, E., Rinaldi, A., Montemurro, F., Catapano, C., Bertoni, F., Alimonti, A., 2015. Interaction of CDCP1 with HER2 Enhances HER2-Driven Tumorigenesis and Promotes Trastuzumab Resistance in Breast Cancer. Cell Rep. 11, 564–576. https://doi.org/10.1016/j.celrep.2015.03.044

Antonarakis, E.S., Lu, C., Wang, H., Luber, B., Nakazawa, M., Roeser, J.C., Chen, Yan, Mohammad, T.A., Chen, Yidong, Fedor, H.L., Lotan, T.L., Zheng, Q., De Marzo, A.M., Isaacs, J.T., Isaacs, W.B., Nadal, R., Paller, C.J., Denmeade, S.R., Carducci, M.A., Eisenberger, M.A., Luo, J., 2014. AR-V7 and Resistance to Enzalutamide and Abiraterone in Prostate Cancer. N. Engl. J. Med. 371, 1028–1038. https://doi.org/10.1056/NEJMoa1315815

Ascione, C.M., Napolitano, F., Esposito, D., Servetto, A., Belli, S., Santaniello, A., Scagliarini, S., Crocetto, F., Bianco, R., Formisano, L., 2023. Role of FGFR3 in bladder cancer: Treatment landscape and future challenges. Cancer Treat. Rev. 115, 102530. https://doi.org/10.1016/j.ctrv.2023.102530

Asim, M., Tarish, F., Zecchini, H.I., Sanjiv, K., Gelali, E., Massie, C.E., Baridi, A., Warren, A.Y., Zhao, W., Ogris, C., McDuffus, L.-A., Mascalchi, P., Shaw, G., Dev, H., Wadhwa, K., Wijnhoven, P., Forment, J.V., Lyons, S.R., Lynch, A.G., O'Neill, C., Zecchini, V.R., Rennie, P.S., Baniahmad, A., Tavaré, S., Mills, I.G., Galanty, Y., Crosetto, N., Schultz, N., Neal, D., Helleday, T., 2017. Synthetic lethality between androgen receptor signalling and the PARP pathway in prostate cancer. Nat. Commun. 8, 374. https://doi.org/10.1038/s41467-017-00393-y

Atiya, H., Frisbie, L., Pressimone, C., Coffman, L., 2020. Mesenchymal Stem Cells in the Tumor Microenvironment, in: Birbrair, A. (Ed.), Tumor Microenvironment, Advances in Experimental Medicine and Biology. Springer International Publishing, Cham, pp. 31–42. https://doi.org/10.1007/978-3-030-37184-5_3

Aurilio, G., Cimadamore, A., Mazzucchelli, R., Lopez-Beltran, A., Verri, E., Scarpelli, M., Massari, F., Cheng, L., Santoni, M., Montironi, R., 2020. Androgen Receptor Signaling Pathway in Prostate Cancer: From Genetics to Clinical Applications. Cells 9, 2653. https://doi.org/10.3390/cells9122653

Benes, C.H., Poulogiannis, G., Cantley, L.C., Soltoff, S.P., 2012. The SRC-associated protein CUB Domain-Containing Protein-1 regulates adhesion and motility. Oncogene 31, 653–663. https://doi.org/10.1038/onc.2011.262

Berdik, C., 2017. Unlocking bladder cancer. Nature 551, S34–S35. https://doi.org/10.1038/551S34a

Bhatt, A.S., Erdjument-Bromage, H., Tempst, P., Craik, C.S., Moasser, M.M., 2005. Adhesion signaling by a novel mitotic substrate of src kinases. Oncogene 24, 5333–5343. https://doi.org/10.1038/sj.onc.1208582

Boevé, L.M.S., Hulshof, M.C.C.M., Vis, A.N., Zwinderman, A.H., Twisk, J.W.R., Witjes, W.P.J., Delaere, K.P.J., Moorselaar, R.J.A. van, Verhagen, P.C.M.S., van Andel, G., 2019. Effect on Survival of Androgen Deprivation Therapy Alone Compared to Androgen Deprivation Therapy Combined with Concurrent Radiation Therapy to the Prostate in Patients with Primary Bone Metastatic Prostate Cancer in a Prospective Randomised Clinical Trial: Data from the HORRAD Trial. Eur. Urol. 75, 410–418. https://doi.org/10.1016/j.eururo.2018.09.008

Bunnell, B.A., Martin, E.C., Matossian, M.D., Brock, C.K., Nguyen, K., Collins-Burow, B., Burow, M.E., 2022. The effect of obesity on adipose-derived stromal cells and adipose tissue and their impact on cancer. Cancer Metastasis Rev. 41, 549–573. https://doi.org/10.1007/s10555-022-10063-1

Cai, M., Song, X.-L., Li, X.-A., Chen, M., Guo, J., Yang, D.-H., Chen, Z., Zhao, S.-C., 2023. Current therapy and drug resistance in metastatic castration-resistant prostate cancer. Drug Resist. Updat. 68, 100962. https://doi.org/10.1016/j.drup.2023.100962

Cao, B., Qi, Y., Zhang, G., Xu, D., Zhan, Y., Alvarez, X., Guo, Z., Fu, X., Plymate, S.R., Sartor, O., Zhang, H., Dong, Y., 2014. Androgen receptor splice variants activating the full-length receptor in mediating resistance to androgen-directed therapy. Oncotarget 5, 1646–1656. https://doi.org/10.18632/oncotarget.1802

Cathomas, R., Lorch, A., Bruins, H.M., Compérat, E.M., Cowan, N.C., Efstathiou, J.A., Fietkau, R., Gakis, G., Hernández, V., Espinós, E.L., Neuzillet, Y., Ribal, M.J., Rouanne, M., Thalmann, G.N., van der Heijden, A.G., Veskimäe, E., Alfred Witjes, J.,

Milowsky, M.I., 2022. The 2021 Updated European Association of Urology Guidelines on Metastatic Urothelial Carcinoma. Eur. Urol. 81, 95–103. https://doi.org/10.1016/j.eururo.2021.09.026

Cheng, L., Montironi, R., Davidson, D.D., Lopez-Beltran, A., 2009. Staging and reporting of urothelial carcinoma of the urinary bladder. Mod. Pathol. Off. J. U. S. Can. Acad. Pathol. Inc 22 Suppl 2, S70-95. https://doi.org/10.1038/modpathol.2009.1

Clarke, N., Wiechno, P., Alekseev, B., Sala, N., Jones, R., Kocak, I., Chiuri, V.E., Jassem, J., Fléchon, A., Redfern, C., Goessl, C., Burgents, J., Kozarski, R., Hodgson, D., Learoyd, M., Saad, F., 2018. Olaparib combined with abiraterone in patients with metastatic castration-resistant prostate cancer: a randomised, double-blind, placebo-controlled, phase 2 trial. Lancet Oncol. 19, 975–986. https://doi.org/10.1016/S1470-2045(18)30365-6

Clarke, N.W., Armstrong, A.J., Thiery-Vuillemin, A., Oya, M., Shore, N., Loredo, E., Procopio, G., de Menezes, J., Girotto, G., Arslan, C., Mehra, N., Parnis, F., Brown, E., Schlürmann, F., Joung, J.Y., Sugimoto, M., Virizuela, J.A., Emmenegger, U., Navratil, J., Buchschacher, G.L., Poehlein, C., Harrington, E.A., Desai, C., Kang, J., Saad, F., 2022. Abiraterone and Olaparib for Metastatic Castration-Resistant Prostate Cancer. NEJM Evid. 1. https://doi.org/10.1056/EVIDoa2200043

Cowell, J.K., Qin, H., Hu, T., Wu, Q., Bhole, A., Ren, M., 2017. Mutation in the FGFR1 tyrosine kinase domain or inactivation of PTEN is associated with acquired resistance to FGFR inhibitors in FGFR1-driven leukemia/lymphomas. Int. J. Cancer 141, 1822–1829. https://doi.org/10.1002/ijc.30848

Datta, J., Damodaran, S., Parks, H., Ocrainiciuc, C., Miya, J., Yu, L., Gardner, E.P., Samorodnitsky, E., Wing, M.R., Bhatt, D., Hays, J., Reeser, J.W., Roychowdhury, S., 2017. Akt Activation Mediates Acquired Resistance to Fibroblast Growth Factor Receptor Inhibitor BGJ398. Mol. Cancer Ther. 16, 614–624. https://doi.org/10.1158/1535-7163.MCT-15-1010

Deryugina, E.I., Conn, E.M., Wortmann, A., Partridge, J.J., Kupriyanova, T.A., Ardi, V.C., Hooper, J.D., Quigley, J.P., 2009. Functional Role of Cell Surface CUB Domain-Containing Protein 1 in Tumor Cell Dissemination. Mol. Cancer Res. 7, 1197–1211. https://doi.org/10.1158/1541-7786.MCR-09-0100

Doshi, B., Athans, S.R., Woloszynska, A., 2023. Biological differences underlying sex and gender disparities in bladder cancer: current synopsis and future directions. Oncogenesis 12, 44. https://doi.org/10.1038/s41389-023-00489-9

Facchinetti, F., Hollebecque, A., Braye, F., Vasseur, D., Pradat, Y., Bahleda, R., Pobel, C., Bigot, L., Déas, O., Florez Arango, J.D., Guaitoli, G., Mizuta, H., Combarel, D., Tselikas, L., Michiels, S., Nikolaev, S.I., Scoazec, J.-Y., Ponce-Aix, S., Besse, B., Olaussen, K.A., Loriot, Y., Friboulet, L., 2023. Resistance to Selective FGFR Inhibitors in *FGFR*- Driven Urothelial Cancer. Cancer Discov. 13, 1998–2011. https://doi.org/10.1158/2159-8290.CD-22-1441

Fajka-Boja, R., Szebeni, G.J., Hunyadi-Gulyás, É., Puskás, L.G., Katona, R.L., 2020. Polyploid Adipose Stem Cells Shift the Balance of IGF1/IGFBP2 to Promote the Growth of Breast Cancer. Front. Oncol. 10, 157. https://doi.org/10.3389/fonc.2020.00157

Garraway, L.A., Jänne, P.A., 2012. Circumventing Cancer Drug Resistance in the Era of Personalized Medicine. Cancer Discov. 2, 214–226. https://doi.org/10.1158/2159-8290.CD-12-0012

Goetz, R., Mohammadi, M., 2013. Exploring mechanisms of FGF signalling through the lens of structural biology. Nat. Rev. Mol. Cell Biol. 14, 166–180. https://doi.org/10.1038/nrm3528

Guercio, B.J., Sarfaty, M., Teo, M.Y., Funt, S.A., Lee, C.-H., Aggen, D.H., Ratna, N., Regazzi, A.M., Chen, Z., Lattanzi, M., Al-Ahmadie, H.A., Brannon, A.R., Berger, M.F., Solit, D.B., Rosenberg, J.E., Bajorin, D.F., Iyer, G., 2022. Abstract 3410: Identifying potential mechanisms of resistance to erdafitinib (erda) via longitudinal analysis of circulating tumor (ct)-DNA of patients (pts) with advanced/metastatic urothelial cancer (mUC). Cancer Res. 82, 3410–3410. https://doi.org/10.1158/1538-7445.AM2022-3410

Gust, K.M., McConkey, D.J., Awrey, S., Hegarty, P.K., Qing, J., Bondaruk, J., Ashkenazi, A., Czerniak, B., Dinney, C.P., Black, P.C., 2013. Fibroblast Growth Factor Receptor 3 Is a Rational Therapeutic Target in Bladder Cancer. Mol. Cancer Ther. 12, 1245–1254. https://doi.org/10.1158/1535-7163.MCT-12-1150

Hahn, N.M., Bivalacqua, T.J., Ross, A., Netto, G.J., Park, J.C., Masterson, T.A., Koch, M.O., Bihrle, R., Foster, R., Gardner, T.A., Cheng, L., Jones, D.R., McElyea, K., Sandusky, G., Liu, Z., Turner, S.A., Tsongalis, G.J., Plimack, E.R., Greenberg, R.E., Geynisman, D.M., 2016. Phase 2 trial of dovitinib in Bacillus Calmette-Guerin (BCG) refractory urothelial carcinoma (UC) with tumor FGFR3 mutations or over-expression: Hoosier Cancer Research Network GU12-157. J. Clin. Oncol. 34, 4526–4526. https://doi.org/10.1200/JCO.2016.34.15_suppl.4526

Harris, W.P., Mostaghel, E.A., Nelson, P.S., Montgomery, B., 2009. Erratum: Androgen deprivation therapy: progress in understanding mechanisms of resistance and optimizing androgen depletion. Nat. Rev. Urol. 6, 173–173. https://doi.org/10.1038/ncpuro1322

He, Y., Wortmann, A., Burke, L.J., Reid, J.C., Adams, M.N., Abdul-Jabbar, I., Quigley, J.P., Leduc, R., Kirchhofer, D., Hooper, J.D., 2010. Proteolysis-induced N-terminal Ectodomain Shedding of the Integral Membrane Glycoprotein CUB Domain-containing Protein 1 (CDCP1) Is Accompanied by Tyrosine Phosphorylation of Its C-terminal Domain and Recruitment of Src and PKCδ. J. Biol. Chem. 285, 26162–26173. https://doi.org/10.1074/jbc.M109.096453

Helsten, T., Elkin, S., Arthur, E., Tomson, B.N., Carter, J., Kurzrock, R., 2016. The FGFR Landscape in Cancer: Analysis of 4,853 Tumors by Next-Generation Sequencing. Clin. Cancer Res. 22, 259–267. https://doi.org/10.1158/1078-0432.CCR-14-3212

Hosni, S., Kilian, V., Klümper, N., Gabbia, D., Sieckmann, K., Corvino, D., Winkler, A., Saponaro, M., Woersdoerfer, K., Schmidt, D., Hahn, O., Zanotto, I., Bertlich, M., Toma, M., Bald, T., Eckstein, M., Hölzel, M., Geyer, M., Ritter, M., Wachten, D., De Martin, S., Alajati, A., 2024. Adipocyte precursor-derived NRG1 promotes resistance to FGFR inhibition in urothelial carcinoma. Cancer Res. https://doi.org/10.1158/0008-5472.CAN-23-1398

Hu, R., Dunn, T.A., Wei, S., Isharwal, S., Veltri, R.W., Humphreys, E., Han, M., Partin, A.W., Vessella, R.L., Isaacs, W.B., Bova, G.S., Luo, J., 2009. Ligand-Independent Androgen

Receptor Variants Derived from Splicing of Cryptic Exons Signify Hormone-Refractory Prostate Cancer. Cancer Res. 69, 16–22. https://doi.org/10.1158/0008-5472.CAN-08-2764

Hughes, S.E., 1997. Differential Expression of the Fibroblast Growth Factor Receptor (FGFR) Multigene Family in Normal Human Adult Tissues. J. Histochem. Cytochem. 45, 1005–1019. https://doi.org/10.1177/002215549704500710

Hussain, M., Daignault-Newton, S., Twardowski, P.W., Albany, C., Stein, M.N., Kunju, L.P., Siddiqui, J., Wu, Y.-M., Robinson, D., Lonigro, R.J., Cao, X., Tomlins, S.A., Mehra, R., Cooney, K.A., Montgomery, B., Antonarakis, E.S., Shevrin, D.H., Corn, P.G., Whang, Y.E., Smith, D.C., Caram, M.V., Knudsen, K.E., Stadler, W.M., Feng, F.Y., Chinnaiyan, A.M., 2018. Targeting Androgen Receptor and DNA Repair in Metastatic Castration-Resistant Prostate Cancer: Results From NCI 9012. J. Clin. Oncol. 36, 991–999. https://doi.org/10.1200/JCO.2017.75.7310

James, N.D., Tannock, I., N'Dow, J., Feng, F., Gillessen, S., Ali, S.A., Trujillo, B., Al-Lazikani, B., Attard, G., Bray, F., Compérat, E., Eeles, R., Fatiregun, O., Grist, E., Halabi, S., Haran, Á., Herchenhorn, D., Hofman, M.S., Jalloh, M., Loeb, S., MacNair, A., Mahal, B., Mendes, L., Moghul, M., Moore, C., Morgans, A., Morris, M., Murphy, D., Murthy, V., Nguyen, P.L., Padhani, A., Parker, C., Rush, H., Sculpher, M., Soule, H., Sydes, M.R., Tilki, D., Tunariu, N., Villanti, P., Xie, L.-P., 2024. The Lancet Commission on prostate cancer: planning for the surge in cases. The Lancet 403, 1683–1722. https://doi.org/10.1016/S0140-6736(24)00651-2

Kamoun, A., de Reyniès, A., Allory, Y., Sjödahl, G., Robertson, A.G., Seiler, R., Hoadley, K.A., Groeneveld, C.S., Al-Ahmadie, H., Choi, W., Castro, M.A.A., Fontugne, J., Eriksson, P., Mo, Q., Kardos, J., Zlotta, A., Hartmann, A., Dinney, C.P., Bellmunt, J., Powles, T., Malats, N., Chan, K.S., Kim, W.Y., McConkey, D.J., Black, P.C., Dyrskjøt, L., Höglund, M., Lerner, S.P., Real, F.X., Radvanyi, F., Aine, M., Al-Ahmadie, H., Allory, Y., Bellmunt, J., Bernard-Pierrot, I., Black, P.C., Castro, M.A.A., Chan, K.S., Choi, W., Czerniak, B., Dinney, C.P., Dyrskjøt, L., Eriksson, P., Fontugne, J., Gibb, E.A., Groeneveld, C.S., Hartmann, A., Hoadley, K.A., Höglund, M., Kamoun, A., Kardos, J., Kim, J., Kim, W.Y., Kwiatkowski, D.J., Lebret, T., Lerner, S.P., Liedberg, F., Malats, N., McConkey, D.J., Mo, Q., Powles, T., Radvanyi, F., Real, F.X., de Reyniès, A., Robertson, A.G., Siefker-Radtke, A., Sirab, N., Seiler, R., Sjödahl, G., Taber, A., Weinstein, J., Zlotta, A., 2020. A Consensus Molecular Classification of Muscle-invasive Bladder Cancer. Eur. Urol. 77, 420–433. https://doi.org/10.1016/j.eururo.2019.09.006

Kanayama, M., Lu, C., Luo, J., Antonarakis, E.S., 2021. AR Splicing Variants and Resistance to AR Targeting Agents. Cancers 13, 2563. https://doi.org/10.3390/cancers13112563

Kanev, P.-B., Atemin, A., Stoynov, S., Aleksandrov, R., 2024. PARP1 roles in DNA repair and DNA replication: The basi(c)s of PARP inhibitor efficacy and resistance. Semin. Oncol. 51, 2–18. https://doi.org/10.1053/j.seminoncol.2023.08.001

Karkera, J.D., Cardona, G.M., Bell, K., Gaffney, D., Portale, J.C., Santiago-Walker, A., Moy, C.H., King, P., Sharp, M., Bahleda, R., Luo, F.R., Alvarez, J.D., Lorenzi, M.V., Platero, S.J., 2017. Oncogenic Characterization and Pharmacologic Sensitivity of Activating Fibroblast Growth Factor Receptor (FGFR) Genetic Alterations to the Selective FGFR

Inhibitor Erdafitinib. Mol. Cancer Ther. 16, 1717–1726. https://doi.org/10.1158/1535-7163.MCT-16-0518

Kirby, M., Hirst, C., Crawford, E.D., 2011. Characterising the castration-resistant prostate cancer population: a systematic review: The Epidemiology of CRPC. Int. J. Clin. Pract. 65, 1180–1192. https://doi.org/10.1111/j.1742-1241.2011.02799.x

Lee, T.H., Pyo, H., Yoo, G.S., Kim, J.H., Jeon, S.S., Seo, S.I., Jeong, B.C., Jeon, H.G., Sung, H.H., Kang, M., Song, W., Chung, J.H., Park, W., 2024. Androgen deprivation alone versus combined with pelvic radiation for adverse events and quality of life in clinically node-positive prostate cancer. Sci. Rep. 14, 8207. https://doi.org/10.1038/s41598-024-54976-z

Li, L., Karanika, S., Yang, G., Wang, J., Park, S., Broom, B.M., Manyam, G.C., Wu, W., Luo, Y., Basourakos, S., Song, J.H., Gallick, G.E., Karantanos, T., Korentzelos, D., Azad, A.K., Kim, J., Corn, P.G., Aparicio, A.M., Logothetis, C.J., Troncoso, P., Heffernan, T., Toniatti, C., Lee, H.-S., Lee, J.-S., Zuo, X., Chang, W., Yin, J., Thompson, T.C., 2017. Androgen receptor inhibitor–induced “BRCAness” and PARP inhibition are synthetically lethal for castration-resistant prostate cancer. Sci. Signal. 10, eaam7479. https://doi.org/10.1126/scisignal.aam7479

Li, Y., Chan, S.C., Brand, L.J., Hwang, T.H., Silverstein, K.A.T., Dehm, S.M., 2013. Androgen Receptor Splice Variants Mediate Enzalutamide Resistance in Castration-Resistant Prostate Cancer Cell Lines. Cancer Res. 73, 483–489. https://doi.org/10.1158/0008-5472.CAN-12-3630

Loriot, Y., Matsubara, N., Park, S.H., Huddart, R.A., Burgess, E.F., Houede, N., Banek, S., Laguerre, B., Guadalupi, V., Ku, J.H., Triantos, S., Akapame, S., Deprince, K., Mukhopadhyay, S., Siefker-Radtke, A.O., 2023. Phase 3 THOR study: Results of erdafitinib (erda) versus chemotherapy (chemo) in patients (pts) with advanced or metastatic urothelial cancer (mUC) with select fibroblast growth factor receptor alterations (*FGFRalt*). J. Clin. Oncol. 41, LBA4619–LBA4619. https://doi.org/10.1200/JCO.2023.41.17_suppl.LBA4619

Loriot, Y., Necchi, A., Park, S.H., Garcia-Donas, J., Huddart, R., Burgess, E., Fleming, M., Rezazadeh, A., Mellado, B., Varlamov, S., Joshi, M., Duran, I., Tagawa, S.T., Zakharia, Y., Zhong, B., Stuyckens, K., Santiago-Walker, A., De Porre, P., O’Hagan, A., Avadhani, A., Siefker-Radtke, A.O., 2019. Erdafitinib in Locally Advanced or Metastatic Urothelial Carcinoma. N. Engl. J. Med. 381, 338–348. https://doi.org/10.1056/NEJMoa1817323

Lu, Y., Yang, Y., Liu, Yan, Hao, Y., Zhang, Y., Hu, Y., Jiang, L., Gong, Y., Wu, K., Liu, Yingbin, 2017. Upregulation of PAG1/Cbp contributes to adipose-derived mesenchymal stem cells promoted tumor progression and chemoresistance in breast cancer. Biochem. Biophys. Res. Commun. 494, 719–727. https://doi.org/10.1016/j.bbrc.2017.10.118

Luo, H., Liu, Y., Li, Y., Zhang, C., Yu, B., Shao, C., 2022. Androgen receptor splicing variant 7 (ARv7) promotes DNA damage response in prostate cancer cells. FASEB J. 36, e22495. https://doi.org/10.1096/fj.202200190R

Maj, M., Kokocha, A., Bajek, A., Drewa, T., 2018. The interplay between adipose-derived stem cells and bladder cancer cells. Sci. Rep. 8, 15118. https://doi.org/10.1038/s41598-018-33397-9

Milowsky, M.I., Dittrich, C., Duran Martinez, I., Jagdev, S., Millard, F.E., Sweeney, C., Bajorin, D.F., Cerbone, L., Dunn, R.M., Sen, P., Shi, M., Kay, A.C.M., Squires, M., Sternberg, C.N., 2013. Final results of a multicenter, open-label phase II trial of dovitinib (TKI258) in patients with advanced urothelial carcinoma with either mutated or nonmutated *FGFR3* . J. Clin. Oncol. 31, 255–255. https://doi.org/10.1200/jco.2013.31.6_suppl.255

Miyazaki, Y., Oda, T., Inagaki, Y., Kushige, H., Saito, Y., Mori, N., Takayama, Y., Kumagai, Y., Mitsuyama, T., Kida, Y.S., 2021. Adipose-derived mesenchymal stem cells differentiate into heterogeneous cancer-associated fibroblasts in a stroma-rich xenograft model. Sci. Rep. 11, 4690. https://doi.org/10.1038/s41598-021-84058-3

Miyazawa, Y., Uekita, T., Hiraoka, N., Fujii, S., Kosuge, T., Kanai, Y., Nojima, Y., Sakai, R., 2010. CUB Domain–Containing Protein 1, a Prognostic Factor for Human Pancreatic Cancers, Promotes Cell Migration and Extracellular Matrix Degradation. Cancer Res. 70, 5136–5146. https://doi.org/10.1158/0008-5472.CAN-10-0220

Necchi, A., Todenhöfer, T., Deville, J.-L., Häckl, M., Marszewska, M., McKernan, P., Saulay, M., Engelhardt, M., De Santis, M., 2023. Efficacy and safety of derazantinib (DZB) in patients with metastatic urothelial carcinoma (mUC) with activating *FGFR1/2/3* genetic aberrations (GA): Results from the phase 1b/2 FIDES-02 study. J. Clin. Oncol. 41, 501–501. https://doi.org/10.1200/JCO.2023.41.6_suppl.501

Ornitz, D.M., Itoh, N., 2015. The Fibroblast Growth Factor signaling pathway. WIREs Dev. Biol. 4, 215–266. https://doi.org/10.1002/wdev.176

Parker, C., Castro, E., Fizazi, K., Heidenreich, A., Ost, P., Procopio, G., Tombal, B., Gillessen, S., 2020. Prostate cancer: ESMO Clinical Practice Guidelines for diagnosis, treatment and follow-up. Ann. Oncol. 31, 1119–1134. https://doi.org/10.1016/j.annonc.2020.06.011

Perera, T.P.S., Jovcheva, E., Mevellec, L., Vialard, J., De Lange, D., Verhulst, T., Paulussen, C., Van De Ven, K., King, P., Freyne, E., Rees, D.C., Squires, M., Saxty, G., Page, M., Murray, C.W., Gilissen, R., Ward, G., Thompson, N.T., Newell, D.R., Cheng, N., Xie, L., Yang, J., Platero, S.J., Karkera, J.D., Moy, C., Angibaud, P., Laquerre, S., Lorenzi, M.V., 2017. Discovery and Pharmacological Characterization of JNJ-42756493 (Erdafitinib), a Functionally Selective Small-Molecule FGFR Family Inhibitor. Mol. Cancer Ther. 16, 1010–1020. https://doi.org/10.1158/1535-7163.MCT-16-0589

Perry, S.E., Robinson, P., Melcher, A., Quirke, P., Bühring, H.-J., Cook, G.P., Blair, G.E., 2007. Expression of the CUB domain containing protein 1 (CDCP1) gene in colorectal tumour cells. FEBS Lett. 581, 1137–1142. https://doi.org/10.1016/j.febslet.2007.02.025

Philip, A.T., Amin, M.B., Tamboli, P., Lee, T.J., Hill, C.E., Ro, J.Y., 2000. Intravesical adipose tissue: a quantitative study of its presence and location with implications for therapy and prognosis. Am. J. Surg. Pathol. 24, 1286–1290. https://doi.org/10.1097/00000478-200009000-00013

Robertson, A.G., Kim, J., Al-Ahmadie, H., Bellmunt, J., Guo, G., Cherniack, A.D., Hinoue, T., Laird, P.W., Hoadley, K.A., Akbani, R., Castro, M.A.A., Gibb, E.A., Kanchi, R.S., Gordenin, D.A., Shukla, S.A., Sanchez-Vega, F., Hansel, D.E., Czerniak, B.A., Reuter, V.E., Su, X., de Sa Carvalho, B., Chagas, V.S., Mungall, K.L., Sadeghi, S., Pedamallu, C.S., Lu, Y., Klimczak, L.J., Zhang, J., Choo, C., Ojesina, A.I., Bullman, S., Leraas,

K.M., Lichtenberg, T.M., Wu, C.J., Schultz, Nicholaus, Getz, G., Meyerson, M., Mills, G.B., McConkey, D.J., Akbani, R., Al-Ahmadie, H., Albert, M., Alexopoulou, I., Ally, A., Antic, T., Aron, M., Balasundaram, M., Bartlett, J., Baylin, S.B., Beaver, A., Bellmunt, J., Birol, I., Boice, L., Bootwalla, M.S., Bowen, J., Bowlby, R., Brooks, D., Broom, B.M., Bshara, W., Bullman, S., Burks, E., Cárcano, F.M., Carlsen, R., Carvalho, B.S., Carvalho, A.L., Castle, E.P., Castro, M.A.A., Castro, P., Catto, J.W., Chagas, V.S., Cherniack, A.D., Chesla, D.W., Choo, C., Chuah, E., Chudamani, S., Cortessis, V.K., Cottingham, S.L., Crain, D., Curley, E., Czerniak, B.A., Daneshmand, S., Demchok, J.A., Dhalla, N., Djaladat, H., Eckman, J., Egea, S.C., Engel, J., Felau, I., Ferguson, M.L., Gardner, J., Gastier-Foster, J.M., Gerken, M., Getz, G., Gibb, E.A., Gomez-Fernandez, C.R., Gordenin, D.A., Guo, G., Hansel, D.E., Harr, J., Hartmann, A., Herbert, L.M., Hinoue, T., Ho, T.H., Hoadley, K.A., Holt, R.A., Hutter, C.M., Jones, S.J.M., Jorda, M., Kahnoski, R.J., Kanchi, R.S., Kasaian, K., Kim, J., Klimczak, L.J., Kwiatkowski, D.J., Lai, P.H., Laird, P.W., Lane, B.R., Leraas, K.M., Lerner, S.P., Lichtenberg, T.M., Liu, J., Lolla, L., Lotan, Y., Lu, Y., Lucchesi, F.R., Ma, Y., Machado, R.D., Maglinte, D.T., Mallery, D., Marra, M.A., Martin, S.E., Mayo, M., McConkey, D.J., Meraney, A., Meyerson, M., Mills, G.B., Moinzadeh, A., Moore, R.A., Mora Pinero, E.M., Morris, S., Morrison, C., Mungall, K.L., Mungall, A.J., Myers, J.B., Naresh, R., O'Donnell, P.H., Ojesina, A.I., Parekh, D.J., Parfitt, J., Paulauskis, J.D., Sekhar Pedamallu, C., Penny, R.J., Pihl, T., Porten, S., Quintero-Aguilo, M.E., Ramirez, N.C., Rathmell, W.K., Reuter, V.E., Rieger-Christ, K., Robertson, A.G., Sadeghi, S., Saller, C., Salner, A., Sanchez-Vega, F., Sandusky, G., Scapulatempo-Neto, C., Schein, J.E., Schuckman, A.K., Schultz, Nikolaus, Shelton, C., Shelton, T., Shukla, S.A., Simko, J., Singh, P., Sipahimalani, P., Smith, N.D., Sofia, H.J., Sorcini, A., Stanton, M.L., Steinberg, G.D., Stoehr, R., Su, X., Sullivan, T., Sun, Q., Tam, A., Tarnuzzer, R., Tarvin, K., Taubert, H., Thiessen, N., Thorne, L., Tse, K., Tucker, K., Van Den Berg, D.J., van Kessel, K.E., Wach, S., Wan, Y., Wang, Z., Weinstein, J.N., Weisenberger, D.J., Wise, L., Wong, T., Wu, Y., Wu, C.J., Yang, L., Zach, L.A., Zenklusen, J.C., Zhang, J. (Julia), Zhang, J., Zmuda, E., Zwarthoff, E.C., Weinstein, J.N., Kwiatkowski, D.J., Lerner, S.P., 2017. Comprehensive Molecular Characterization of Muscle-Invasive Bladder Cancer. Cell 171, 540-556.e25. https://doi.org/10.1016/j.cell.2017.09.007

Saha, A., Kolonin, M.G., DiGiovanni, J., 2023. Obesity and prostate cancer - microenvironmental roles of adipose tissue. Nat. Rev. Urol. 20, 579–596. https://doi.org/10.1038/s41585-023-00764-9

Saponaro, M., Flottmann, S., Eckstein, M., Hommerding, O., Klümper, N., Corvino, D., Hosni, S., Schmidt, A., Mönig, N., Schmidt, D., Ellinger, J., Toma, M., Kristiansen, G., Bald, T., Alimonti, A., Ritter, M., Hölzel, M., Alajati, A., 2023. CDCP1 expression is frequently increased in aggressive urothelial carcinoma and promotes urothelial tumor progression. Sci. Rep. 13, 73. https://doi.org/10.1038/s41598-022-26579-z

Scherl-Mostageer, M., Sommergruber, W., Abseher, R., Hauptmann, R., Ambros, P., Schweifer, N., 2001. Identification of a novel gene, CDCP1, overexpressed in human colorectal cancer. Oncogene 20, 4402–4408. https://doi.org/10.1038/sj.onc.1204566

Schiewer, M.J., Goodwin, J.F., Han, S., Brenner, J.C., Augello, M.A., Dean, J.L., Liu, F., Planck, J.L., Ravindranathan, P., Chinnaiyan, A.M., McCue, P., Gomella, L.G., Raj,

G.V., Dicker, A.P., Brody, J.R., Pascal, J.M., Centenera, M.M., Butler, L.M., Tilley, W.D., Feng, F.Y., Knudsen, K.E., 2012. Dual Roles of PARP-1 Promote Cancer Growth and Progression. Cancer Discov. 2, 1134–1149. https://doi.org/10.1158/2159-8290.CD-12-0120

Sharp, A., Coleman, I., Yuan, W., Sprenger, C., Dolling, D., Rodrigues, D.N., Russo, J.W., Figueiredo, I., Bertan, C., Seed, G., Riisnaes, R., Uo, T., Neeb, A., Welti, J., Morrissey, C., Carreira, S., Luo, J., Nelson, P.S., Balk, S.P., True, L.D., de Bono, J.S., Plymate, S.R., 2018. Androgen receptor splice variant-7 expression emerges with castration resistance in prostate cancer. J. Clin. Invest. 129, 192–208. https://doi.org/10.1172/JCI122819

Siegel, R.L., Miller, K.D., Wagle, N.S., Jemal, A., 2023. Cancer statistics, 2023. CA. Cancer J. Clin. 73, 17–48. https://doi.org/10.3322/caac.21763

Sohl, C.D., Ryan, M.R., Luo, B., Frey, K.M., Anderson, K.S., 2015. Illuminating the Molecular Mechanisms of Tyrosine Kinase Inhibitor Resistance for the FGFR1 Gatekeeper Mutation: The Achilles' Heel of Targeted Therapy. ACS Chem. Biol. 10, 1319–1329. https://doi.org/10.1021/acschembio.5b00014

Spassov, D.S., Baehner, F.L., Wong, C.H., McDonough, S., Moasser, M.M., 2009. The Transmembrane src Substrate Trask Is an Epithelial Protein that Signals during Anchorage Deprivation. Am. J. Pathol. 174, 1756–1765. https://doi.org/10.2353/ajpath.2009.080890

Steelman, L.S., Chappell, W.H., Abrams, S.L., Kempf, C.R., Long, J., Laidler, P., Mijatovic, S., Maksimovic-Ivanic, D., Stivala, F., Mazzarino, M.C., Donia, M., Fagone, P., Malaponte, G., Nicoletti, F., Libra, M., Milella, M., Tafuri, A., Bonati, A., Bäsecke, J., Cocco, L., Evangelisti, C., Martelli, A.M., Montalto, G., Cervello, M., McCubrey, J.A., 2011. Roles of the Raf/MEK/ERK and PI3K/PTEN/Akt/mTOR pathways in controlling growth and sensitivity to therapy-implications for cancer and aging. Aging 3, 192–222. https://doi.org/10.18632/aging.100296

Sweis, R.F., Spranger, S., Bao, R., Paner, G.P., Stadler, W.M., Steinberg, G., Gajewski, T.F., 2016. Molecular Drivers of the Non–T-cell-Inflamed Tumor Microenvironment in Urothelial Bladder Cancer. Cancer Immunol. Res. 4, 563–568. https://doi.org/10.1158/2326-6066.CIR-15-0274

Tolkach, Y., Kremer, A., Lotz, G., Schmid, M., Mayr, T., Förster, S., Garbe, S., Hosni, S., Cronauer, M.V., Kocsmár, I., Kocsmár, É., Riesz, P., Alajati, A., Ritter, M., Ellinger, J., Ohlmann, C.-H., Kristiansen, G., 2022. Androgen Receptor Splice Variants Contribute to the Upregulation of DNA Repair in Prostate Cancer. Cancers 14, 4441. https://doi.org/10.3390/cancers14184441

Tomlinson, D.C., Baldo, O., Harnden, P., Knowles, M.A., 2007. FGFR3 protein expression and its relationship to mutation status and prognostic variables in bladder cancer. J. Pathol. 213, 91–98. https://doi.org/10.1002/path.2207

Tran, L., Xiao, J.-F., Agarwal, N., Duex, J.E., Theodorescu, D., 2021. Advances in bladder cancer biology and therapy. Nat. Rev. Cancer 21, 104–121. https://doi.org/10.1038/s41568-020-00313-1

Tsuji, W., 2014. Adipose-derived stem cells: Implications in tissue regeneration. World J. Stem Cells 6, 312. https://doi.org/10.4252/wjsc.v6.i3.312

Turner, N., Grose, R., 2010. Fibroblast growth factor signalling: from development to cancer. Nat. Rev. Cancer 10, 116–129. https://doi.org/10.1038/nrc2780

Uekita, T., Jia, L., Narisawa-Saito, M., Yokota, J., Kiyono, T., Sakai, R., 2007. CUB Domain-Containing Protein 1 Is a Novel Regulator of Anoikis Resistance in Lung Adenocarcinoma. Mol. Cell. Biol. 27, 7649–7660. https://doi.org/10.1128/MCB.01246-07

Uekita, T., Tanaka, M., Takigahira, M., Miyazawa, Y., Nakanishi, Y., Kanai, Y., Yanagihara, K., Sakai, R., 2008. CUB-Domain-Containing Protein 1 Regulates Peritoneal Dissemination of Gastric Scirrhous Carcinoma. Am. J. Pathol. 172, 1729–1739. https://doi.org/10.2353/ajpath.2008.070981

van Rhijn, B.W.G., Vis, A.N., van der Kwast, T.H., Kirkels, W.J., Radvanyi, F., Ooms, E.C.M., Chopin, D.K., Boevé, E.R., Jöbsis, A.C., Zwarthoff, E.C., 2003. Molecular Grading of Urothelial Cell Carcinoma With Fibroblast Growth Factor Receptor 3 and MIB-1 is Superior to Pathologic Grade for the Prediction of Clinical Outcome. J. Clin. Oncol. 21, 1912–1921. https://doi.org/10.1200/JCO.2003.05.073

Wang, L., Šuštić, T., Leite de Oliveira, R., Lieftink, C., Halonen, P., van de Ven, M., Beijersbergen, R.L., van den Heuvel, M.M., Bernards, R., van der Heijden, M.S., 2017. A Functional Genetic Screen Identifies the Phosphoinositide 3-kinase Pathway as a Determinant of Resistance to Fibroblast Growth Factor Receptor Inhibitors in FGFR Mutant Urothelial Cell Carcinoma. Eur. Urol. 71, 858–862. https://doi.org/10.1016/j.eururo.2017.01.021

Watson, P.A., Chen, Y.F., Balbas, M.D., Wongvipat, J., Socci, N.D., Viale, A., Kim, K., Sawyers, C.L., 2010. Constitutively active androgen receptor splice variants expressed in castration-resistant prostate cancer require full-length androgen receptor. Proc. Natl. Acad. Sci. 107, 16759–16765. https://doi.org/10.1073/pnas.1012443107

Wong, C.H., Baehner, F.L., Spassov, D.S., Ahuja, D., Wang, D., Hann, B., Blair, J., Shokat, K., Welm, A.L., Moasser, M.M., 2009. Phosphorylation of the src Epithelial Substrate Trask Is Tightly Regulated in Normal Epithelia but Widespread in Many Human Epithelial Cancers. Clin. Cancer Res. 15, 2311–2322. https://doi.org/10.1158/1078-0432.CCR-08-2533

Wright, H.J., Arulmoli, J., Motazedi, M., Nelson, L.J., Heinemann, F.S., Flanagan, L.A., Razorenova, O.V., 2016. CDCP1 cleavage is necessary for homodimerization-induced migration of triple-negative breast cancer. Oncogene 35, 4762–4772. https://doi.org/10.1038/onc.2016.7

Xie, Y., Su, N., Yang, J., Tan, Q., Huang, S., Jin, M., Ni, Z., Zhang, B., Zhang, D., Luo, F., Chen, H., Sun, X., Feng, J.Q., Qi, H., Chen, L., 2020. FGF/FGFR signaling in health and disease. Signal Transduct. Target. Ther. 5, 181. https://doi.org/10.1038/s41392-020-00222-7

Yin, Y., Li, R., Xu, K., Ding, Sentai, Li, J., Baek, G., Ramanand, S.G., Ding, Sam, Liu, Z., Gao, Y., Kanchwala, M.S., Li, X., Hutchinson, R., Liu, X., Woldu, S.L., Xing, C., Desai, N.B., Feng, F.Y., Burma, S., de Bono, J.S., Dehm, S.M., Mani, R.S., Chen, B.P.C., Raj, G.V., 2017. Androgen Receptor Variants Mediate DNA Repair after Prostate Cancer

Irradiation. Cancer Res. 77, 4745–4754. https://doi.org/10.1158/0008-5472.CAN-17-0164

Zhang, L., Wang, Z., Liu, K., Liu, Y., Wang, S., Jiang, W., Lu, F., Dang, Y., 2024. Targets of tumor microenvironment for potential drug development. MedComm – Oncol. 3, e68. https://doi.org/10.1002/mog2.68

Zhang, Y., 2013. Understanding the Gender Disparity in Bladder Cancer Risk: The Impact of Sex Hormones and Liver on Bladder Susceptibility to Carcinogens. J. Environ. Sci. Health Part C 31, 287–304. https://doi.org/10.1080/10590501.2013.844755

Zheng, J., Zhang, W., Li, L., He, Y., Wei, Y., Dang, Y., Nie, S., Guo, Z., 2022. Signaling Pathway and Small-Molecule Drug Discovery of FGFR: A Comprehensive Review. Front. Chem. 10, 860985. https://doi.org/10.3389/fchem.2022.860985

3. Publications

3.1 Publication 1: Androgen Receptor Splice Variants Contribute to the Upregulation of DNA Repair in Prostate Cancer.

cancers

MDPI

Article

Androgen Receptor Splice Variants Contribute to the Upregulation of DNA Repair in Prostate Cancer

Yuri Tolkach [1,2,*,†], Anika Kremer [1,†], Gábor Lotz [3], Matthias Schmid [4], Thomas Mayr [1], Sarah Förster [1], Stephan Garbe [5], Sana Hosni [6], Marcus V. Cronauer [1], Ildikó Kocsmár [7], Éva Kocsmár [3], Péter Riesz [7], Abdullah Alajati [6], Manuel Ritter [6], Jörg Ellinger [6], Carsten-Henning Ohlmann [8] and Glen Kristiansen [1,*]

1 Institute of Pathology, University Hospital Bonn, 53127 Bonn, Germany
2 Institute of Pathology, University Hospital Cologne, 50937 Cologne, Germany
3 Department of Pathology, Forensic and Insurance Medicine, Semmelweis University, 1085 Budapest, Hungary
4 Department of Medical Biometry, Informatics, and Epidemiology (IMBIE), University Hospital Bonn, 53127 Bonn, Germany
5 Department of Radiation Oncology, University Hospital Bonn, 53127 Bonn, Germany
6 Clinic of Urology, University Hospital Bonn, 53127 Bonn, Germany
7 Department of Urology, Semmelweis University, 1085 Budapest, Hungary
8 Department of Urology, Johanniter Krankenhaus Bonn, 53113 Bonn, Germany
* Correspondence: iurii.tolkach@uk-koeln.de (Y.T.); glen.kristiansen@ukbonn.de (G.K.); Tel.: +49-221-4788-7023 (Y.T.); +49-228-2871-5375 (G.K.); Fax: +49-221-478-6360 (Y.T.); +49-228-2871-5030 (G.K.)
† These authors contributed equally to this work.

Simple Summary: Ligand-independent androgen receptor splice variants emerge during androgen deprivation therapy and are suspected to render prostate carcinomas castration-resistant. In a retrospective analysis of a large cohort of primary and advanced prostate tumors, we observed increased expression of androgen receptor splice variants in therapy refractory tumors. Our hypothesis was that AR splice variants exert their tumor-promoting activity by modulating the intrinsic DNA repair machinery. In the sequence from primary over advanced tumors under androgen-deprivation therapy to castration resistance, AR splice variant expression increases and is linked to increased expression of DNA repair genes. This effect of AR splice variants appeared independent of their known impact on tumor cell proliferation. These clinical findings were validated in an androgen-sensitive prostate cancer cell line that mimics a castration-resistant phenotype by overexpression of AR-V7. Modulated DNA repair gene expression in the presence of AR splice variants is linked to increased DNA repair activity, pointing at a novel therapeutic approach for castration-resistant prostate cancer.

Abstract: Background: Canonical androgen receptor (AR) signaling regulates a network of DNA repair genes in prostate cancer (PCA). Experimental and clinical evidence indicates that androgen deprivation not only suppresses DNA repair activity but is often synthetically lethal in combination with PARP inhibition. The present study aimed to elucidate the impact of AR splice variants (AR-Vs), occurring in advanced or late-stage PCA, on DNA repair machinery. Methods: Two hundred and seventy-three tissue samples were analyzed, including primary hormone-naïve PCA, primary metastases, hormone-sensitive PCA on androgen deprivation therapy (ADT) and castration refractory PCA (CRPC group). The transcript levels of the target genes were profiled using the nCounter platform. Experimental support for the findings was gained in AR/AR-V7-expressing LNCaP cells subjected to ionizing radiation. Results: AR-Vs were present in half of hormone-sensitive PCAs on androgen deprivation therapy (ADT) and two-thirds of CRPC samples. The presence of AR-Vs is highly correlated with increased activity in the AR pathway and DNA repair gene expression. In AR-V-expressing CRPC, the DNA repair score increased by 2.5-fold as compared to AR-V-negative samples. Enhanced DNA repair and the deregulation of DNA repair genes by AR-V7 supported the clinical data in a cell line model. Conclusions: The expression of AR splice variants such as AR-V7 in PCA patients following ADT might be a reason for reduced or absent therapy effects in patients on additional PARP inhibition due to the modulation of DNA repair gene expression. Consequently, AR-Vs should be further studied as predictive biomarkers for therapy response in this setting.

check for updates

Citation: Tolkach, Y.; Kremer, A.; Lotz, G.; Schmid, M.; Mayr, T.; Förster, S.; Garbe, S.; Hosni, S.; Cronauer, M.V.; Kocsmár, I.; et al. Androgen Receptor Splice Variants Contribute to the Upregulation of DNA Repair in Prostate Cancer. *Cancers* **2022**, *14*, 4441. https://doi.org/10.3390/cancers14184441

Academic Editors: Philippe Pourquier and Alfonso Urbanucci

Received: 18 July 2022
Accepted: 7 September 2022
Published: 13 September 2022

Keywords: prostate cancer; DNA repair; BRCA1; BRCA2; androgen receptor; splice variant; AR-V7; castration-refractory prostate cancer; androgen deprivation therapy

1. Introduction

Androgen receptor (AR) signaling and DNA repair are tightly interconnected in prostate cancer (PCA) [1–8]. The presence of pathogenic mutations in genes responsible for homologous recombination (HR) DNA repair opens up the possibility of therapy with PARP inhibitors (PARPi) in up to 25% of patients with metastatic castration-refractory PCA (CRPC) [9,10]. In cases of insufficiency in HR DNA repair, PARP is a reserve system that operates through base excision. Blocking base excision repair with PARPi renders tumor cells incapable of effectively repairing DNA damage, which then eventually accumulates lethal mutations [5,6]. However, there is early evidence that PARPi might be effective in CRPC in the absence of HR DNA gene mutations [5,6,11]. Androgen deprivation therapy (ADT) on PCA cells induces a so-called functional "BRCAness". The term BRCAness defines an insufficiency in the HR DNA repair system [2,5,6], originally caused by the functional loss of the BRCA1 and BRCA2 genes. BRCA-deficient cells use error-prone DDR pathways that consequently increase their genome instability [12]. ADT treatment mimics this loss of BRCA1/2 expression. In this situation, PARPi deepens the DNA repair insufficiency, resulting in synthetic lethality for tumor cells. It has also been shown in vitro that both *PARP1* and *PARP2* are critical effectors of the AR pathway activity. Besides their function in DNA repair, PARP enzymes are known to be transcriptional coactivators of the AR. Notably, PARP-1 appears to activate AR function and affect downstream signaling [13,14], which is another rationale for targeting PARP in PCA [5–8,15,16].

The synthetic lethality of ADT and PARPi might, however, be dependent on AR alterations (splice variants, amplification, mutations) often present in advanced PCA [17–20] and responsible for sustained AR pathway activity during ADT. The upregulation of AR-V7 in clinical samples of advanced PCA patients was reported by Sharp et al. [21]. DNA repair in PCA cell lines exposed to ionizing radiation was found to be diminished following AR blockade with enzalutamide but largely preserved in the case of AR-V7 and ARv567es splice variant expression [3]. There is limited evidence that both full-length AR (AR-FL) and AR splice variants (AR-Vs) directly activate the expression of key genes necessary for DNA repair [2,3,8,22]. Apparently, both non-homologous end-joining and HR DNA repair are the main effectors of AR-FL and AR-Vs in prostate cancer [1,2,4]. Blocking AR-FL using antiandrogens has been shown to retain AR-V activity with regard to supporting the DNA repair system. However, so far, this has mainly been shown in cell line models [3,8,23].

The present study aimed to clarify, in clinical PCA samples, whether the expression of key DNA repair genes is affected by ADT, particularly in the presence of AR-Vs. A cohort of patients in different stages of PCA was analyzed to characterize AR pathway activity, and these data were correlated with the expression of DNA repair genes. Luo et al. reported that DNA repair is modulated by androgen receptor splice variant 7 [23]. The present study provides evidence that DNA repair is partly dependent on AR pathway activity in PCA. As enhanced DNA repair is induced in the presence of AR-Vs through the modulation of DNA repair gene expression, the application of synthetic lethality concepts, such as the combination of ADT and PARPi, might be questionable.

2. Materials and Methods

2.1. Patient Cohort

The study cohort consisted of 184 patients: 167 patients with PCA in different disease stages and 17 patients from control groups (Table 1). All patients received ADT (LHRH analogs/antagonists) alone or in combination with abiraterone or antiandrogens (bicalutamide, etc.). Two patients with primary small-cell carcinoma of the prostate and sarcomatous carcinoma lacking prostate epithelial differentiation after ADT were also

included. Materials on twenty-two patients with CRPC were provided by the Department of Pathology, Forensic and Insurance Medicine, Semmelweis University, Budapest, Hungary (2005–2016). All other patients were diagnosed at the Institute of Pathology of the University Hospital Bonn, Bonn, Germany (2003–2018).

Table 1. Clinical characteristics of the study cohort.

	Number of Patients	Number of Samples
PCA, primary tumor, hormone-naïve	77	136
pT-stage		
pT1b (TURP)	20	
pT2	14	
pT3a	9	
pT3b	21	
pT4	3	
unknown	10	
pN stage		
pN0	32	
pN1	12	
pNx	33	
Prostatectomy		
ISUP/WHO grade group		
ISUP 1	3	
ISUP 2	6	
ISUP 3	1	
ISUP 4	37	
ISUP 5	30	
Morphology		
Acinar adenocarcinoma	52	
Ductal/mixed adenocarcinoma [§]	25	
PCA, metastases, hormone-naïve	23	28
PCA ADT *	42	55
PCA CRPC *,[#]	32	35
BPH	10	10
Benign prostate tissue without hyperplasia	7	7
Neuroendocrine carcinoma of the prostate	1	1
Sarcomatoid carcinoma [$]	1	1
OVERALL	184	273

Comments: *—CRPC samples from primary (untreated) tumor in the prostate or from metastases; [§]—only samples containing ductal adenocarcinoma were included in the analysis in case of mixed ductal/acinar morphology; [#]—four samples of CRPC bone metastases that failed quality control are not showed here. [$]—primary tumor sample, after androgen deprivation therapy.

2.2. Samples

All samples were harvested from formalin-fixed paraffin-embedded (FFPE) tissue blocks (flow chart: see Figure 1). Multiple samples (up to 4) from tumors of selected patients were analyzed to address heterogeneity of primary and metastatic tumors with an overall number of 273 samples passing quality control (Figure 2A). All tumor samples had a purity of >90% tumor cells and were macrodissected. Among included CRPC samples, 29 were from primary tumor (no treatment with curative intent) and 6 from metastatic lesions (2 from bone and 2 from soft tissue metastases, 1 from liver and 1 from retroperitoneal lymph node).

2.3. RNA Extraction

One or several 10 µm sections from paraffin block were used for macrodissection and total mRNA extraction. PureLink™ FFPE RNA Isolation Kit (ThermoFisher Scientific, Waltham, MA, USA) was used according to the manufacturer's instructions. NanoDrop 2000 spectrophotometer (Thermo Scientific, USA) was applied for mRNA quality control and quantification.

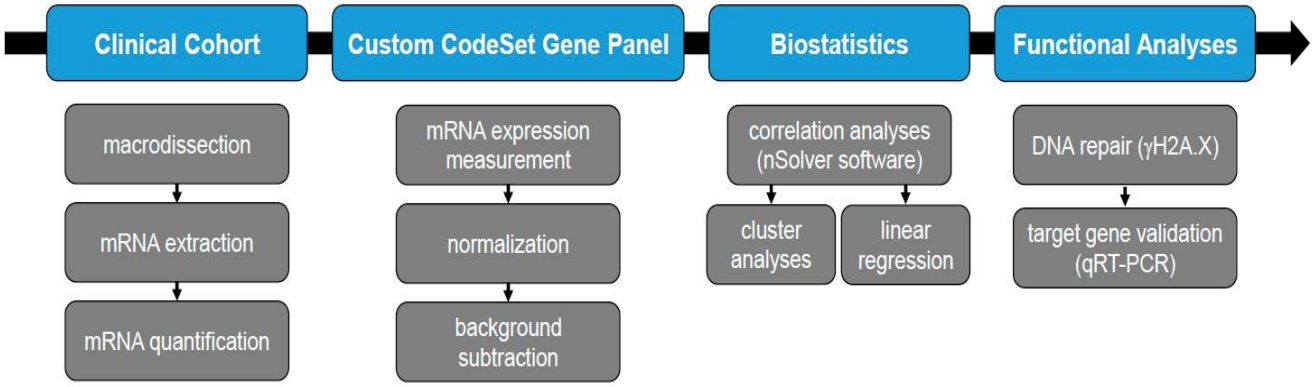

Figure 1. Flow chart of the main steps in this study: material processing, data acquisition, biostatistical analyses and experimental validation.

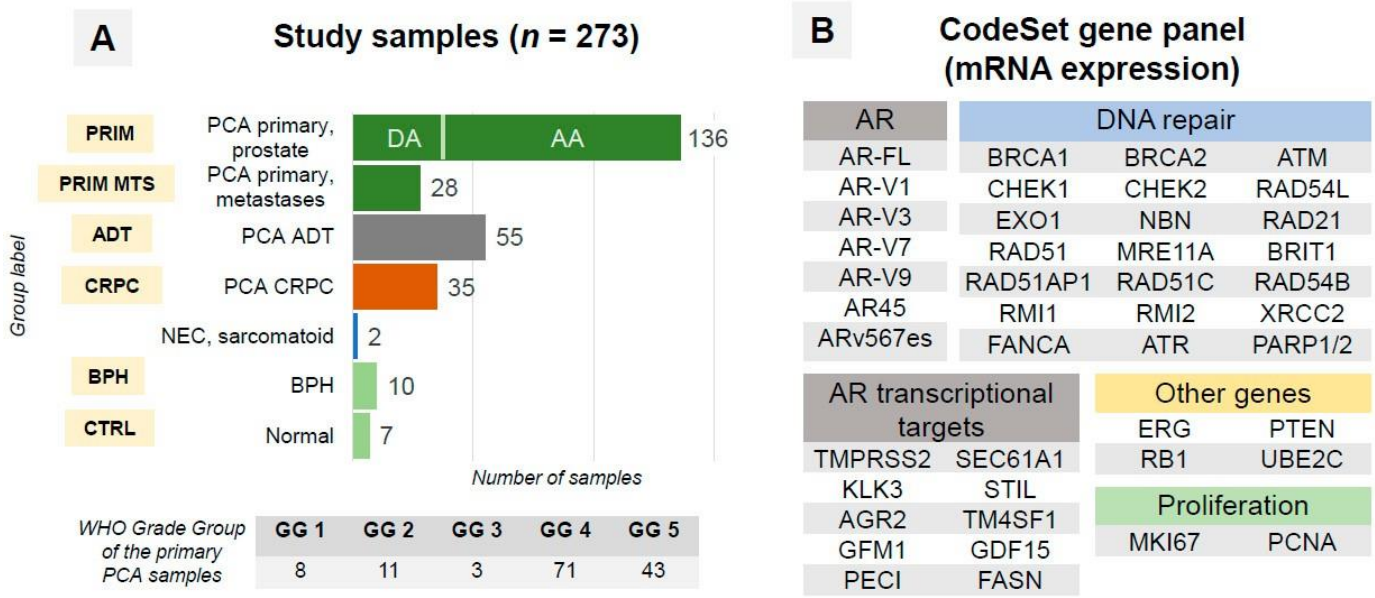

Figure 2. (**A**) Structure of the samples in study cohort and group labels used in further Figures. Among primary prostate cancer samples, 33 ductal adenocarcinoma (DA) samples were analyzed. Abbreviations: AA—acinar adenocarcinoma, ADT—androgen deprivation therapy (primary tumor and metastases), BPH—benign prostatic hyperplasia, CRPC—castration-refractory prostate cancer (primary tumor and metastases), CTRL—normal prostate tissue, GG—grade group, NEC—neuroendocrine carcinoma, PCA—prostate cancer, WHO—World Health Organization. (**B**) Composition of the gene panel for mRNA expression analysis using nCounter technology. AR—androgen receptor, FL—full-length. Additionally, four housekeeping genes (HPRT1, ALAS1, ARF1, PGK1) were included in the panel.

2.4. RNA Expression Analysis

All RNA expression analyses were performed using the nCounter platform (NanoString Technologies, Inc.; Seattle, WA, USA). A custom CodeSet gene panel (Supplementary Table S1) included 45 target genes: (1) AR-FL and splice variants (AR-Vs; junction-specific probes), (2) AR transcriptional targets, (3) DNA repair-associated genes, (4) proliferation-related genes, and (5) further genes relevant for PCA (Figure 2B). Four housekeeping genes (*HPRT1, ALAS1, ARF1, PGK1*) were included. All samples were titrated to 100 ng of the total mRNA amount. Internal nCounter negative and positive controls as well as other internal metrics (RNA quantity, binding density) were used for quality control.

2.5. Statistical Analysis

Raw RNA expression data were processed by nSolver Analysis Software v. 4.0.70 (Nanostring Technologies, Seattle, WA, USA). Negative controls were used for background subtraction (geometric mean) of the called expression values. Internal positive controls and reference genes were used for normalization of expression levels. All further analyses were carried out in R (v. 3.6.0, The R Foundation for Statistical Computing). AR pathway score (AR score) was calculated from 10 genes representing transcriptional targets of AR (Figure 2B), as described in [19], with benign non-hyperplastic prostatic tissue used as reference. In brief, for each gene, a z-score was calculated by subtracting the pooled mean of expression in reference tissue samples divided by the pooled standard deviation of expression in reference tissue samples. AR score output was calculated as the sum of z-scores for all ten target genes divided by the number of genes. The HRDNA repair score (DNA-R score) was calculated using the same principle using all genes (n = 20) from our panel related to HR DNA repair (excluding *PARP1* and *PARP2*). The expression of AR-Vs was evaluated both quantitatively (correlation analyses, heatmap) and qualitatively. For qualitative estimation of AR-Vs (present/not present), a threshold of 20 normalized counts (approximately 5 standard deviations above mean AR-V expression for control tissue samples) was used after background subtraction of the geometric mean of negative control samples. Appropriate parametric (*t*-test), non-parametric (Mann–Whitney U test) and correlation statistical tests (Pearson's r) were used for comparison between groups and parameters. Expression heatmaps were created in nSolver 4.0 analysis software (nanoString, Seattle, WA, USA) using Pearson's correlation for clustering.

2.6. Linear Regression Analysis

To analyze the joint effects of AR-Vs and proliferation on DNA repair, score variables that quantified either AR-Vs or the proliferation of tumor cells were constructed. These scores were set up in the same way as the DNA-R score using z-scores of the AR splice variants (AR-V1, -V3, -V7, -V9) and proliferation genes (MKI67, PCNA) for both the splice variant (SV score) and proliferation (P score) scores, respectively. Values of multiple samples from single patients were averaged. In the next step, the scores were used to fit linear regression models with the DNA-R score as the dependent variable and the SV and P scores as independent variables. The fits of the linear regression models were used to investigate whether AR-Vs had an effect on DNA repair when accounting for the effect of tumor cell proliferation on DNA repair (Supplementary Figure S9).

2.7. Cell Culture and Irradiation

LNCaP cells were obtained from the German Collection of Microorganisms and Cell Cultures (Braunschweig, Germany). LNCaP cells stably overexpressing AR-FL (LNCaP/AR) or AR-V7 (LNCaP/V7) were generated by lentiviral transduction. Lentivirus was generated in HEK 293T cells via co-transfection of VSV-G, Gag-Pol and AR-FL/ V7 expressing plasmids using jetPRIME (Polyplus, Illkirch, France). pLENTI6.3/AR-GC-E2325 (lentiviral vector for AR-FL expression [24]) was a gift from Karl-Henning Kalland, and AR-V7-pcw107, described in Martz et al., 2014 [25], was a gift from David Sabatini and Kris Wood. LNCaP/AR cells were selected with 5.5 µg/mL Blasticidin (Life Technologies, Paisley, UK) for 2 weeks, and LNCaP/V7 cells were selected with 1 µg/mL Puromycin (Cayman Chemical, Ann Arbor, USA) for 5 days.

Cells were cultured in RPMI1640 medium containing GlutaMax supplemented with 1% penicillin/streptomycin (10,000 U/mL) and 10% fetal bovine serum (Life Technologies, Paisley, UK) or 10% charcoal-stripped fetal bovine serum (DCC) (Biowest, Nuaillé, France) at 37 ˚C in a humidified atmosphere containing 5% CO_2. Cells were routinely checked to exclude mycoplasma contamination.

Radiation experiments were performed on a linear accelerator (Truebeam Stx, Varian Medical System, Palo Alto, CA, USA) using 6 MeV photon energy at a dose rate of 4 Gy/min at dose maximum (D_{max} = 20 mm). Depending on the experimental setting, the applied

dose to the cells varied between 2 to 6 Gy. For this purpose, cells seeded in 6-well plates (for Western Blot and RNA analysis) or on glass coverslips placed in 12-well plates (for IF) were positioned in a tissue-equivalent RW3-plasticphantom (PTW, Freiburg, Germany) at a depth of D_{max}. The field size was adapted according to the number of plates irradiated.

2.8. γH2A.X Assay

DNA double-strand breaks were determined by γH2A.X staining cells [26]. Cells were grown for 24 h in androgen-deprived medium and then subjected to 2 Gy irradiation. Immunofluorescence was performed 24 h post-irradiation, as previously described [27]. Foci were visualized using phospho-Histone H2A.X (catalog number 05-636; Millipore, Temecula, CA, USA) and anti-mouse IgG/IgM Alexa Fluor 488-conjugated secondary antibodies (Dianova, Hamburg, Germany). Subsequently, cells were embedded in Fluoromount-G with DAPI (Life Technologies, Carlsbad, CA, USA). Fluorescent images were acquired on an Olympus CKX53 microscope (Tokyo, Japan) and foci were counted using QuPath Software v0.3.2 [28]. At least 200 cells per condition were counted.

2.9. Immunoblot

Cell lysates were prepared using RIPA lysis buffer supplemented with protease and phosphatase inhibitors (Complete Protease Inhibitor Cocktail, Roche, Basel, Switzerland and Halt Protease and Phosphatase Inhibitor Thermo Scientific, Rockford, IL, USA) as previously described [29]. Primary antibodies used included AR-V7 (31-1109-00, RevMab Biosciences, San Francisco, CA, USA), γH2A.X (05-636, Merck Millipore, Darmstadt, Germany), and β-Actin (ab6276, Abcam, Cambridge, UK). As a secondary antibody, a horseradish peroxidase-conjugated antibody (ab6789, Abcam) was used. Signals were detected using ECL Western Blot Substrate or SuperSignal West Dura Extended Duration Substrate (Thermo Scientific, Rockford, IL, USA) on a Fusion S imaging system (Vilber Lourmat, Radolfzell, Germany).

2.10. Quantitative qRT-PCR

To study the mRNA expression of DNA repair genes (Supplementary Table S1) in LNCaP cells stably overexpressing AR-FL or AR-V7, cells were seeded 24 h prior to irradiation in androgen-deprived medium. Six hours after irradiation (6Gy), either protein lysates or total RNA were recovered from the cells, followed by qRT-PCR as previously described [29]. Oligonucleotide primers specific for DNA repair genes and PPIA (peptidylprolyl isomerase A, used as housekeeping gene) were purchased from biomers.net (Ulm, Germany). Primer sequences are provided in Supplementary Table S2. Sequence verification of the amplification products was performed with Sanger sequencing. Gene expression was measured in triplicates per gene. Relative gene expression was assessed using the $\Delta\Delta C_\tau$ method with PPIA as a housekeeping gene (Supplementary Tables S3 and S4).

2.11. Ethical Considerations

The study was approved by the ethical committees of the University of Bonn (Votum 124/19) and Semmelweis University (#177/2016).

3. Results

3.1. Quality Control (QC)

Three and five samples were excluded at the QC stage from the ADT and CRPC groups, respectively, due to low RNA quality (the final composition is in Table 1, excluding samples failing QC). The excluded samples were small, decalcified bone biopsies and transurethral resections.

3.2. AR-Vs Appear Mostly as a Response to ADT

An analysis of AR-FL and AR-V mRNA expression (AR-V1, AR-V3, AR-V7, AR-V9, AR45, ARv567es) was performed on the nCounter platform (Figures 1 and 3). AR-Vs were

detected in approximately two-thirds of CRPC samples and half of ADT samples but in only 14% of hormone-naïve cases (84% with Gleason Score > 4 + 3; no statistical association with ductal/acinar morphology). We detected no expression of AR-Vs in normal tissue and BPH samples (Figure 3A,B). AR-V1 was the most common AR-V in hormone-naïve PCA. AR-V7 was most common during ADT and in the CRPC stage (Figure 3B–D). In fact, in CRPC samples, AR-V7 was present in 100% of the samples expressing any of the other AR-Vs (Figure 3D). One of two CRPC patients on abiraterone therapy in our cohort expressed AR-Vs.

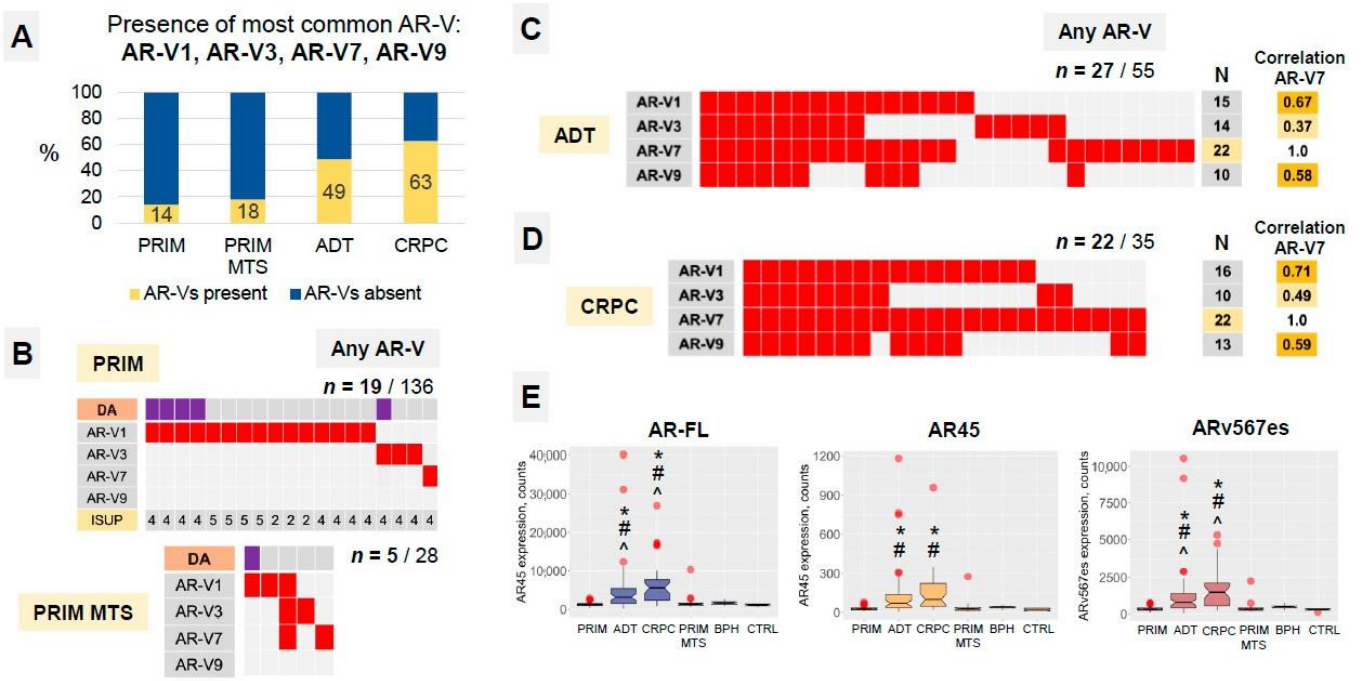

Figure 3. (**A**) Analysis of samples expressing any of the four androgen receptor splice variants in the four main study groups. BPH and CTRL groups were negative for AR-Vs. Numbers represent percentages of samples containing AR-Vs. (**B**–**D**) Stratification of the samples expressing any of the AR-V splice variants (V1, V3, V7, V9) in study groups. Boxes represent single samples. Stratification according to histological subtype (acinar or ductal (DA) adenocarcinoma) in primary hormone-naïve tumor samples. As other AR-Vs are co-expressed with AR-V7 in CRPCs, the latter appears a reasonable surrogate marker for the presence of AR-Vs. Correlation (co-existence) measure is presented for AR-V1, -V3 and -V9 compared to AR-V7 splice variant. "*n*" represents the number of samples positive for single AR splice variants. (**E**) Expression of full-length AR (AR-FL) and two other splice variants (AR45 and ARv567es) in tumor and benign study groups. Statistical significance ($p < 0.05$): * vs. PRIM group, ^ CRPC vs. ADT group, # vs. CTRL group (Mann–Whitney U-test).

Both AR45 and ARv567es mRNA were detectable in tumor and benign samples (Figure 3E). AR-FL, AR45 and ARv567es mRNA expressions were significantly higher in ADT and CRPC samples (all $p < 0.001$). AR45 and ARv567es mRNA expressions were highly correlated with the expression of AR-FL (Pearson's r 0.86 and 0.99, respectively, both $p < 1.0 \times 10^{-10}$). ARv567es mRNA expression was approximately three and four times higher (both $p < 0.0001$) in presence of any of the other AR-V splice variants in the CRPC and ADT groups, correspondingly.

A certain level of intra-patient heterogeneity was evident regarding the presence of AR-Vs. The AR-V status of multiple samples from single patients was heterogeneous in 9 out of 41 patients in the PRIM group, 1 of 4 patients in PRIM MTS, and 3 of 10 patients in the ADT group, but not in the CRPC group.

Both samples with primary small cell neuroendocrine carcinoma of the prostate and sarcomatoid carcinoma (post-ADT) showed no or almost undetectable expression levels of AR-Vs and AR-FL, respectively [30].

3.3. AR Signaling and Proliferation Depend on the Presence of AR-Vs in ADT and CRPC Tumors

To measure the activation of the AR pathway, we calculated an AR score from cumulative levels of expression for 10 established transcriptional targets of AR (Figure 2B) with CTRL samples as a reference.

The median AR-FL expression increased with the progression of the disease (Figure 3E). However, AR target gene (positive AR score) induction was significantly reduced in the ADT and CRPC samples (despite ongoing ADT), while AR signaling was significantly activated in samples from both the PRIM and PRIM MTS groups (Figure 4A). In fact, a smaller part of the ADT and CRPC samples revealed the downregulation of known AR target genes (negative AR score) (Figure 4A).

The decrease in the AR score, as observed for ADT and CRPC, however, does not translate into a significant change in the proliferative index. Similar to the PRIM MTS group, MKI67 expression was significantly elevated in ADT and CRPC compared to the PRIM samples (Figure 4B), but only in ADT and CRPC (Figure 4D, Supplementary Figure S1A,B), but MKI67 expression correlated with AR-Vs only in ADT and CRPC samples (Figure 4D, Supplementary Figure S1A,B). A similar upregulation of the PRIM MET, ADT and CRPC cohort was detected for the ubiquitin-conjugating enzyme E2C *(UBE2C)* in comparison to the CTRL, BPH and PRIM groups (Supplementary Figure S2A). The progressive loss of AR target gene expression, in combination with an increasing proliferative index, may hint at a progredient dedifferentiation of tumors ranging from the PRIM to CRPC cohorts.

The expression of UBE2C is driven by AR-V- and not by AR-signaling in CRPC tumors [31]. Our analyses support this finding, as UBE2C expression was significantly upregulated only in CRPC tumors expressing AR-Vs (Figure 4E, Supplementary Figure S2B). In the same group, we found a significant association between AR-V expression with increased proliferation (MKI67) and the AR-V^{+}-dependent elevation of AR target gene expression, while in AR-V negative CRPCs, AR target gene induction was in the range of the CTRL group ($p = 0.003$; Figure 4C). We did not find evidence for a correlation between AR pathway activity and *PTEN* or *RB1* expression in any of the groups (all $p > 0.05$).

In both ADT and CRPC groups (Figure 4D), significantly higher *MKI67* mRNA expression was evident in tumors expressing AR-V splice variants. *PCNA* expression strongly correlated with the *MKI67* expression (Pearson's r 0.52, $p < 2.2 \times 10^{-16}$; not shown) without any evidence of dependence on AR-Vs (Supplementary Figure S1C,D).

3.4. Homologous Recombination DNA Repair Activity Depends on the Presence of AR-Vs and AR Pathway Activation

Overall, the mRNA expression of 20 genes associated with HR DNA repair was analyzed in our study. Unsupervised heatmap clustering analysis showed evidence of two major clusters of DNA repair genes, one of them containing *BRCA1* and the other containing *BRCA2* expression. With the introduction of AR-Vs in this analysis as a quantitative parameter, AR-V expression was preferentially associated with the CRPC phenotype (11/45 in the AR-V low-expressing group vs. 23/45 in the AR-V high-expressers, Figure 5). In the AR-V high-expressing group, DNA repair gene expression was more abundantly deregulated as compared to the AR-V low-expressing group, where a more stable expression of DNA repair genes was observed.

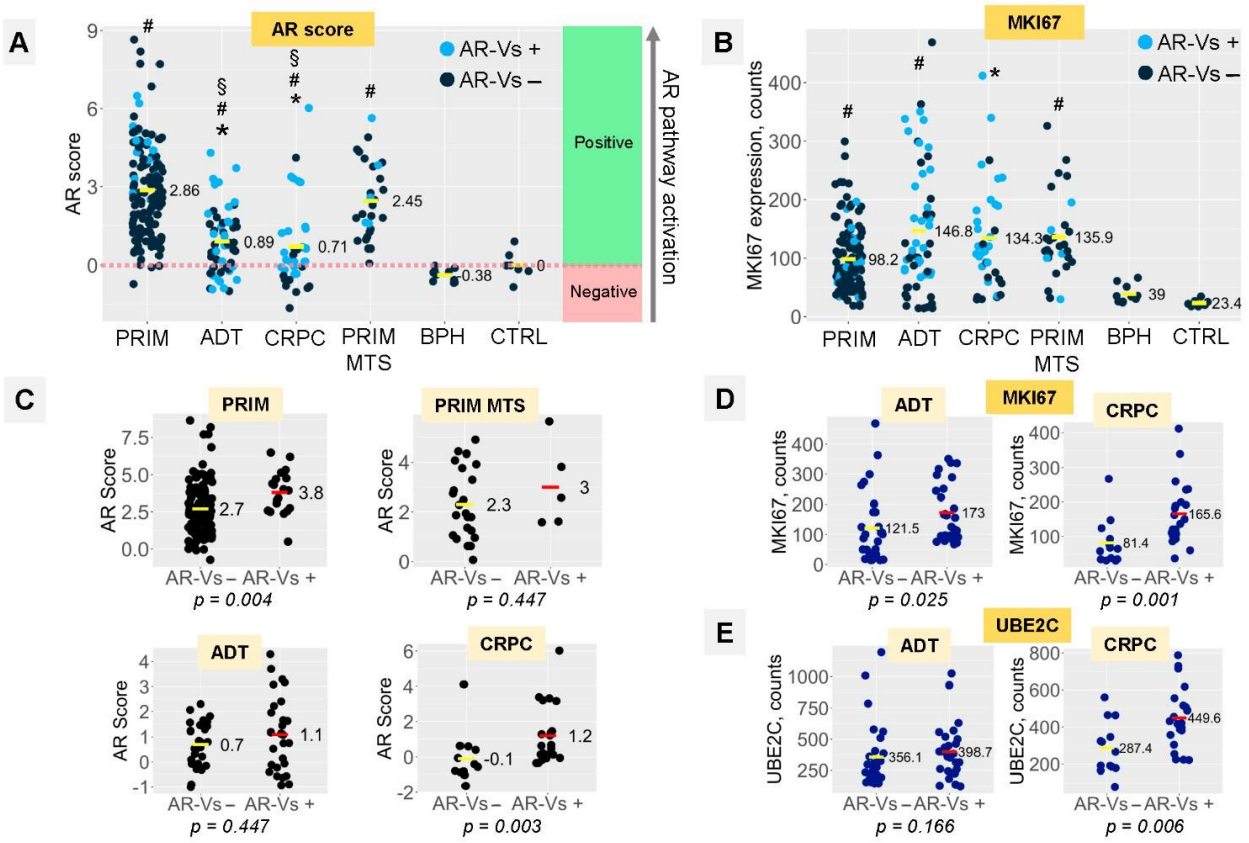

Figure 4. (**A**) Distribution of AR scores in study groups (cumulative score of AR pathway activation, calculated based on mRNA expression of 10 transcriptional targets of AR). Light blue points express any of the AR-V splice variants (V1, V3, V7, V9); dark blue points do not express AR-V splice variants. "Positive" area represents AR score in "activated" range compared to reference group (CTRL: benign non-hyperplastic prostate tissue). "Negative" area represents depression in AR signaling. (**B**) mRNA expression of proliferation marker MKI67. (**C**) Analysis of AR score distribution in four "tumor" study groups in relation to dependence on AR-V splice variant expression. (**D**) Analysis of MKI67 mRNA expression in ADT and CRPC groups in relation to dependence on AR-V splice variant expression. (**E**) Analysis of UBE2C mRNA expression in ADT and CRPC groups in relation to dependence on AR-V splice variant expression. *p*-levels calculated using Mann–Whitney U-test. Statistical significance ($p < 0.05$): * vs. PRIM group, # vs. CTRL group, § vs. PRIM MTS group.

To quantify DNA repair gene expression, we calculated a DNA repair activity score (DNA-R score) from the expression levels of 20 genes (excluding *PARP1* and *PARP2*) using CTRL samples as a reference, analogous to the AR score introduced above (Figures 6 and S3). The DNA-R score significantly increased in all groups, including BPH, compared to the reference group (Figure 6A). In the presence of AR-Vs, the DNA-R score increased significantly in CRPCs. We observed a similar trend in the ADT group (Figure 6B). In the PRIM and ADT groups, as well as in the CRPC group (statistical trend), the DNA-R score significantly correlated with the AR score (Figure 6C). In linear regression models, the effect of proliferation on DNA repair was clearly visible (Table 2, lower panel). However when accounting for this effect, residual coefficient estimates revealed a positive association between the presence of AR-Vs and enhanced DNA repair in both primary tumors (ADT, $p = 0.0377$) and tumors that that underwent androgen deprivation therapy (ADT, $p = 0.0297$). Statistical analysis revealed a strong trend for CRPC within the latter group (Table 2, upper panel). An analysis of the CRPC group ($p = 0.0551$) showed a strong trend in the same direction in the respective regression models. The DNA-R score was not found to be correlated with *RB1*, *PTEN* or *ERG* mRNA expression (all $p > 0.05$).

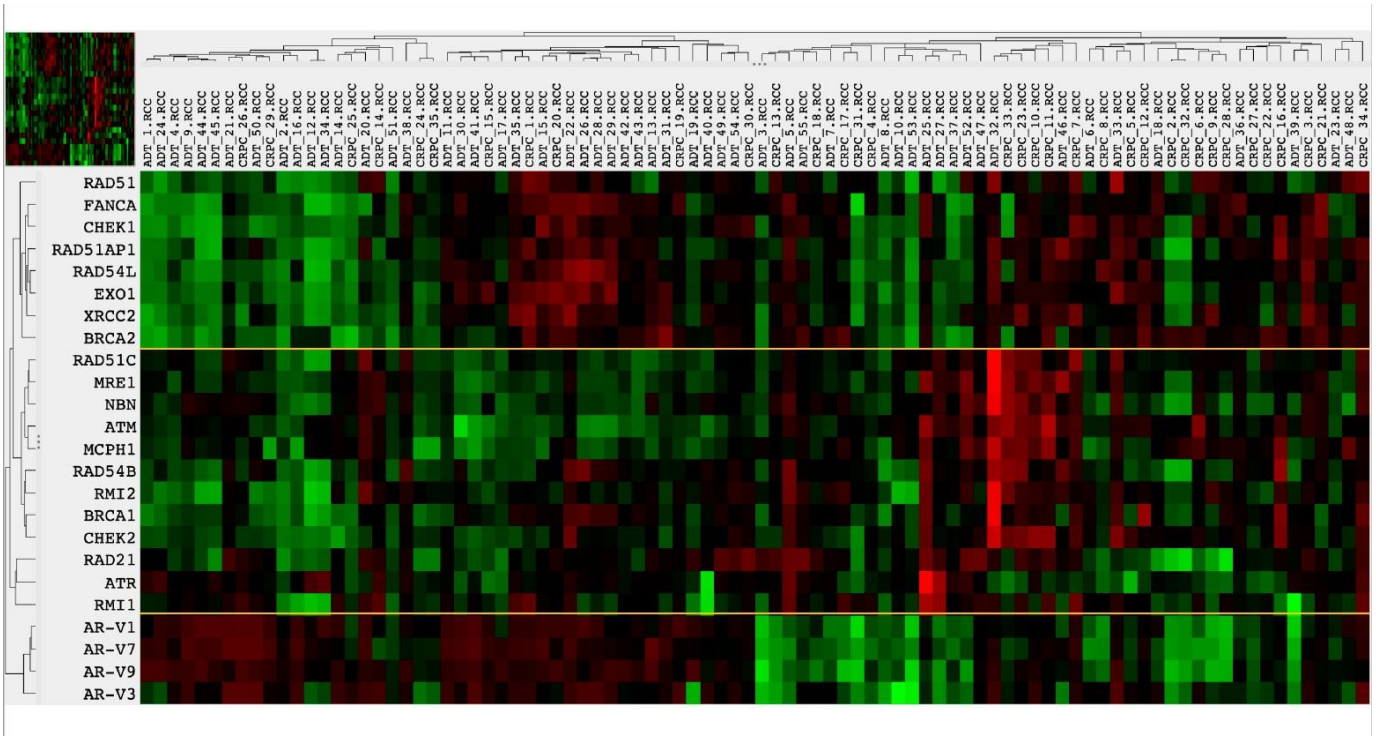

Figure 5. Heatmap plot of mRNA expression levels of DNA repair genes and AR-V splice variants as a quantitative parameter (**left side**). Samples represent pooled tumor samples from ADT and CRPC groups. Note similarities in the expression levels of the upper cluster of DNA repair genes (RAD51 to BRCA2) and AR-V splice variants, with the exception of 15 samples on the **left side** (mostly ADT samples). Clusters are separated by yellow lines.

To quantify DNA repair gene expression, we calculated a DNA repair activity score (DNA-R score) from the expression levels of 20 genes (excluding *PARP1* and *PARP2*) using CTRL samples as a reference, analogous to the AR score introduced above (Figures 6 and S3). The DNA-R score significantly increased in all groups, including BPH, compared to the reference group (Figure 6A). In the presence of AR-Vs, the DNA-R score increased significantly in CRPCs. We observed a similar trend in the ADT group (Figure 6B). In the PRIM and ADT groups, as well as in the CRPC group (statistical trend), the DNA-R score significantly correlated with the AR score (Figure 6C). In linear regression models, the effect of proliferation on DNA repair was clearly visible (Table 2, lower panel). However when accounting for this effect, residual coefficient estimates revealed a positive association between the presence of AR-Vs and enhanced DNA repair in both primary tumors (ADT, $p = 0.0377$) and tumors that that underwent androgen deprivation therapy (ADT, $p = 0.0297$). Statistical analysis revealed a strong trend for CRPC within the latter group (Table 2, upper panel). An analysis of the CRPC group ($p = 0.0551$) showed a strong trend in the same direction in the respective regression models. The DNA-R score was not found to be correlated with *RB1*, *PTEN* or *ERG* mRNA expression (all $p > 0.05$).

An analysis of expression and dependence on the presence of AR-Vs for single HR DNA repair genes is presented in Supplementary Figures S4–S7. The trends in mRNA expression for the individual DNA repair genes were similar to the ADT and CRPC groups. Some genes (*ATM*, *RAD51C*, *BRCA2*, *MRE1*, *RMI1*) were more profoundly downregulated in the CRPC group (Figure 7A). A number of DNA repair genes showed statistically significant altered expression in the PRIM, ADT and CRPC groups in the presence of AR-Vs (Figure 7B).

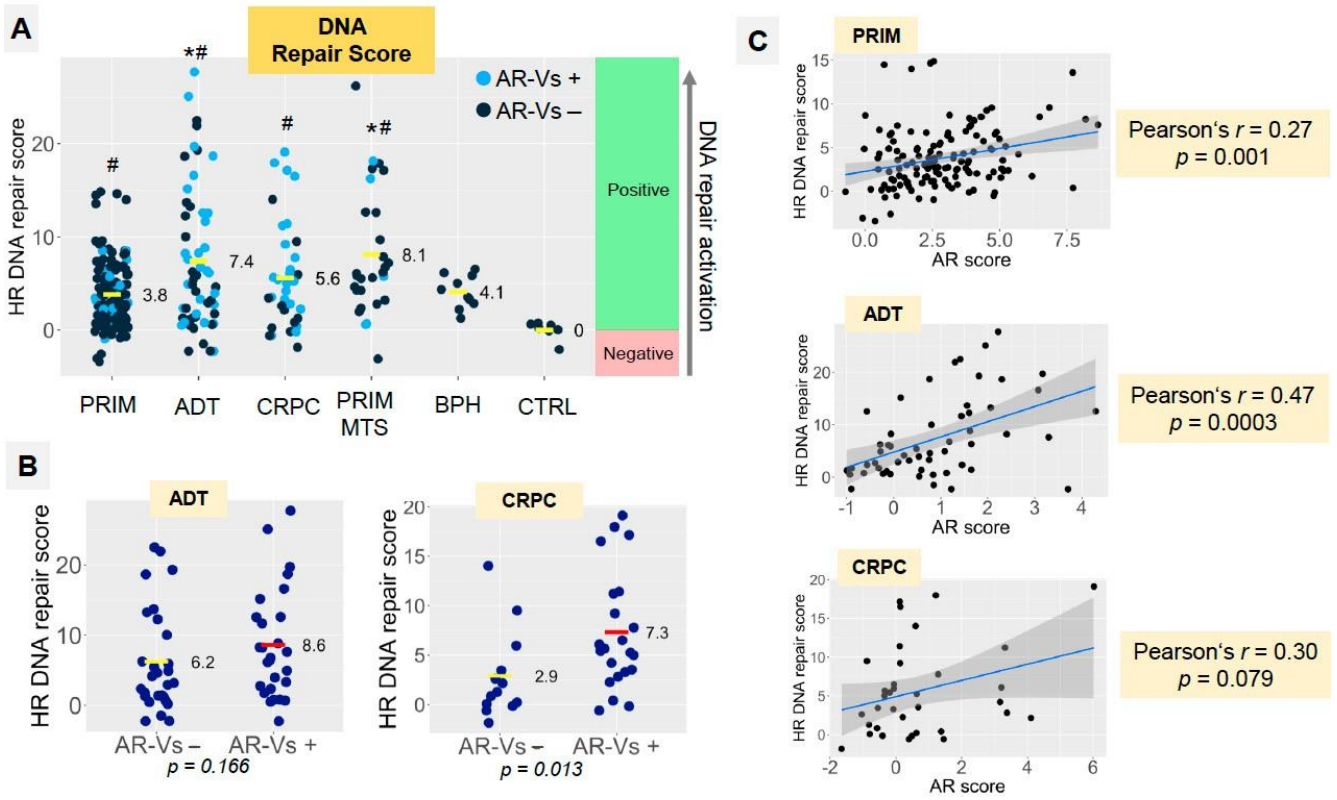

Figure 6. (**A**) Distribution of DNA repair scores in study groups (cumulative score based on mRNA expression of 20 DNA repair genes). Light blue points express any of the AR-V splice variants (V1, V3, V7, V9); dark blue points do not express AR-V splice variants. (**B**) Dependence of DNA repair score on the presence of AR-V splice variants (V1, V3, V7, V9) in ADT and CRPC groups. *p*-levels calculated using Mann–Whitney U-test. Statistical significance ($p < 0.05$): * vs. PRIM group, # vs. CTRL group. (**C**) Correlation analysis shows dependence of the AR score and DNA repair score in PRIM, ADT and CRPC groups.

Table 2. Estimates of associations between AR splice variants, proliferation and DNA repair, as obtained from fitting group-wise linear regression models with the DNA-R score as a dependent variable and splice variant and proliferation scores as independent variables. * $p < 0.05$, *** $p < 0.0005$.

AR splice variants vs. DNA repair.				
	Patients	**Coefficient Estimate**	**SD**	***p*-Value**
ADT	88	0.008013	0.003624	0.0297 *
ADT nonCRPC	53	0.007468	0.004472	0.101
CRPC	35	0.012147	0.006103	0.0551
Prim	136	0.080467	0.038329	0.0377 *
AR splice variants vs. proliferation.				
	Patients	**Coefficient Estimate**	**SD**	***p*-Value**
ADT	88	0.028671	0.002070	$<2 \times 10^{-16}$ ***
ADT nonCRPC	53	0.030869	0.002317	$<2 \times 10^{-16}$ ***
CRPC	35	0.023398	0.003974	1.5×10^{-6} ***
Prim	136	0.030435	0.002304	$<2 \times 10^{-16}$ ***

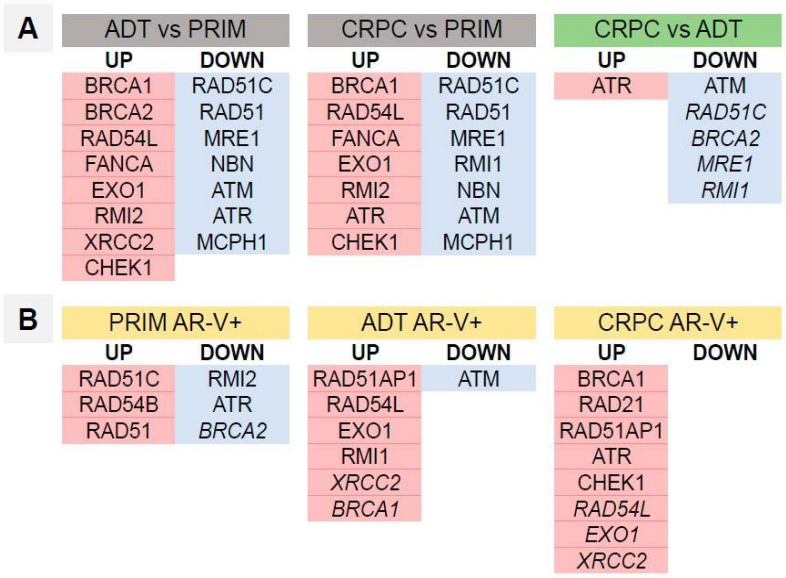

Figure 7. DNA repair genes differentially expressed in samples from different ADT, CRPC and PRIM groups ($p < 0.05$; in italic—$p = 0.05–0.1$) in relation to AR-V expression. Detailed expression analysis of individual DNA repair genes is provided in Supplementary Figures S4–S7. Upregulated genes are shown with a red background and downregulated genes with a blue background. (**A**) Cumulative analysis of all samples in study groups independent of AR-V status. (**B**) Analysis of genes affected in samples positive for any of AR-V splice variants (V1, V3, V7, V9) compared to those without AR-V splice variant expression.

It is known that DNA repair genes are also involved in various aspects of cell cycle progression. Gene ontology (GO) analyses of our gene set further validated the involvement of our gene set in DNA repair, as compared to the cell cycle and mitotic processes (Supplementary Figure S11A). We found BRCA1 genes as well as the BRCA2 cluster upregulated in processes related to DNA repair, but only to a low extent were they involved in cell cycle-related pathways. Ranking the pathways using GO Panther hierarchical cluster analysis (Supplementary Figure S11B) revealed our gene set to be significantly linked to multiple DNA repair pathways (DNA repair, double-strand break repair, double-strand break repair via homologous recombination, cellular response to DNA damage stimulus, recombinational repair, DNA recombination), followed by cell cycle pathways. It is striking that DDR pathways showed up to five times higher "fold enrichment" (13.91–62.22) compared to cell cycle pathways (9.25–13.34).

PARP1 and *PARP2* mRNA expression was not found to correlate with the AR score in any of the groups. Both *PARP1* and *PARP2* were statistically significantly downregulated in the CRPC group compared to primary tumors (both $p < 0.05$; Supplementary Figure S8), where were not dependent on the presence of AR-Vs.

3.5. AR-V7 Enhances DNA Double-Strand Break Repair in an In Vitro PCA Model

The induction of DNA repair genes by AR splice variants can be measured by γH2A.X foci formation after the introduction of double-strand breaks. We used the LNCaP/V7 PCA in vitro tumor model for irradiation and assayed for γH2A.X foci formation over time. In contrast to primary foci, which correlate in number with DSBs, residual foci indicate the number of DBSs in the repair process [32]. We screened for foci formation at three timepoints (1 h, 24 h and 48 h after irradiation) and verified a strong induction of γH2AX focus formation at the early timepoint (1 h), a gradual decline of foci after 24 h and an almost complete loss of detectable foci 2 days after irradiation (Supplementary Figure S12). Compared to LNCaP cells overexpressing AR-FL (Supplementary Figure S10), we observed a modest but significantly reduced number of residual foci 24 h after irradiation (−8.5%,

$p < 0.01$) in the presence of AR-V7, indicating accelerated DNA repair in LNCaP cells containing this AR splice variant [32] (Figure 8). Consequently, the presence of AR-V7 in PCA cells improves DNA repair provoked by X-ray irradiation.

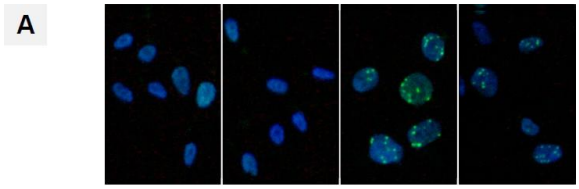

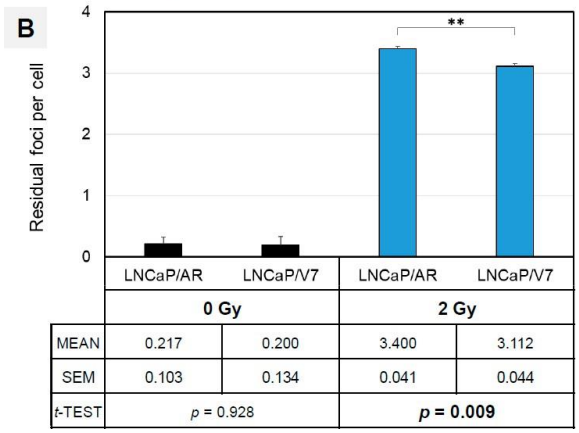

MEAN	0.217	0.200	3.400	3.112
SEM	0.103	0.134	0.041	0.044
t-TEST	$p = 0.928$		**$p = 0.009$**	

Figure 8. (**A**) The presence of AR-V7 enhances DNA repair in vitro. Increased DNA repair is visualized by a diminished number of residual γH2Ax foci 24 h after irradiation. Nuclear counterstain with DAPI from left to right: LNCaP/AR (0 Gy), LNCaP/V7 (0 Gy), LNCaP/AR (2 Gy), LNCaP/V7 (2 Gy). (**B**) Quantification of residual γH2A.X foci 24 h after irradiation (2 Gy, blue). Non-irradiated cells were used for comparison (0 Gy, black). In total, >200 nuclei were counted per cell line, irradiative condition and experiment, with a mean of three independent experiments. ** = $p < 0.01$.

3.6. In Vitro Validation of Findings in Clinical Samples

With the first proof that AR-V7 expression in tumor cells enhances DNA repair, our next step was to investigate the AR-V7-specific regulation of DNA repair gene expression (mRNA). DNA repair gene upregulation was observed in CRPC tumors (Figure 7B) expressing androgen receptor splice variants (CRPC AR-V+) in comparison to ADT refractory tumors in the absence of AR-Vs. We translated the CRPC AR-V+ phenotype in our tumor model to LNCaP cells expressing AR-V7, while androgen-resistant LNCaP cells overexpressing AR-FL mimicked the reference cohort (CRPC) [33]. We induced DNA damage in order to study the transcriptional regulation of DNA repair genes in vitro 6 h after irradiation. We observed only a minimal alteration of DNA repair genes in unirradiated reference samples of both LNCaP/AR and LNCaP/V7 cells. This finding disproves the assumption of a gross impact of AR-V7 on repair genes prior to DNA damage (Figure 9). Upon irradiation, however, a set of four genes (CHEK1, EXO1, RAD54L, XRCC2) was strongly upregulated, specifically in cells expressing AR-V7, confirming and validating the expression data generated from clinical samples, as described above. These similarities point to the representative nature of LNCaP/V7 cells as an in vitro model of CRPC tumor cells that express AR splice variants (CRPC AR-V+, Figure 7B).

A similar in vitro analysis was performed to corroborate the results achieved by comparing clinical CRPC and PRIM sub-cohorts (CRPC vs. PRIM; Figure 7A), where alterations in DNA repair gene expression were associated with the CRPC phenotype. *In vitro*, clinical CRPC was phenocopied by our LNCaP/V7 cell line, while the PRIM phenotype was represented by androgen-responsive LNCaP cells. As a primary result in the absence of DNA damage, we observed minor alterations in DNA repair gene mRNA expression. DNA repair induced by double-strand breaks resulted in a substantial shift in a

subset of genes (RAD54L, EXO1, RMI2; Figure 10A), earlier identified as upregulated in clinical CRPC samples. Three additional genes (ATM, NBN, MCPH1) were confirmed as downregulated in vitro in the LNCaP/V7 CRPC model (Figure 10B). The genes identified by in vitro analyses can be equally assigned to either the group of DNA damage sensors (ATM, CHEK1/CHK1, MCPH1, NBN) or HR repair genes (EXO1, RAD54L, RMI2, XRCC2), in accordance with published data [3,5,8,34,35].

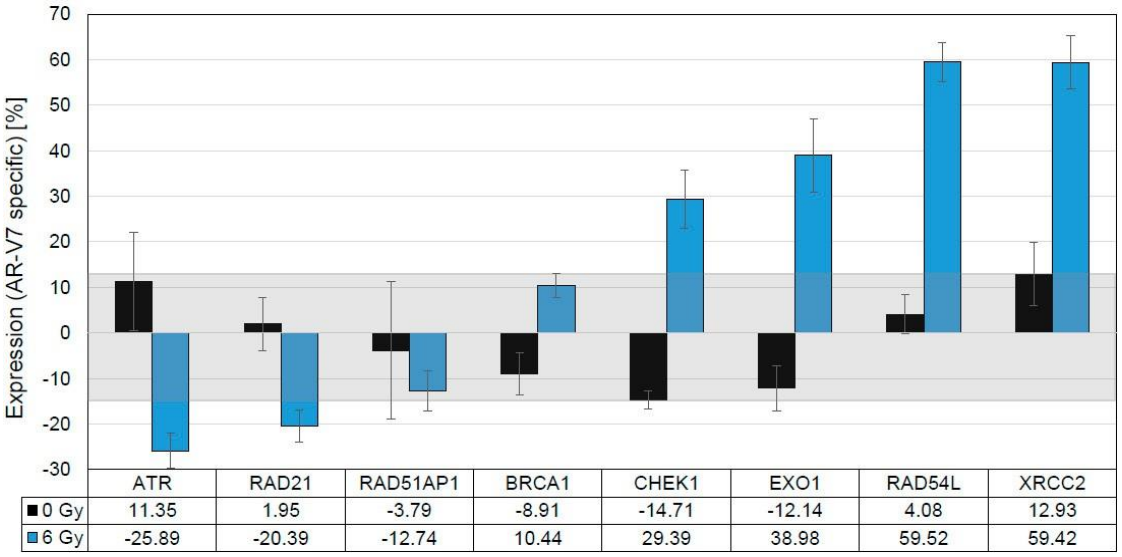

	ATR	RAD21	RAD51AP1	BRCA1	CHEK1	EXO1	RAD54L	XRCC2
0 Gy	11.35	1.95	-3.79	-8.91	-14.71	-12.14	4.08	12.93
6 Gy	-25.89	-20.39	-12.74	10.44	29.39	38.98	59.52	59.42

Figure 9. Validation of upregulated DNA repair genes of the AR splice variant expressing CRPC. LNCaP overexpressing AR-V7 served as a surrogate for CRPCs expressing AR-Vs. DNA repair genes upregulated in CRPC+AR-Vs (Figure 7B) were validated by qRT-PCR under irradiated (6 Gy, IR, blue bars) and non-irradiated (0 Gy, Ø, black bars) androgen-deprived conditions. The latter condition, with generally lower AR-V7-specific expression, served as the threshold (light gray box) to identify genes (CHEK1, EXO1, RAD54L, XRCC2) strongly upregulated by irradiation.

A

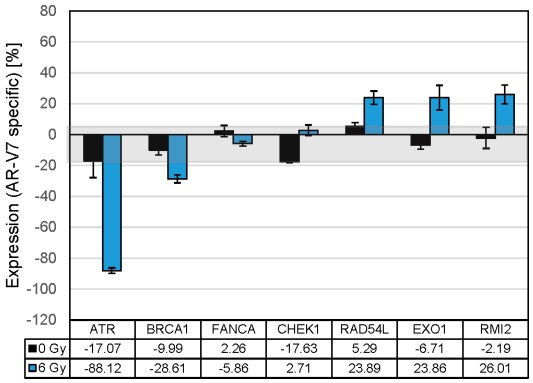

	ATR	BRCA1	FANCA	CHEK1	RAD54L	EXO1	RMI2
0 Gy	-17.07	-9.99	2.26	-17.63	5.29	-6.71	-2.19
6 Gy	-88.12	-28.61	-5.86	2.71	23.89	23.86	26.01

Figure 10. *Cont.*

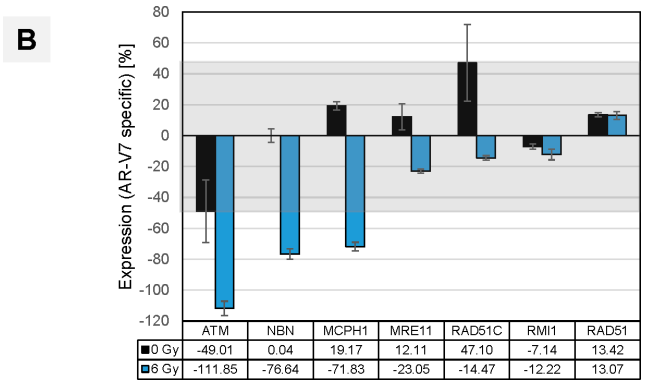

Figure 10. (**A**) Impact of AR splice variants in clinical CRPC via the validation of deregulated DNA repair genes in vitro. LNCaP cells overexpressing AR-V7 served as a surrogate for CRPCs expressing AR splice variants. DNA repair genes deregulated in CRPC vs. PRIM (Figure 7A) were validated by qRT-PCR under irradiated (6 Gy, IR, blue bars) and non-irradiated (0 Gy, Ø, black bars), androgen-deprived conditions. The latter condition, with generally lower AR-V7-specific expression, served as the threshold (light grey box) to identify genes visibly upregulated by irradiation such as RAD54L, EXO1, RMI2. (**B**) Under the same experimental conditions, genes such as ATM, NBN, MPCH1 were confirmed as downregulated.

4. Discussion

The recognition of the commonly impaired DNA damage response by defects in HR has enabled new, targeted therapeutic interventions in many malignant tumors, including PCA [9,36]. The connection between the AR pathway and DNA repair in PCA proved to be so tight that, even in the absence of pathogenic mutations in DNA repair genes, there is a possibility of targeted therapeutic interventions using PARPi. ADT causes the significant downregulation of DNA repair genes given direct and indirect transcriptional regulation of the latter through AR [1–3,5–8,15,37]. This functional impairment of HR is sufficient to induce synthetic lethality under treatment with PARPi. Several major studies [5,6] provided a proof of principle for such synthetic lethality in cell line experiments, and two clinical trials have been conducted to date on patients with CRPC. A pilot study (NCI 9012) showed no differences in response rates between CRPC cohorts receiving abiraterone versus abiraterone/veliparib [38]. Abiraterone/olaparib, however, was effective in unselected patients with CRPC compared to abiraterone only [11], in particular, in a subgroup of patients with pathogenic mutations in HR DNA repair genes (NCT03732820) [39].

These studies [5,6] of synthetic lethality [11,38] analyzed AR function in the context of mutant DNA repair genes in CRPC tumors. AR splice variants showed activating effects in DNA repair genes similar to full-length androgen receptors [3,8], thus provoking the examination of the effect of AR-Vs on DNA repair genes in a clinical setting.

An appropriate in vitro model system has to fulfill several aspects to closely mimic the physiological situation of AR-V7-expressing PCA tumor cells [40]. The expression of AR-V7 is only observed in the context of full-length AR. The choice of an LNCaP cell model with high endogenous AR-FL expression caused by lentiviral transduction avoids clonal effects. To compensate for higher total AR expression in LNCaP/V7, we generated an LNCaP control cell line that overexpresses full-length AR (LNCaP/AR). Original LNCaP cells harbor the AR T878A mutation [41], which is known to cause aberrant AR behavior. However, the use of steroid-depleted media minimizes the effect of mutant AR signaling, and comparison with the control cell line LNCaP/AR, which overexpresses the wild-type full-length androgen receptor, ensures the analysis of AR-V7-specific effects in this in vitro tumor model. Hence, we are confident that our experimental setup allows for the analysis of AR-V7-specific effects in DDR even in the presence of the endogenous AR T878A mutation in LNCaP cells.

Cell lines such as VCaP might be used to analyze endogenous AR-V7 effects on DNA repair. However, VCaP cells are infected with and secrete the retrovirus Bxv-1, a xenotropic

mouse leukemia virus, as shown by Sfanos et al. [42]. In the course of retroviral infection, γH2AX foci are detectable at sites of proviral integration [43], limiting the use of this assay to study DNA repair in VCaP cells.

Thus, we cannot exclude the impact of this virus on cellular physiology and AR-FL/AR-V7-signaling in these cells. We chose the transgenic approach using LNCaP cells, as these cells are not known to produce any viruses, closely mimicking the clinical situation.

To the best of our knowledge, this is the first study to analyze the link between AR pathway activation, the presence of AR splice variants and the transcription of DNA repair genes in multiple subgroups of clinical PCA tumor samples that reflect the development of ADT resistance. While the upregulation of AR-V7 under ADT treatment in patient samples was already reported by Sharp et al. [21], our approach provides data for those subgroups, including a CRPC specimen. Additionally, these data were substantiated by cell line models, mimicking the CRPC phenotype of the clinical samples. Importantly, we provide evidence that crucial components of the DNA repair machinery might be induced in the presence of AR-Vs in CRPC. Thus, approximately two-thirds of patients with CRPC and half of the patients on ADT (but still hormone-sensitive) in our study harbored AR-V1, -V3, -V7, and -V9. Additionally, our study demonstrated the presence of AR-Vs is correlated to the increased activity of the AR pathway measured by the AR score in CRPC. Furthermore, the cellular proliferation index doubled in CRPC in the presence of AR-Vs as measured by MKI67 expression (Figure 4C,D).

This study shows that the expression of DNA repair genes, summarized as a DNA repair score, is 2.5 times higher in the presence of AR-Vs in CRPC (Figure 6B,C). This validates the results of previous experimental studies, which showed that, even in the absence of AR-FL, AR splice variants can provide the necessary transcriptional support for DNA repair genes [3] and the loss of AR-Vs sensitizes them to ionizing radiation [8]. As was demonstrated by Luo et al. [23], AR-V7 significantly promotes the DDR of PCA cells under severe DNA damage. The impact of AR-Vs on the DDR machinery may have clinical implications, as the activity of DNA repair in CRPC in the presence of AR-V splice variants seems to be similar or even higher than in hormone-naïve tumors. This may explain the rather inconclusive findings concerning the combination therapy of ADT with PARPi [11,38], implying that AR-Vs may be predictive of the efficacy of synthetic lethality-based therapeutic regimens (in a negative way), and this should be clarified in further studies.

The expression signature of DNA repair genes in primary tumors differs from that of tumors under ADT and CRPC (Figure 7). Most of the genes analyzed are similarly affected in ADT and CRPC samples: among upregulated genes (BRCA1, RAD54L, FANCA, EXO1, RMI2, XRCC1, CHEK1), the majority were found to have the same tendency in CRPC tumors in studies by Taylor et al. [44] and Grasso et al. [45] Only RAD51 was downregulated in our study, but it was upregulated in the aforementioned studies. Interestingly, the majority of regulated genes in our study (ADT and CRPC) were shown to be transcriptionally downregulated by androgen blockade in experimental studies [1–3,6–8,15,37], contradicting the findings of Taylor et al. [44], Grasso et al. [45] and our results. Our study provides evidence that AR-Vs may account for this discrepancy, as the genes induced by AR-Vs largely overlap with regulated genes in tumors under androgen depletion or CRPCs (compared to hormone-naïve tumors; Figure 7A,B).

Specifically, BRCA1, RAD54L, EXO1 and CHEK1 are identically upregulated. It is now tempting to draw the following conclusions. First, elevated levels of AR-Vs detectable during ADT provide transcriptional support for DNA repair gene activity. This is corroborated by two experimental studies utilizing PCA cell lines [3,8]. Second, the activating effect of AR-Vs applies to some, but not all, DNA repair genes. Indeed, AR-Vs and AR-FL transcriptomes are, to some extent, different [31], even in regard to DNA damage response genes [1,8,34,35]. However, the precise differences in the transcriptional effects of AR-FL and AR-Vs concerning DNA repair are, to date, understudied by far and warrant further investigations.

PARP1 and *PARP2* were characterized earlier as important effectors of AR, functioning in positive regulatory loops [6–8,15]. In our study, mRNA expression in both genes was, to some extent, downregulated in CRPC samples compared to hormone-naïve tumors (Supplementary Figure S8) but did not show any dependency on AR splice variant expression. This could be related to the fact that mRNA expression in these genes is not a reliable measure of PARylation activity, which was also shown earlier [6].

Our analysis of clinical CRPC samples demonstrates the specific upregulation of DNA repair genes in two clinical settings: CRPC vs. PRIM and CRPC AR-V+ vs. CRPC AR-V-. This points to the initiation of DNA damage repair (DDR) in CRPC tumors. However, the precise mechanisms leading to AR-V-mediated modulations in DDR remain largely unknown. In our study, we constructed two in vitro cell line models simulating clinical CRPC tumor phenotypes with and without AR-V7 overexpression, derived from the initially hormone-sensitive LNCaP cell line (corresponding to the hormone-naïve phenotype in our experimental setup). In an in vitro CRPC model using LNCaP cells that overexpress AR-V7, DDR was induced by ionizing radiation. The presence of AR-V7 yielded a significant reduction in γH2A.X foci, which mark positions in the genome with actively ongoing DDR [32]. The resulting superior DDR has a beneficial impact on AR-V7 tumor cells. Upon DNA damage induced by irradiation, AR is known to translocate to the nucleus and initiate the expression of DNA repair genes such as XRCC2 [2]. AR splice variants such as AR-V7 are already located at a high fraction in the nuclei of primary PCA cells [46], while AR-FL remains cytoplasmatic in the absence of activating ligands. An augmented transcriptional activation of DNA repair genes in the presence of AR-Vs, therefore, appears plausible and was substantiated by our PCA tumor model.

DNA repair genes with de-regulated expression in CRPC clinical samples can either be classified in the group of DNA damage sensors (ATM, CHEK1/CHK1, MCPH1, NBN) or HR genes (EXO1, RAD54L, RMI2, XRCC2). Their altered expression was confirmed by our in vitro analyses. These data indicate that AR-Vs indeed play a multidirectional role in augmenting DDR in CRPC tumors (Figures 8–10) and mirror the findings of Yin et al., 2017 [3], who reported a causal link between AR-Vs and DNA repair after irradiation.

Furthermore, we confirmed three genes (ATM, NBN and MCPH1) to be downregulated in clinical CRPC tumor samples in our in vitro models. Various publications reported a downregulation of genes with a potential tumor-suppressive function in DNA repair [40,47], with ATM being one of the crucial and most thoroughly studied. One publication showed an association between NBN mutations and high-grade PCA in a Polish patient cohort [48], suggesting a tumor-suppressive function in this gene in normal prostate tissue. MCPH1, also downregulated in our clinical CRPC tumor samples, was previously reported to be downregulated in prostate carcinoma [49]. MCPH1 is functionally tightly associated with ATM and NBN. MCPH1 recruits ATM and NBN to DNA damage repair foci as part of the early DNA damage response [50]. The functional loss of ATM or NBN, two genes that are downregulated in our study, is associated with poor survival in PCa patients [50–52] and sensitizes PARP inhibitor therapies. Androgen receptor splice variant expression, in contrast, appears to reactivate DNA damage repair gene expression previously thwarted by ADT. In summary, our experiments using the AR-V7 in vitro PCA model suggest that the PARPi sensitization of CRPC tumors will likely not occur in the presence of AR-Vs [8], despite the observed loss of ATM expression. To the best of our knowledge, for the first time, the AR-V-dependent alteration of DDR gene expression has been shown in CRPC patients (Figure 7), and accelerated DDR in an AR-V7-dependent CRPC tumor model was confirmed.

In contrast to our expectations, we found an independent impact of AR-V expression on DDR gene expression in the clinical cohort. The employment of a linear regression model provided not only a significant positive association of AR-V expression with proliferation but also independently for DNA repair gene expression in primary tumors (Table 2). Calculations for the other groups resulted in corresponding associations, concluding that AR-Vs have an independent impact on DDR gene expression. Corroborating these findings

in vitro, analogous alterations of DDR gene expression, as found in the clinical samples, appeared within a timeframe that excludes the involvement of proliferative aspects of the functionality of AR-V7.

This study is not devoid of limitations, as DNA repair is a very complex process. Other important components of the DNA repair system, such as Ku70 protein [53], DNA protein kinase catalytic subunit [54] and some other genes, which have been shown to be AR-dependent, were not studied. Several other AR rearrangements (gene amplification and mutations) were also not targets of our study.

5. Conclusions

This study confirms the tight interconnection between AR signaling, alterations in AR expression and the transcription of DNA repair genes in clinical tumor samples and in vitro prostate cancer models. Of particular importance is the modulation of DNA repair gene expression in the presence of AR splice variants in CRPC. The expression of AR splice variants might be a reason for the reduced or absent effect of therapeutic concepts exploiting the principle of synthetic lethality between ADT and PARP inhibition. Thus, AR-Vs show potential as predictive biomarkers for the efficacy of PARPi therapy, as previously suggested [23].

Supplementary Materials: The following supporting information can be downloaded at: https://www.mdpi.com/article/10.3390/cancers14184441/s1. Table S1: CodeSet gene panel used in the study with probe sequences for RNA expression analysis. Table S2: Primer sequences used for qPCR analysis. Table S3: Validation of DNA repair genes by qRT-PCR analysis that were significantly deregulated in clinical samples (CRPC + AR-V). Table S4: Validation of DNA repair genes by qRT-PCR analysis that were significantly deregulated in clinical samples (CRPC vs PRIM). Figure S1: MKI67 and PCNA mRNA expression in study groups. Figure S2: UBE2C mRNA expression in study groups. Figure S3: mRNA expression of 20 DNA repair genes in study groups and correlation of DNA repair and AR scores. Figure S4: mRNA expression of 20 DNA repair genes in dependence on AR-V status in the PRIM group. Figure S5: mRNA expression of 20 DNA repair genes in dependence on AR-V status in the CRPC group. Figure S6: mRNA expression of 20 DNA repair genes in dependence on AR-V status in the ADT group. Figure S7: mRNA expression of 20 DNA repair genes in dependence on AR-V status. Figure S8: mRNA expression of PARP1 (A) and PARP2 (B) in study groups. Figure S9: Separation of the impact of AR splice variants on proliferation and DNA repair using a linear regression model. Figure S10: Expression of total androgen receptor and splice variant 7 in the LNCaP/AR in vitro tumor models. Figure S11: Gene ontology analysis of genes de-regulated in clinical samples reveals association with DNA repair. Figure S12: AR-V7 improves DNA repair after irradiation in an in vitro tumor model.

Author Contributions: Conceptualization, Y.T. and G.K.; data curation, Y.T., A.K., G.L., I.K., É.K., P.R., M.R., J.E. and C.-H.O.; formal analysis, Y.T., A.K. and M.S.; funding acquisition, Y.T. and G.K.; investigation, Y.T., A.K. and S.F.; methodology, Y.T., A.K. and S.F.; resources, Y.T., G.L., S.G., S.H., M.V.C., I.K., É.K., P.R., A.A., M.R., J.E., C.-H.O. and G.K.; software, Y.T.; supervision, Y.T. and G.K.; visualization, Y.T.; writing—original draft, Y.T., A.K. and T.M.; writing—review and editing, Y.T., A.K., G.L., M.S., T.M., S.F., S.G., S.H., M.V.C., I.K., É.K., P.R., A.A., M.R., J.E., C.-H.O. and G.K. All authors have read and agreed to the published version of the manuscript.

Funding: This work was supported by the Astellas research grant (Y.T., G.K.) and the BONFOR research grant (Y.T., A.K.) from the University of Bonn (Bonn, Germany). Partial support was provided by a startup grant from Semmelweis University, Budapest, Hungary (G.L.), and by the New National Excellence Program (ÚNKP-21-4-I-SE-32) of the Ministry for Innovation and Technology of Hungary (É.K.). M.V.C. is supported by a research grant (FC/2020/01A/ERVT) from Fondation Cancer, Luxembourg. T.M. and S.F. were financed by the Rudolf Becker Foundation for translational prostate carcinoma research (Essen, Germany). The funding organizations were not involved in any aspects of study design, implementation, data analysis or interpretation.

Institutional Review Board Statement: The study was approved by the ethics committees of the University of Bonn, Germany (#124/2019) and Semmelweis University, Budapest, Hungary (#177/2016). The study was conducted in accordance with the Declaration of Helsinki.

Informed Consent Statement: This is a retrospective study with tissue samples from anonymized patients who are not identifiable from the data set. Written informed consent is not available for the patients of this data set.

Data Availability Statement: Data generated in this study are available upon request.

Acknowledgments: We would like to thank Thomas Müdder (Department of Radiation Oncology, University Hospital Bonn, Germany) for helping with the irradiation.

Conflicts of Interest: The authors declare no conflict of interest.

References

1. Polkinghorn, W.R.; Parker, J.S.; Lee, M.X.; Kass, E.M.; Spratt, D.E.; Iaquinta, P.J.; Arora, V.K.; Yen, W.F.; Cai, L.; Zheng, D.; et al. Androgen receptor signaling regulates DNA repair in prostate cancers. *Cancer Discov.* **2013**, *3*, 1245–1253. [CrossRef] [PubMed]
2. Goodwin, J.F.; Schiewer, M.J.; Dean, J.L.; Schrecengost, R.S.; de Leeuw, R.; Han, S.; Ma, T.; Den, R.B.; Dicker, A.P.; Feng, F.Y.; et al. A hormone-DNA repair circuit governs the response to genotoxic insult. *Cancer Discov.* **2013**, *3*, 1254–1271. [CrossRef] [PubMed]
3. Yin, Y.; Li, R.; Xu, K.; Ding, S.; Li, J.; Baek, G.; Ramanand, S.G.; Ding, S.; Liu, Z.; Gao, Y.; et al. Androgen Receptor Variants Mediate DNA Repair after Prostate Cancer Irradiation. *Cancer Res.* **2017**, *77*, 4745–4754. [CrossRef] [PubMed]
4. Zhang, W.; Liao, C.Y.; Chtatou, H.; Incrocci, L.; van Gent, D.C.; van Weerden, W.M.; Nonnekens, J. Apalutamide Sensitizes Prostate Cancer to Ionizing Radiation via Inhibition of Non-Homologous End-Joining DNA Repair. *Cancers* **2019**, *11*, 1593. [CrossRef] [PubMed]
5. Li, L.; Karanika, S.; Yang, G.; Wang, J.; Park, S.; Broom, B.M.; Manyam, G.C.; Wu, W.; Luo, Y.; Basourakos, S.; et al. Androgen receptor inhibitor-induced 'BRCAness' and PARP inhibition are synthetically lethal for castration-resistant prostate cancer. *Sci. Signal.* **2017**, *10*, eaam7479. [CrossRef]
6. Asim, M.; Tarish, F.; Zecchini, H.I.; Sanjiv, K.; Gelali, E.; Massie, C.E.; Baridi, A.; Warren, A.Y.; Zhao, W.; Ogris, C.; et al. Synthetic lethality between androgen receptor signalling and the PARP pathway in prostate cancer. *Nat. Commun.* **2017**, *8*, 374. [CrossRef]
7. Schiewer, M.J.; Goodwin, J.F.; Han, S.; Brenner, J.C.; Augello, M.A.; Dean, J.L.; Liu, F.; Planck, J.L.; Ravindranathan, P.; Chinnaiyan, A.M.; et al. Dual roles of PARP-1 promote cancer growth and progression. *Cancer Discov.* **2012**, *2*, 1134–1149. [CrossRef]
8. Kounatidou, E.; Nakjang, S.; McCracken, S.; Dehm, S.M.; Robson, C.N.; Jones, D.; Gaughan, L. A novel CRISPR-engineered prostate cancer cell line defines the AR-V transcriptome and identifies PARP inhibitor sensitivities. *Nucleic Acids Res.* **2019**, *47*, 5634–5647. [CrossRef]
9. Mateo, J.; Carreira, S.; Sandhu, S.; Miranda, S.; Mossop, H.; Perez-Lopez, R.; Nava Rodrigues, D.; Robinson, D.; Omlin, A.; Tunariu, N.; et al. DNA-Repair Defects and Olaparib in Metastatic Prostate Cancer. *N. Engl. J. Med.* **2015**, *373*, 1697–1708. [CrossRef]
10. Armenia, J.; Wankowicz, S.; Liu, D.; Gao, J.; Kundra, R.; Reznik, E.; Chatila, W.K.; Chakravarty, D.; Han, G.C.; Coleman, I.; et al. The long tail of oncogenic drivers in prostate cancer. *Nat. Genet.* **2018**, *50*, 645–651. [CrossRef]
11. Clarke, N.; Wiechno, P.; Alekseev, B.; Sala, N.; Jones, R.; Kocak, I.; Chiuri, V.E.; Jassem, J.; Fléchon, A.; Redfern, C.; et al. Olaparib combined with abiraterone in patients with metastatic castration-resistant prostate cancer: A randomised, double-blind, placebo-controlled, phase 2 trial. *Lancet Oncol.* **2018**, *19*, 975–986. [CrossRef]
12. Byrum, A.K.; Vindigni, A.; Mosammaparast, N. Defining and Modulating 'BRCAness'. *Trends Cell Biol.* **2019**, *29*, 740–751. [CrossRef] [PubMed]
13. Deshmukh, D.; Qiu, Y. Role of PARP-1 in prostate cancer. *Am. J. Clin. Exp. Urol.* **2015**, *3*, 1–12. [PubMed]
14. Schiewer, M.J.; Knudsen, K.E. Transcriptional roles of PARP1 in cancer. *Mol. Cancer Res.* **2014**, *12*, 1069–1080. [CrossRef]
15. Gui, B.; Gui, F.; Takai, T.; Feng, C.; Bai, X.; Fazli, L.; Dong, X.; Liu, S.; Zhang, X.; Zhang, W.; et al. Selective targeting of PARP-2 inhibits androgen receptor signaling and prostate cancer growth through disruption of FOXA1 function. *Proc. Natl. Acad. Sci. USA* **2019**, *116*, 14573–14582. [CrossRef]
16. Jividen, K.; Kedzierska, K.Z.; Yang, C.S.; Szlachta, K.; Ratan, A.; Paschal, B.M. Genomic analysis of DNA repair genes and androgen signaling in prostate cancer. *BMC Cancer* **2018**, *18*, 960. [CrossRef]
17. Li, Y.; Yang, R.; Henzler, C.M.; Ho, Y.; Passow, C.; Auch, B.; Carreira, S.; Nava Rodrigues, D.; Bertan, C.; Hwang, T.H.; et al. Diverse AR Gene Rearrangements Mediate Resistance to Androgen Receptor Inhibitors in Metastatic Prostate Cancer. *Clin. Cancer Res.* **2020**, *26*, 1965–1976. [CrossRef]
18. Wang, Q.; Li, W.; Zhang, Y.; Yuan, X.; Xu, K.; Yu, J.; Chen, Z.; Beroukhim, R.; Wang, H.; Lupien, M.; et al. Androgen receptor regulates a distinct transcription program in androgen-independent prostate cancer. *Cell* **2009**, *138*, 245–256. [CrossRef]
19. The Cancer Genome Atlas Research Network. The Molecular Taxonomy of Primary Prostate Cancer. *Cell* **2015**, *163*, 1011–1025. [CrossRef]
20. Kallio, H.M.L.; Hieta, R.; Latonen, L.; Brofeldt, A.; Annala, M.; Kivinummi, K.; Tammela, T.L.; Nykter, M.; Isaacs, W.B.; Lilja, H.G.; et al. Constitutively active androgen receptor splice variants AR-V3, AR-V7 and AR-V9 are co-expressed in castration-resistant prostate cancer metastases. *Br. J. Cancer* **2018**, *119*, 347–356. [CrossRef]
21. Sharp, A.; Coleman, I.; Yuan, W.; Sprenger, C.; Dolling, D.; Rodrigues, D.N.; Russo, J.W.; Figueiredo, I.; Bertan, C.; Seed, G.; et al. Androgen receptor splice variant-7 expression emerges with castration resistance in prostate cancer. *J. Clin. Investig.* **2019**, *129*, 192–208. [CrossRef] [PubMed]

22. Culig, Z. The way towards understanding possible multiple functions of AR V7 in prostate cancer. *BJU Int.* **2018**, *122*, 169. [CrossRef]
23. Luo, H.; Liu, Y.; Li, Y.; Zhang, C.; Yu, B.; Shao, C. Androgen receptor splicing variant 7 promotes DNA damage response in prostate cancer cells. *FASEB J.* **2022**, *36*, e22495. [CrossRef] [PubMed]
24. Olsen, J.R.; Azeem, W.; Hellem, M.R.; Marvyin, K.; Hua, Y.; Qu, Y.; Li, L.; Lin, B.; Ke, X.; Øyan, A.M.; et al. Context dependent regulatory patterns of the androgen receptor and androgen receptor target genes. *BMC Cancer* **2016**, *16*, 377. [CrossRef] [PubMed]
25. Martz, C.A.; Ottina, K.A.; Singleton, K.R.; Jasper, J.S.; Wardell, S.E.; Peraza-Penton, A.; Anderson, G.R.; Winter, P.S.; Wang, T.; Alley, H.M.; et al. Systematic identification of signaling pathways with potential to confer anticancer drug resistance. *Sci. Signal.* **2014**, *7*, ra121. [CrossRef]
26. Deville, S.S.; Luft, S.; Kaufmann, M.; Cordes, N. Keap1 inhibition sensitizes head and neck squamous cell carcinoma cells to ionizing radiation via impaired non-homologous end joining and induced autophagy. *Cell Death Dis.* **2020**, *11*, 887. [CrossRef]
27. Becker, Y.; Förster, S.; Gielen, G.H.; Loke, I.; Thaysen-Andersen, M.; Laurini, C.; Wehrand, K.; Pietsch, T.; Diestel, S. Paucimannosidic glycoepitopes inhibit tumorigenic processes in glioblastoma multiforme. *Oncotarget* **2019**, *10*, 4449–4465. [CrossRef]
28. Bankhead, P.; Loughrey, M.B.; Fernández, J.A.; Dombrowski, Y.; McArt, D.G.; Dunne, P.D.; McQuaid, S.; Gray, R.T.; Murray, L.J.; Coleman, H.G.; et al. QuPath: Open source software for digital pathology image analysis. *Sci. Rep.* **2017**, *7*, 16878. [CrossRef]
29. Mathy, C.S.; Mayr, T.; Kürpig, S.; Meisenheimer, M.; Dolscheid-Pommerich, R.C.; Stoffel-Wagner, B.; Kristiansen, G.; Essler, M.; Muders, M.H.; Bundschuh, R.A. Antihormone treatment differentially regulates PSA secretion, PSMA expression and 68 Ga-PSMA uptake in LNCaP cells. *J. Cancer Res. Clin. Oncol.* **2021**, *147*, 1733–1743. [CrossRef]
30. Wright, M.E.; Tsai, M.J.; Aebersold, R. Androgen receptor represses the neuroendocrine transdifferentiation process in prostate cancer cells. *Mol. Endocrinol.* **2003**, *17*, 1726–1737. [CrossRef]
31. Hu, R.; Lu, C.; Mostaghel, E.A.; Yegnasubramanian, S.; Gurel, M.; Tannahill, C.; Edwards, J.; Isaacs, W.B.; Nelson, P.S.; Bluemn, E.; et al. Distinct transcriptional programs mediated by the ligand-dependent full-length androgen receptor and its splice variants in castration-resistant prostate cancer. *Cancer Res.* **2012**, *72*, 3457–3462. [CrossRef] [PubMed]
32. Roggero, C.M.; Jin, L.; Cao, S.; Sonavane, R.; Kopplin, N.G.; Ta, H.Q.; Ekoue, D.N.; Witwer, M.; Ma, S.; Liu, H.; et al. A detailed characterization of stepwise activation of the androgen receptor variant 7 in prostate cancer cells. *Oncogene* **2021**, *40*, 1106–1117. [CrossRef] [PubMed]
33. Chen, C.D.; Welsbie, D.S.; Tran, C.; Baek, S.H.; Chen, R.; Vessella, R.; Rosenfeld, M.G.; Sawyers, C.L. Molecular determinants of resistance to antiandrogen therapy. *Nat. Med.* **2004**, *10*, 33–39. [CrossRef] [PubMed]
34. He, Y.; Lu, J.; Ye, Z.; Hao, S.; Wang, L.; Kohli, M.; Tindall, D.J.; Li, B.; Zhu, R.; Wang, L.; et al. Androgen receptor splice variants bind to constitutively open chromatin and promote abiraterone-resistant growth of prostate cancer. *Nucleic Acids Res.* **2018**, *46*, 1895–1911. [CrossRef]
35. Jones, D.; Wade, M.; Nakjang, S.; Chaytor, L.; Grey, J.; Robson, C.N.; Gaughan, L. FOXA1 regulates androgen receptor variant activity in models of castrate-resistant prostate cancer. *Oncotarget* **2015**, *6*, 29782–29794. [CrossRef]
36. Yap, T.A.; Plummer, R.; Azad, N.S.; Helleday, T. The DNA Damaging Revolution: PARP Inhibitors and Beyond. *Am. Soc. Clin. Oncol. Educ. Book* **2019**, *39*, 185–195. [CrossRef]
37. Spratt, D.E.; Evans, M.J.; Davis, B.J.; Doran, M.G.; Lee, M.X.; Shah, N.; Wongvipat, J.; Carnazza, K.E.; Klee, G.G.; Polkinghorn, W.; et al. Androgen Receptor Upregulation Mediates Radioresistance after Ionizing Radiation. *Cancer Res.* **2015**, *75*, 4688–4696. [CrossRef]
38. Hussain, M.; Daignault-Newton, S.; Twardowski, P.W.; Albany, C.; Stein, M.N.; Kunju, L.P.; Siddiqui, J.; Wu, Y.M.; Robinson, D.; Lonigro, R.J.; et al. Targeting Androgen Receptor and DNA Repair in Metastatic Castration-Resistant Prostate Cancer: Results from NCI 9012. *J. Clin. Oncol. Off. J. Am. Soc. Clin. Oncol.* **2018**, *36*, 991–999. [CrossRef]
39. Clarke, N.W.; Armstrong, A.J.; Thiery-Vuillemin, A.; Oya, M.; Shore, N.; Loredo, E.; Procopio, G.; de Menezes, J.; Girotto, G.; Arslan, C.; et al. Abiraterone and Olaparib for Metastatic Castration-Resistant Prostate Cancer. *NEJM Evid.* **2022**, *1*, 1–16. [CrossRef]
40. Cato, L.; de Tribolet-Hardy, J.; Lee, I.; Rottenberg, J.T.; Coleman, I.; Melchers, D.; Houtman, R.; Xiao, T.; Li, W.; Uo, T.; et al. ARv7 Represses Tumor-Suppressor Genes in Castration-Resistant Prostate Cancer. *Cancer Cell* **2019**, *35*, 401–413.e6. [CrossRef]
41. Veldscholte, J.; Berrevoets, C.A.; Ris-Stalpers, C.; Kuiper, G.G.; Jenster, G.; Trapman, J.; Brinkmann, A.O.; Mulder, E. The androgen receptor in LNCaP cells contains a mutation in the ligand binding domain which affects steroid binding characteristics and response to antiandrogens. *J. Steroid Biochem. Mol. Biol.* **1992**, *41*, 665–669. [CrossRef]
42. Sfanos, K.S.; Aloia, A.L.; Hicks, J.L.; Esopi, D.M.; Steranka, J.P.; Shao, W.; Sanchez-Martinez, S.; Yegnasubramanian, S.; Burns, K.H.; Rein, A.; et al. Identification of replication competent murine gammaretroviruses in commonly used prostate cancer cell lines. *PLoS ONE* **2011**, *6*, e20874. [CrossRef] [PubMed]
43. Daniel, R.; Ramcharan, J.; Rogakou, E.; Taganov, K.D.; Greger, J.G.; Bonner, W.; Nussenzweig, A.; Katz, R.A.; Skalka, A.M. Histone H2AX is phosphorylated at sites of retroviral DNA integration but is dispensable for postintegration repair. *J. Biol. Chem.* **2004**, *279*, 45810–45814. [CrossRef] [PubMed]
44. Taylor, B.S.; Schultz, N.; Hieronymus, H.; Gopalan, A.; Xiao, Y.; Carver, B.S.; Arora, V.K.; Kaushik, P.; Cerami, E.; Reva, B.; et al. Integrative Genomic Profiling of Human Prostate Cancer. *Cancer Cell* **2010**, *18*, 11–22. [CrossRef]
45. Grasso, C.S.; Wu, Y.M.; Robinson, D.R.; Cao, X.; Dhanasekaran, S.M.; Khan, A.P.; Quist, M.J.; Jing, X.; Lonigro, R.J.; Brenner, J.C.; et al. The mutational landscape of lethal castration-resistant prostate cancer. *Nature* **2012**, *487*, 239–243. [CrossRef]

46. Chen, X.; Bernemann, C.; Tolkach, Y.; Heller, M.; Nientiedt, C.; Falkenstein, M.; Herpel, E.; Jenzer, M.; Grüllich, C.; Jäger, D.; et al. Overexpression of nuclear AR-V7 protein in primary prostate cancer is an independent negative prognostic marker in men with high-risk disease receiving adjuvant therapy. *Urol. Oncol.* **2018**, *36*, 161.e19–161.e30. [CrossRef]
47. Xu, L.; Ma, E.; Zeng, T.; Zhao, R.; Tao, Y.; Chen, X.; Groth, J.; Liang, C.; Hu, H.; Huang, J. ATM deficiency promotes progression of CRPC by enhancing Warburg effect. *Endocr.-Relat. Cancer* **2019**, *26*, 59–71. [CrossRef]
48. Wokołorczyk, D.; Kluz´niak, W.; Huzarski, T.; Gronwald, J.; Szymiczek, A.; Rusak, B.; Stempa, K.; Gliniewicz, K.; Kashyap, A.; Morawska, S.; et al. Mutations in ATM, NBN and BRCA2 predispose to aggressive prostate cancer in Poland. *Int. J. Cancer* **2020**, *147*, 2793–2800. [CrossRef]
49. Rai, R.; Dai, H.; Multani, A.S.; Li, K.; Chin, K.; Gray, J.; Lahad, J.P.; Liang, J.; Mills, G.B.; Meric-Bernstam, F.; et al. BRIT1 regulates early DNA damage response, chromosomal integrity, and cancer. *Cancer Cell* **2006**, *10*, 145–157. [CrossRef]
50. de Bono, J.S.; Mehra, N.; Scagliotti, G.V.; Castro, E.; Dorff, T.; Stirling, A.; Stenzl, A.; Fleming, M.T.; Higano, C.S.; Saad, F.; et al. Talazoparib monotherapy in metastatic castration-resistant prostate cancer with DNA repair alterations (TALAPRO-1): An open-label, phase 2 trial. *Lancet. Oncol.* **2021**, *22*, 1250–1264. [CrossRef]
51. Abida, W.; Armenia, J.; Gopalan, A.; Brennan, R.; Walsh, M.; Barron, D.; Danila, D.; Rathkopf, D.; Morris, M.; Slovin, S.; et al. Prospective Genomic Profiling of Prostate Cancer Across Disease States Reveals Germline and Somatic Alterations That May Affect Clinical Decision Making. *JCO Precis. Oncol.* **2017**, *1*, 1–16. [CrossRef] [PubMed]
52. Zhou, S.; Dai, Z.; Wang, L.; Gao, X.; Yang, L.; Wang, Z.; Wang, Q.; Liu, Z. MET inhibition enhances PARP inhibitor efficacy in castration-resistant prostate cancer by suppressing the ATM/ATR and PI3K/AKT pathways. *J. Cell. Mol. Med.* **2021**, *25*, 11157–11169. [CrossRef] [PubMed]
53. Al-Ubaidi, F.L.T.; Schultz, N.; Loseva, O.; Egevad, L.; Granfors, T.; Helleday, T. Castration therapy results in decreased Ku70 levels in prostate cancer. *Clin. Cancer Res. Off. J. Am. Assoc. Cancer Res.* **2013**, *19*, 1547–1556. [CrossRef] [PubMed]
54. Dylgjeri, E.; McNair, C.; Goodwin, J.F.; Raymon, H.K.; McCue, P.A.; Shafi, A.A.; Leiby, B.E.; de Leeuw, R.; Kothari, V.; McCann, J.J.; et al. Pleiotropic Impact of DNA-PK in Cancer and Implications for Therapeutic Strategies. *Clin. Cancer Res. Off. J. Am. Assoc. Cancer Res.* **2019**, *25*, 5623–5638. [CrossRef] [PubMed]

3.2 Publication 2: CDCP1 expression is frequently increased in aggressive urothelial carcinoma and promotes urothelial tumor progression.

scientific reports

Check for updates

OPEN

CDCP1 expression is frequently increased in aggressive urothelial carcinoma and promotes urothelial tumor progression

Miriam Saponaro[1,6], Sina Flottmann[1,6], Markus Eckstein[2], Oliver Hommerding[3], Niklas Klümper[1,4], Dillon Corvino[4], Sana Hosni[1], Anja Schmidt[1], Nicolas Mönig[1], Doris Schmidt[1], Jörg Ellinger[1], Marieta Toma[3], Glen Kristiansen[3], Tobias Bald[4], Andrea Alimonti[5], Manuel Ritter[1], Michael Hölzel[4] & Abdullah Alajati[1]✉

The prognosis of patients with advanced urothelial carcinoma (UC) remains poor and improving treatment continues to be a major medical need. CUB domain containing protein 1 (CDCP1) is a known oncogene in various types of solid cancers and its overexpression is associated with impaired prognosis. However, its role in UC remains undetermined. Here we assessed the clinical relevance of CDCP1 in two cohorts of UC at different stages of the disease. Immunohistochemistry showed that CDCP1 is highly expressed in advanced UC, which significantly correlates with shorter overall survival. Importantly, the basal/squamous UC subtype showed significantly enriched CDCP1 at the mRNA and protein levels. The functional role of CDCP1 overexpression was assessed taking advantage of ex vivo organoids derived from the CDCP1$^{pcLSL/+}$ transgenic mouse model. Furthermore, CDCP1 knockout UC cell lines were generated using CRISPR/Cas9 technology. Interestingly, CDCP1 overexpression significantly induced the activation of MAPK/ERK pathways in ex vivo organoids and increased their proliferation. Similarly, CDCP1 knockout in UC cell lines reduced their proliferation and migration, concomitant with MAPK/ERK pathway activity reduction. Our results highlight the relevance of CDCP1 in advanced UC and demonstrate its oncogenic role, suggesting that targeting CDCP1 could be a rational therapeutic strategy for the treatment of advanced UC.

The standard treatment for advanced urothelial cancer (UC) is radical cystectomy preceded or followed by platinum-based chemotherapy[1]. The advent of immunotherapy and, more recently, the use of antibody–drug conjugates (ADC) has broadened the therapeutic armamentarium[2]. However, the prognosis of patients with advanced UC remains poor and effective treatment remains a major medical need. CUB domain containing protein 1 (CDCP1), also known as SIMA135[3], gp140[4], CD318[5], or Trask[4], is a transmembrane protein that is frequently overexpressed in a variety of human cancers[6]. In the cell membrane, CDCP1 exists in two forms as the 135 kDa full-length (FL) protein can be cleaved by serine proteases at arginine-368 and lysine-369. Its proteolysis results in the formation of a soluble 65 kDa fragment and a membrane-spanning fragment of 70 kDa[7]. Both the cleaved (C) and FL forms act as substrates for Src, promoting interactions with several receptor tyrosine kinases (RTKs) thereby representing a key factor for pro-tumoral downstream signaling[7–10]. Accordingly, several studies demonstrated that CDCP1 is a potent oncogene and suggest that its overexpression is functionally involved in disease progression[6,11–13]. Indeed, elevated levels of this protein are associated with more advanced stages, poorer prognoses, and/or therapy responses in all studied malignancies[11,12,14–24]. Our recent study carried out on a novel spontaneous mouse model of prostate cancer showed that CDCP1 promotes progression and metastasis through the upregulation of MAPK/ERK and AKT pathways[12]. Similarly, other studies describe CDCP1 overexpression as a driver of MAPK/ERK- and AKT-dependent tumor progression[8,11]. Interestingly, CDCP1 targeting, either

[1]Department of Urology and Pediatric Urology, University Medical Center Bonn (UKB), Venusberg-Campus 1, 53127 Bonn, Germany. [2]Institute of Pathology, University Hospital Erlangen, Friedrich-Alexander-Universität Erlangen-Nürnberg (FAU), Erlangen, Germany. [3]Institute of Pathology, University Medical Center Bonn (UKB), Bonn, Germany. [4]Institute of Experimental Oncology, University Medical Center Bonn (UKB), Bonn, Germany. [5]Institute of Oncology Research, Università Della Svizzera Italiana, Bellinzona, Switzerland. [6]These authors contributed equally: Miriam Saponaro and Sina Flottmann. ✉email: abdullah.alajati@ukbonn.de

with monoclonal antibodies or small molecule inhibitors, has demonstrated effectiveness in inhibiting tumor growth and metastasis in vivo[25]. Moreover, a recent study identified CDCP1 as a suitable target for CAR T-cell-based immunotherapy in pancreatic cancer[26]. Since treatments with either SRC or MAPK/ERK inhibitors have been associated with poor tolerability in the clinic[27], CDCP1 targeting could represent an excellent alternative therapeutic option. However, to the best of our knowledge, the role of CDCP1 in UC has not been well described, and more studies to assess it are needed[28].

Results

UC exhibits an elevated expression of CDCP1, which correlates with shorter overall survival in UC patients. To assess the clinical relevance of CDCP1 in UC, we first performed immunohistochemistry (IHC) staining of human CDCP1 on paraffin-embedded human bladder cancer samples based on the previously described protocol[12]. We examined a cohort of 147 specimens spanning from T1 to T4 stages (Table 1)[29, 30] and stratified samples based on their membrane staining for CDCP1 into four groups (negative, weak, moderate and strong). All groups with negative or weak staining intensity were classified as CDCP1-low, while moderate and strong groups were classified as CDCP1-high (Fig. 1A). In line with previous results[28, 31], CDCP1 expression was negatively or weakly expressed in normal urothelium or normal adjacent tissue (NAT) (Supplementary Fig. 1). A large portion of urothelial tumors at T1 and T2 stages were classified as negative/weak for CDCP1 (CDCP1-low), while the 35% of T3 and 50% of T4 showed high expression levels of CDCP1 (CDCP1-high) (Fig. 1B). Of note, levels of CDCP1 in muscular invasive bladder cancer (MIBC) stages (T2-T4) are significantly higher than in the non-invasive stage (T1) (Fig. 1C). Most importantly, patients with CDCP1-high expression showed a significant poorer outcome compared to patients with CDCP1-low expression levels (Log Rank mantel cox test $P < 0.0001$) (Fig. 1D). In parallel, we performed western blot and real-time PCR (RT-PCR) analyses ($n = 10$ and $n = 107$ respectively) on additional UC frozen samples and the corresponding NAT. These analyses demonstrated a robust increase of CDCP1 expression at protein and RNA levels in UC when compared to NAT (Fig. 1E,F). Taken together, these data showed that CDCP1 is overexpressed in UC compared to normal tissues, and its overexpression is associated with advanced UC and shorter overall survival (OS).

CDCP1 expression is elevated in advanced UC and enriched in Ba/Sq subtype. To gain further insights about the expression of CDCP1 in UC, we analyzed CDCP1 expression in two publically available data sets. The first, consisting of 405 tissue specimens of bladder cancer from the cancer genome atlas (TCGA), was classified according to the consensus subtyping approach of muscle-invasive urothelial bladder cancer (MIBC)[32]. In line with our previous results, we observed elevated levels of CDCP1 in UC compared to its NAT (Fig. 2A). Importantly, we found that CDCP1 levels were strongly associated with the Ba/Sq subtype (Fig. 2B). This was confirmed using a second data set, a single-cell-RNA-sequencing (scRNAseq) of human UC samples[33]. Indeed, analysis of this dataset for cells annotated as epithelial origin revealed that expression of CDCP1 and that of markers reported to be enriched in the Ba/Sq subtype, such as EGFR, KRT5 (CK5) and KRT14 (CK14), have a high degree of co-localization (Fig. 2C). Thereafter, we performed IHC of CDCP1 on a well-established prospectively recruited consecutive cohort of MIBC patients treated with radical cystectomy and adjuvant chemotherapy as previously described (Table 2)[32]. The multivariate analysis on this cohort demonstrated that CDCP1 is not an independent variable for the prediction of patients´ prognosis (Table 3). However, out of 184 analyzed tumors 56% were positive for CDCP1 (Fig. 2D) and we found a strong association between CDCP1 protein expression and the Ba/Sq subtype (Fig. 2E). This association with the Ba/Sq subtype of UC was further validated using the Ba/Sq subtype markers CK5 and CK14[32] (Fig. 2F). Of note, the mRNA levels of CDCP1 reflected the protein levels observed in this cohort (Fig. 2G) and were enriched in the Ba/Sq subtype (Kruskal Wallis: $P < 000.1$) (Fig. 2H). Together, these results confirm the association of CDCP1 expression with the aggressive Ba/Sq UC subtype. Moreover, considering that several studies have already reported the association of CDCP1 with therapy resistance[6], we questioned whether this protein has the same impact on MIBC. The OS of chemo-treated patients expressing high CDCP1 levels is clearly reduced (Fig. 2I), suggesting that CDCP1 may be a suitable marker for chemotherapy sensitivity and targeting CDCP1 could serve as a novel therapeutic strategy to treat resistant patients.

Transgenic overexpression of CDCP1 induces proliferation in ex vivo mouse organoids and its knockout inhibits proliferation and migration of UC cells. To model the effect of CDCP1 overexpression in UC, we exploited the previously generated transgenic mouse model for CDCP1 ($CDCP1^{pCLSL/+}$) and established an ex vivo 3D organoids system that overexpresses CDCP1[12]. Briefly, the bladder of 8 weeks old male $CDCP1^{pCLSL/+}$ mice was excised and dissociated into single cells, as previously described[33]. Bladder cells were infected with an adeno-Cre virus to induce the expression of CDCP1 and seeded in Matrigel (Fig. 3A). We examined the effect of CDCP1 expression on the growth of bladder mouse organoids over two weeks. CDCP1 overexpression resulted in the formation of larger and morphologically distinctive organoids compared to the controls (Fig. 3B). Quantification of the organoids area revealed a significant increase in their size when CDCP1 is overexpressed compared to the controls (Fig. 3C). At the molecular level, IHC analysis on mouse organoids confirmed the expression of CDCP1 (Fig. 3D). Importantly, CDCP1 overexpressing organoids expressed high levels of Ki67 and pERK (Fig. 3D). To further assess the relevance of these findings in human UC, we aimed to perform CDCP1 knockout (KO) in CDCP1 expressing cells with the CRISPR/Cas9 method. Firstly, we screened several UC cell lines for their CDCP1 expression. Western blot analysis indicated variable expression of CDCP1 among the tested UC cell lines (Supplementary Fig. 2A). Given the fact that CDCP1 expression was associated with Ba/Sq subtype and it is highly expressed in the Ba/Sq SCaBER cells, we generated KO of CDCP1 in this cell line (Fig. 3E). Interestingly, loss of CDCP1 in SCaBER cells reduced pAKT, pMEK and pERK1/2 levels (Fig. 3E

Age		
Average (range)	68 (38; 94)	
Sex	**N**	**% of total**
Female	46	25.7%
Male	132	74.3%
Primary tumor (location)	**N**	**% of total**
Control	31	19.0%
BCa	136	81.0%
Tumor stage	**N**	**% of total**
Control	31	–
min.pT1	38	26.0%
min.pT2	40	27.0%
min.pT3	45	31.0%
min.pT4	24	16.0%
Tumor type	**N**	**% of total**
Control	31	–
Non-muscle invasive (NMIBC)	38	26.0%
Muscle invasive (MIBC)	109	74.0%
Survival time (months)		
Median (range)	50 (1; 283)	
CDCP1 level	**N**	**% of total**
Low	115	78.3%
High	32	21.7%

Table 1. Characterization of cohort 1.

and supplementary Fig. 2B). Functional analyses showed that CDCP1 depletion reduced both 2D and 3D proliferation (Fig. 3F,G) and migration in this cell line (Fig. 3H). Interestingly, T24 and TCCSUP cells, which are considered non-type[34, 35], showed a similar behavior to SCaBER when knocked out for CDCP1, with the exception for the 2D proliferation (Supplementary Fig. 2C–F). Collectively, these results demonstrate that CDCP1 expression promotes UC proliferation, while its downregulation reduces proliferation and migration of UC cell lines.

Discussion

Despite the preponderance of studies identifying CDCP1 as a key contributor to oncogenic events in several cancers[6], the functional role of CDCP1 and its clinical relevance in UC remains poorly characterized. Only two previous studies from the same laboratory indicate its involvement in BCa[28, 31]. Yang et al. showed that N6-methyladenosine modified the mRNA levels of CDCP1 in response to chemical carcinogens, which promoted CDCP1 translation. The same group also showed that CDCP1 is moderately or highly expressed in most of the BCa samples (n = 33) when compared to para-tumor controls and correlated CDCP1 expression with BCa progression[31]. In line with these results, the first part of our study demonstrated that CDCP1 is overexpressed in UC when compared to NAT and is associated with MIBC. Moreover, the impact of elevated CDCP1 expression in UC was investigated by Kaplan–Meier analysis, which indicated that patients expressing high levels of CDCP1 have significantly poorer OS (Fig. 1D).

In the second part of this study, we further explored the clinical relevance of CDCP1 in UC. Indeed, our results obtained from three different data sets, showed significant enrichment of CDCP1 expression in the Ba/Sq subtype (Fig. 2B,C,E,H). Since CDCP1 is reported to interact with the epidermal growth factor receptor (EGFR)[36], whose activity is also associated with Ba/Sq tumors in BCa[37, 38], and a cross-talk between these two proteins is already described in other tumor types[39–41], further studies investigating the potential CDCP1/EGFR cross-talk are needed. Such studies may show that a combinational therapy targeting CDCP1 and EGFR may be effective for the treatment of Ba/Sq bladder tumors.

Another important clinical aspect presented by our study is the association of CDCP1 with therapy resistance, which has been reported in breast and ovarian cancers[6, 11, 18]. Indeed, the OS of chemotherapy-treated patients expressing high CDCP1 levels was clearly reduced, supporting the hypothesis that CDCP1 is involved in resistance to first-line chemotherapy in UC.

To determine the oncogenic role of CDCP1 in UC, we took advantage of the previously generated mouse model for CDCP1 overexpression in a Cre-dependent manner[12]. Remarkably, CDCP1 overexpression in bladder organoids obtained from this mouse model resulted in larger and well-defined organoids compared to the control groups (Fig. 3B,C). These preliminary results suggest that CDCP1 overexpression may support oncogenesis in bladder urothelium. Additionally, these results encourage the development of a bladder-specific CDCP1-overexpressing transgenic mouse model to further analyze the oncogenic potential of CDCP1 in UC.

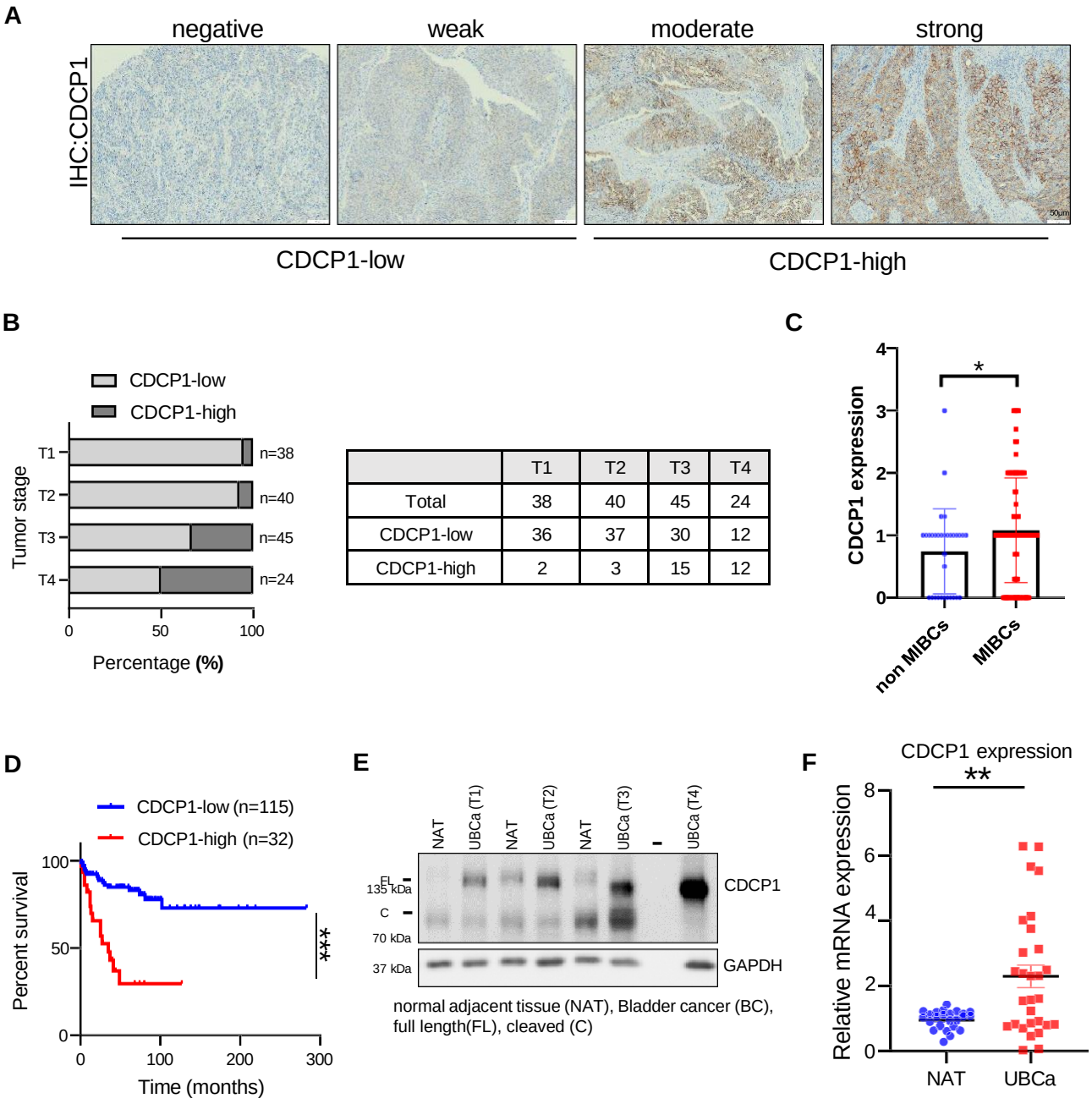

	T1	T2	T3	T4
Total	38	40	45	24
CDCP1-low	36	37	30	12
CDCP1-high	2	3	15	12

Figure 1. UC exhibits elevated expression of CDCP1, which correlates with shorter overall survival in UC patients. (**A**) Representative images of CDCP1-low and CDCP1-high tumors. (**B**) Percentage of patients expressing low and high CDCP1 levels, divided by the tumor stage (T1, T2, T3, T4). The table indicates the relative number of patients, which express low and high CDCP1 divided per tumor stage. (**C**) Column bar graph comparing the expression of CDCP1 in NMIBC (T1) and MIBC (T2–T4). Error bars indicate SD. *P < 0.05. Statistical test: two-tailed unpaired t test. (**D**) Kaplan–Meier survival analysis of UC patients stratified based on the semi-quantitative expression of CDCP1 (CDCP1-low: negative, weak; CDCP1-high: moderate, strong). ***P < 0.001. Statistical test: log-rank test. (**E**) Western blot analysis of CDCP1 and GAPDH expression on representative tumor samples from patients presenting lesions at different stages (T1, T2, T3 and T4). CDCP1 tumor expression is compared with its expression in the NAT from the same patients. (**F**) Comparison between the expression of CDCP1 in UC samples and NAT at the transcriptional level. Expression was quantified via real-time quantitative PCR, and normalized to GAPDH. Error bars indicate SD. **P < 0.01. Statistical test: two-tailed unpaired t test.

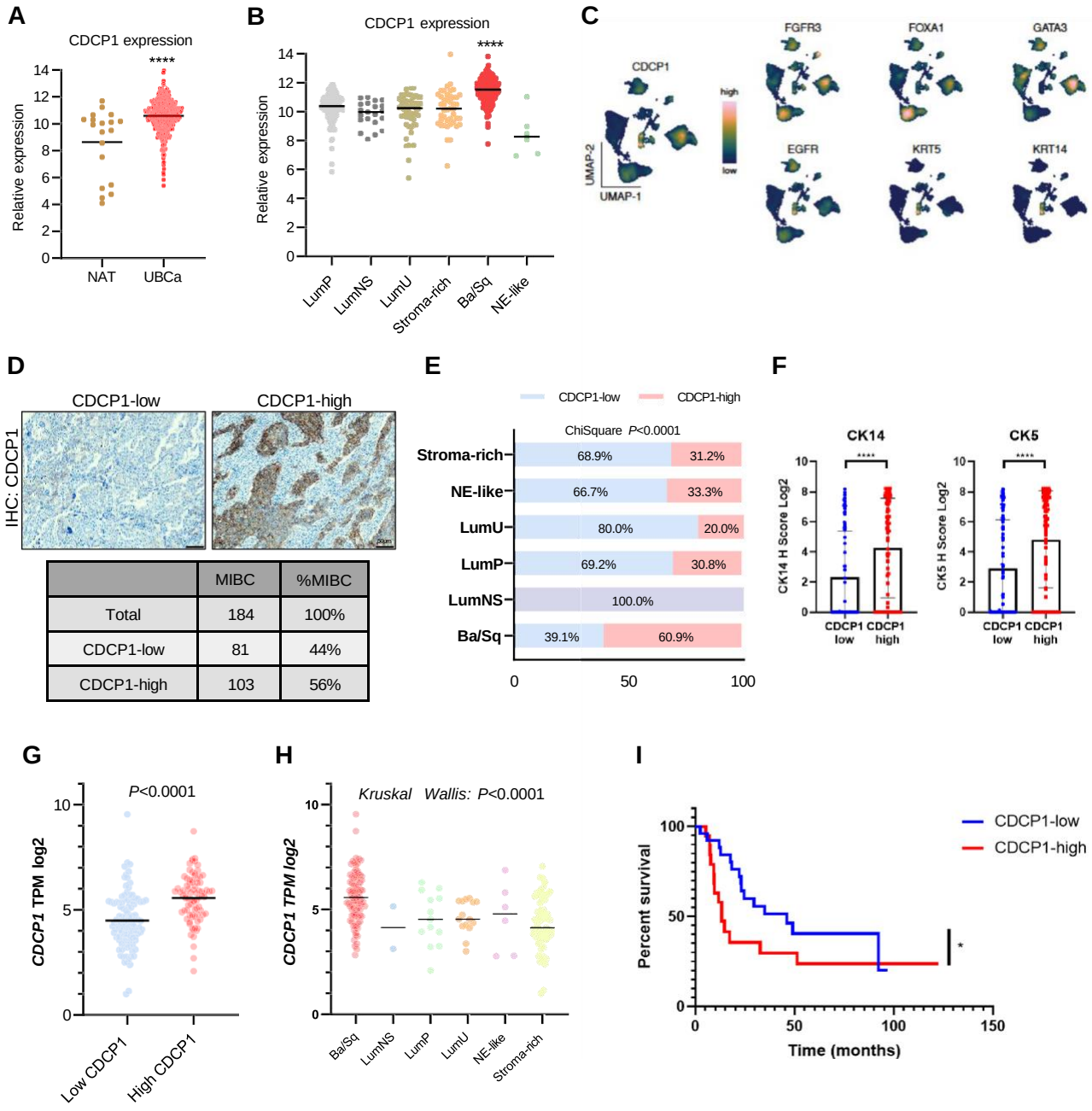

	MIBC	%MIBC
Total	184	100%
CDCP1-low	81	44%
CDCP1-high	103	56%

Figure 2. CDCP1 expression is elevated in advanced UC and enriched in Ba/Sq subtype. (**A**) Expressional levels of CDCP1 in UC tissue compared to NAT. Data obtained from the TCGA BLCA data set. ****P < 0.0001. Statistical test: two-tailed unpaired t test. (**B**) Comparison of CDCP1 levels between the UC molecular subtypes from TCGA BLCA data set. ****P < 0.0001. Statistical test: one-way analysis of variance. (**C**) Visualization via scRNAseq analysis of the expressional levels of CDCP1, and different Lu subtype molecular markers (FGFR3, FOXA1, GATA3) and Ba/Sq subtype molecular markers (EGFR, KRT5, KRT14) in the UC cohort from Chen et al., 2020. (**D**) Representative images of tumors from the MIBC TMA showing tumors with CDCP1-low and CDCP1-high. Table showing the total number of MIBC tumors, CDCP1-low and CDCP1-high. (**E**) Percentage of tumors from the MIBC TMA which show a low or high CDCP1 expression, clustered on the base of the UC subtype. (**F**) Bar graphs indicating the expression of CK5 and CK14 in CDCP1-high tumors compared to CDCP1-low tumors. The expression is evaluated by IHC in the MIBC TMA. Error bars indicate SD. ****P < 0.0001. Statistical test: two-tailed unpaired t test. (**G**) Transcriptional expression of CDCP1 (TPM: transcripts per million reads) compared to CDCP1-low and CDCP1-high levels in the MIBC TMA confirming the correlation between CDCP1 transcripts and protein levels. (**H**) CDCP1 TPM across the UC subtypes showing the high expression of CDCP1 in the Ba/Sq subtype. Tumor samples are correspondent to the ones from the MIBC TMA. (**I**) Kaplan–Meier survival analysis of UC patients treated with chemotherapy stratified based on the semi-quantitative expression of CDCP1 (CDCP1-low: negative, weak; CDCP1-high: moderate, strong). *P < 0.05. Statistical test: Gehan–Breslow–Wilcoxon test.

Age (years)		
Average (range)	68,7 (37; 91)	
Sex	**N**	**% of total**
Female	46	25.0%
Male	138	75.0%
Primary tumor (location)	**N**	**% of total**
BCa	184	100.0%
Grading 2004/2016	**N**	**% of total**
High grade	184	100.0%
Grading 1973	**N**	**% of total**
G2	5	3.0%
G3	179	97.0%
Initial tumor stage	**N**	**% of total**
pT2	53	29.0%
pT3	88	48.0%
pT4	43	23.0%
pN-stage	**N**	**% of total**
NX	13	7.0%
pN0	118	64.0%
pN1	19	10.0%
pN2	34	18.0%
Adjuvant chemotherapy	**N**	**% of total**
No	139	76.0%
Yes	45	24.0%
Survival time (months)		
Average (range)	37 (0; 153,33)	
CDCP1 level	**N**	**% of total**
Low	81	44.0%
High	103	56.0%
Molecular variant	**N**	**% of total**
Ba/Sq	87	47.0%
LumNS	2	1.0%
LumP	13	7.0%
LumU	15	8.0%
NE-like	6	3.0%
Stroma-rich	61	33.0%

Table 2. Characterization of cohort 2.

At the molecular level, we showed that CDCP1 depletion reduced MEK, ERK and AKT phosphorylation in western blot analyses on SCaBER cells knocked out for CDCP1. The reliance of MAPK/ERK and AKT pathways activation on CDCP1 expression in SCaBER suggests that this protein may play a crucial role in UC progression. Indeed, it was previously reported that the activation of MAPK/ERK and AKT pathways increased tumor growth and cancer cells motility[8, 12]. Functional analysis performed with SCaBER cells showed that CDCP1 depletion reduced their 2D and 3D proliferation and migration (Fig. 3F,G,H). Altogether, these findings demonstrate that the growth and migration abilities of SCaBER cells rely on CDCP1 expression, suggesting that Ba/Sq UC patients could benefit from CDCP1-targeting therapies. Therefore, further studies validating the efficacy of CDCP1 inhibition are clearly encouraged.

Materials and methods

Patient cohort and case report. The study was approved by the ethical review board of the Medical Faculty of the University of Bonn (approval number: 036/08 and 093/12) and the Friedrich-Alexander-University Erlangen-Nürnberg (approval number: 329_16B and 97_18Bc). The study was performed in accordance with the Declaration of Helsinki. The study participants were anonymized before their specimens were included in the study cohort. Informed consent was obtained for all the participants. In the first TMA, CDCP1 expression was assessed from patient samples obtained via radical cystectomy or transurethral resection and provided by the University Hospital of Bonn, including benign bladder urothelium and BCa with different stages of disease (T1-T4) as previously described (Table 1)[29, 30]. In the second TMA, CDCP1 expression was assessed in a well-characterized prospective homogenous MIBC cohort treated by radical cystectomy in conjunction with bilateral lymphadenectomy in curative intent at the Department of Urology of the University Hospital of Erlangen[32].

Cox proportional hazards fit				
Censor: disease specific survival censor				
Effect summary				
Source	**LogWorth**		**P value**	
pN-stage summary	2.798	+++++++	0.00159	
pT-stage summary	1.64	++++	0.02293	
L	0.908	++	0.12351	
Resection margin	0.888	++	0.12938	
Age	0.782	++	0.1653	
Histology summary	0.771	++	0.16948	
Gender	0.217	+	0.60618	
CDCP1 low vs. high	0.148		0.71175	
V	0.007		0.98386	
WHO 2016 grading	–	–	–	
Whole model				
Number of events	95			
Number of censorings	89			
Total number	184			
AICc	**BIC**			
858.166	903.533			
Model	**−LogLikelihood**	**ChiSquare**	**DF**	**Prob > Chisq**
Difference	34.3554	68.7108	15	0
Full	412.6543			
Reduced	447.0097			
Parameter estimates				
Term	**Estimate**	**Std error**	**Lower 95%**	**Upper 95%**
CDCP1 low vs. high [low]	0.043	0.117	−0.18	0.28
pT-stage summary [pT2]	−0.55	0.228	−1.02	−0.11
pT-stage summary [pT3]	0.057	0.153	−0.24	0.36
pN-stage summary [pN+]	0.047	0.178	−0.3	0.4
pN-stage summary [pN0]	−0.677	0.187	−1.04	−0.31
Gender [female]	0.063	0.122	−0.18	0.3
Age	0.013	0.01	−0.01	0.03
Resection margin [R1-R0]	0.29	0.281	−0.28	0.82
Resection margin [RX-R1]	2.301	1.098	−0.66	4.1
L[1-0]	0.433	0.283	−0.12	1
V[1-0]	0.005	0.252	−0.5	0.49
Variant summary [neuroendocrine]	1.258	0.512	0.08	2.15
Variant summary [urothelial-NOS]	−0.505	0.209	−0.91	−0.08
Variant summary [urothelial-sarcomatoid/rhabdoid]	−0.022	0.286	-0.61	0.53
Variant summary [urothelial-squamous]	−0.371	0.253	-0.87	0.12
Effect Wald tests				
Source	**Nparm**	**DF**	**Wald ChiSquare**	**Prob > ChiSq**
CDCP1 low vs. high	1	1	0.14	0.712
pT-stage summary	2	2	7.49	0.024
pN-stage summary	2	2	13.24	0.001
Gender	1	1	0.27	0.604
Age	1	1	1.89	0.169
Resection margin	2	2	6.48	0.039
WHO 2016 grading	0	0	0	
L	1	1	2.34	0.126
V	1	1	0	0.984
Variant summary	4	4	8.54	0.074
Continued				

Source	Nparm	DF	Wald ChiSquare	Prob > ChiSq	
Risk ratios					
Unit risk ratios					
Per unit change in regressor					
Term	**Risk ratio**	**Lower 95%**	**Upper 95%**	**Reciprocal**	
Age	1.01	0.99	1.03	0.9867414	
Range risk ratios					
Per change in regressor over entire range					
Term	**Risk ratio**	**Lower 95%**	**Upper 95%**	**Reciprocal**	
Age	2.06	0.75	5.86	0.4863856	
Risk ratios for CDCP1 low vs. high					
Level1	**/Level2**	**Risk ratio**	**Prob > Chisq**	**Lower 95%**	**Upper 95%**
High	Low	0.92	0.712	0.58	1.45
Low	High	1.09	0.712	0.69	1.74
Risk ratios for pT-stage summary					
Level1	**/Level2**	**Risk ratio**	**Prob > Chisq**	**Lower 95%**	**Upper 95%**
pT3	pT2	1.84	0.069	0.96	3.69
pT4	pT2	2.83	0.006	1.34	6.16
pT4	pT3	1.54	0.087	0.94	2.52
pT2	pT3	0.54	0.069	0.27	1.05
pT2	pT4	0.35	0.006	0.16	0.75
pT3	pT4	0.65	0.087	0.4	1.07
Risk ratios for pN-stage summary					
Level1	**/Level2**	**Risk ratio**	**Prob > Chisq**	**Lower 95%**	**Upper 95%**
pN0	pN+	0.48	0.009	0.28	0.83
pNX	pN+	1.79	0.131	0.83	3.66
pNX	pN0	3.7	0.002	1.68	7.76
pN+	pN0	2.06	0.009	1.2	3.56
pN+	pNX	0.56	0.131	0.27	1.2
pN0	pNX	0.27	0.002	0.13	0.6
Risk ratios for gender					
Level1	**/Level2**	**Risk ratio**	**Prob > Chisq**	**Lower 95%**	**Upper 95%**
Male	female	0.88	0.606	0.55	1.44
Female	Male	1.14	0.606	0.69	1.82
Risk ratios for resection margin					
Level1	**/Level2**	**Risk ratio**	**Prob > Chisq**	**Lower 95%**	**Upper 95%**
R1	R0	1.34	0.312	0.75	2.28
RX	R0	13.34	0.074	0.7	76.53
RX	R1	9.98	0.104	0.52	60.06
R0	R1	0.75	0.312	0.44	1.33
R0	RX	0.07	0.074	0.01	1.42
R1	RX	0.1	0.104	0.02	1.93
Risk ratios for L					
Level1	**/Level2**	**Risk ratio**	**Prob > Chisq**	**Lower 95%**	**Upper 95%**
1	0	1.54	0.124	0.89	2.71
0	1	0.65	0.124	0.37	1.12
Risk ratios for V					
Level1	**/Level2**	**Risk ratio**	**Prob>Chisq**	**Lower 95%**	**Upper 95%**
1	0	1.01	0.984	0.61	1.64
0	1	0.99	0.984	0.61	1.64
Risk ratios for variant summary					
Level1	**/Level2**	**Risk ratio**	**Prob>Chisq**	**Lower 95%**	**Upper 95%**
Urothelial-NOS	Neuroendocrine	0.17	0.024	0.05	0.61
Urothelial-sarcomatoid/ rhabdoid	Neuroendocrine	0.28	0.1	0.07	1.1
Urothelial-sarcomatoid/ rhabdoid	Urothelial-NOS	1.62	0.192	0.8	3.28
Urothelial-squamous	Neuroendocrine	0.2	0.038	0.05	0.73
Continued					

Risk ratios for variant summary					
Level1	**/Level2**	**Risk ratio**	**Prob>Chisq**	**Lower 95%**	**Upper 95%**
Urothelial-squamous	Urothelial-NOS	1.14	0.669	0.62	2.11
Urothelial-squamous	Urothelial-sarcomatoid/ rhabdoid	0.71	0.385	0.32	1.53
Urothelial-variant histology	Neuroendocrine	0.2	0.038	0.05	0.74
Urothelial-variant histology	Urothelial-NOS	1.16	0.6	0.67	1.98
Urothelial-variant histology	Urothelial-sarcomatoid/ rhabdoid	0.71	0.365	0.35	1.46
Urothelial-variant histology	Urothelial-squamous	1.01	0.976	0.52	1.97
Neuroendocrine	Urothelial-NOS	5.83	0.024	1.63	20.81
Neuroendocrine	Urothelial-sarcomatoid/ rhabdoid	3.6	0.1	0.91	14.27
Urothelial-NOS	Urothelial-sarcomatoid/ rhabdoid	0.62	0.192	0.31	1.25
Neuroendocrine	Urothelial-squamous	5.1	0.038	1.36	19.11
Urothelial-NOS	Urothelial-squamous	0.87	0.669	0.47	1.61
Urothelial-sarcomatoid/ rhabdoid	Urothelial-squamous	1.42	0.385	0.65	3.08
Neuroendocrine	Urothelial-variant histology	5.05	0.038	1.36	18.76
Urothelial-NOS	Urothelial-variant histology	0.87	0.6	0.51	1.48
Urothelial-sarcomatoid/ rhabdoid	Urothelial-variant histology	1.4	0.365	0.68	2.88
Urothelial-squamous	Urothelial-variant histology	0.99	0.976	0.51	1.93

Table 3. Multivariate analysis for CDCP1.

Immunohistochemistry. IHC of CDCP1 protein was performed on a VENTANA BenchMark ULTRA autostainer (Ventana) according to an accredited staining protocol in a routine immunohistochemistry facility. A polyclonal anti-CDCP1 primary antibody (#4115, rabbit polyclonal, Cell Signaling, Danvers, MA, US, dilution: 1:75) was used in this study. This antibody was previously used and validated in several other studies[11, 12, 17, 21]. CDCP1 staining was evaluated by two experienced pathologists (OH and GK) and only specific membrane expression of CDCP1 was assessed. Staining intensity was classified as negative (0), weak (1), moderate (2) and strong (3). Negative and weak specimens were considered CDCP1-low, whereas moderate and strong staining were considered CDCP1-high.

TCGA data analysis. Log2-transformed RSEM (RNA-Seq by Expectation Maximization) RNA sequencing data (RNA-Seq v2) of CDCP1 generated by The Cancer Genome Atlas Research Network (TCGA, http://cancergenome.nih.gov/) were downloaded from the UCSC Xena browser (http://xena.ucsc.edu) for n = 408 UC.

scRNAseq analysis. Data was downloaded as from Chen et al., 2020[33], using their interactive Shiny R interface. Analysis and dataset processing was performed using Seurat version 4.1.1 running on a mac OS version 12.2.1 (Monterey). Analysis was performed using standard Seurat dataset processing pipeline. In brief, data was subsetted to include only cells annotated as "epithelial". Data was visualised using the Nebulosa (version 1.4.0) and scCustomize (version 0.7.0) packages (Table 2). The colour-blind friendly, perceptually uniform and ordered "batlow" colour pallet was used via the R package scico (version 1.3.0). The figure was layed out using Adobe Illustrator version 24.1. Data availability: Publically available scRNAseq data was obtained from chen et al., 2020. Code availability: Code to reproduce scRNAseq data can be found at https://github.com/Eomesodermin.

Cell culture and functional assays. The human UC cell lines used were purchased from ATCC (ATCC, Manassas, VA, US). Cells were cultured in RPMI1640 (Thermo Fisher Scientific) supplemented with 10% FCS (Thermo Fisher Scientific), 1% streptomycin/penicillin (10.000 units/ml Penicillin and 10.000 µg/ml Streptomycin; Thermo Fisher Scientific) and 1% l-glutamine (200 mM; Thermo Fisher Scientific). For the spheroids formation assay, cells were grown in 1.2% Methylcellulose (Sigma-Aldrich) at a density of 25×10^3 cells/mL as hanging drops and incubated under standard culture conditions for 72 h. The diameter of the formed spheroids was measured with Image J and spheroids volume was calculated with the formula $V = 4/3 \times \pi \times r^3$. For the migration assay we put 20×10^3 cells on 24-well plate inserts and incubate for 12 h. We then fixed the cells with PFA 4%, performed crystal violet assay and swapped the internal part of the insert´s membrane to eliminate cells which didn´t migrate. We finally counted the migrated cells on the external part of the membrane. For the establishment of the ex vivo organoids model, single cells from the bladder of male CDCP1$^{pcLSL/+}$ mice were isolated as previously described[33]. Single cells were suspended (10^5 cells/mL) in DMEM, 10% FBS, 100 U/mL penicillin, and 100 µg/mL streptomycin and infected with adenoviruses (rAAV2/1-CMV-GFP and rAAV2/1-CBA-Cre) via spinoculation at 600*g, 1 h, 32 °C. Cells were then incubated for 1 h at 37 °C and 5% CO_2. 10^6 cells were suspended in 1 mL of Matrigel (Corning, New York, United States) and 40 µL drops were formed in pre-warmed flat bottom 24-well plates. Matrigel drops were left 30 min to solidify at 37 °C and 5% CO_2 inverting the 24-well

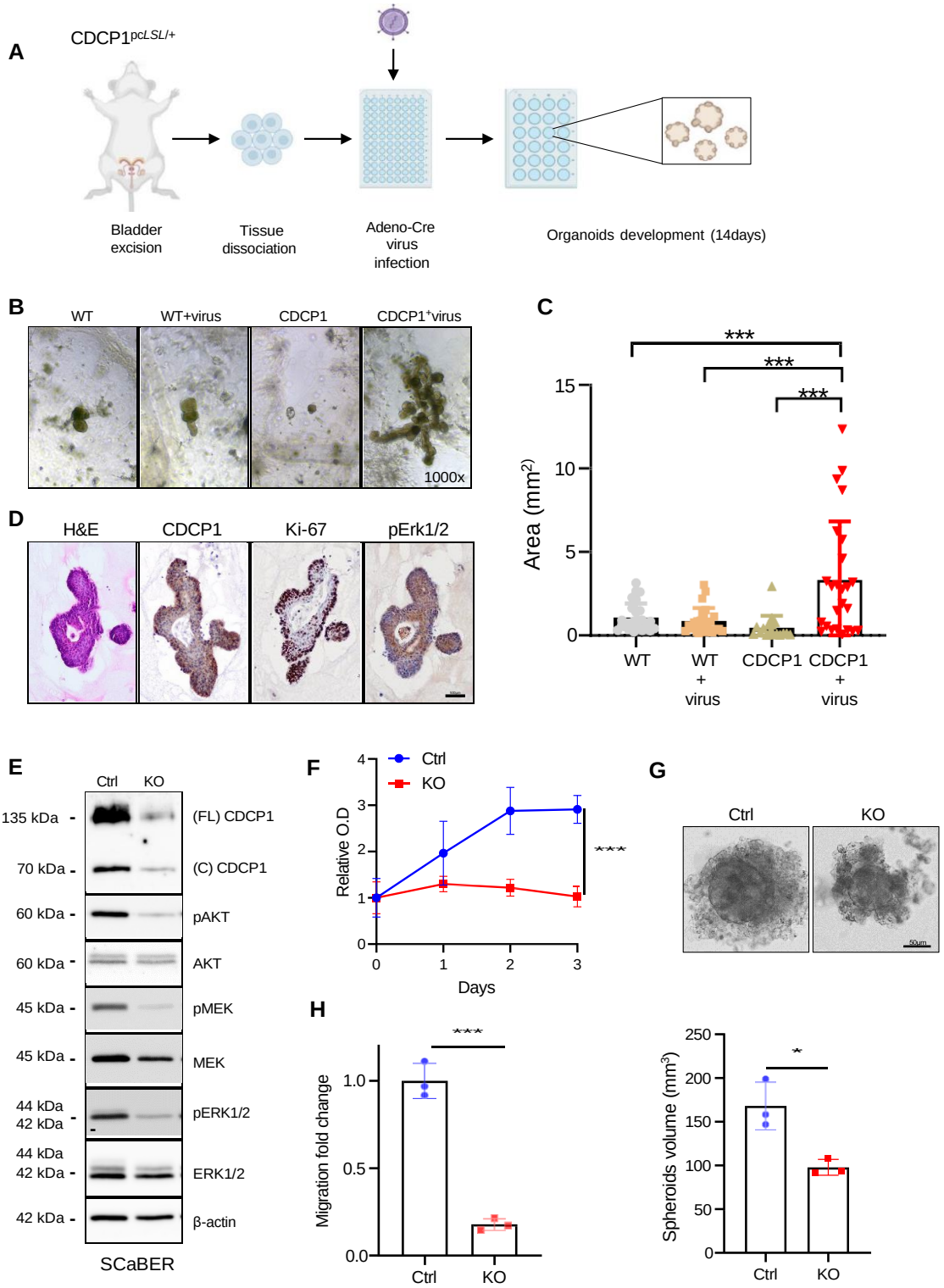

Figure 3. Transgenic overexpression of CDCP1 induces proliferation in ex vivo mouse organoids and its knockout inhibits proliferation and migration of UC cells. (**A**) Schematic representation of the generation of mouse organoids. (**B**) Representative images of the organoids generated from the C57BL/6 (WT) and transgenic (CDCP1) mice after 14 days of culture. The WT+virus and the CDCP1+virus conditions are transduced with the adeno-CRE virus. The WT and the CDCP1 conditions are processed as WT+virus and CDCP1+virus in the absence of the adeno-CRE virus. WT, WT+virus and CDCP1 conditions are all controls. (**C**) Quantification of the approximate area of the organoids. Error bars indicate SD. ***$P < 0.001$. Statistical test: one-way analysis of variance. (**D**) Representative images of H&E and IHC (CDCP1, Ki67, p-ERK1/2) performed on the organoids. (**E**) Western blot analysis of CDCP1 and major downstream targets of CDCP1 signaling in SCaBER UC cell line (Ctrl) and its CDCP1$^{-/-}$ counterpart (KO). (**F**) Relative O.D (proliferation) change of the CDCP1 expressing SCaBER cells (Ctrl) compared to the CDCP1$^{-/-}$ (KO). Error bars indicate SD. ***$P < 0.001$. Statistical test: two-tailed unpaired t test. (**G**) Representative images of the spheroids originated from the CDCP1+(Ctrl) and CDCP1$^{-/-}$ (KO) SCaBER cells. Bar graphs show the quantification of the spheres volume. Error bars indicate SD. *$P < 0.05$. Statistical test: two-tailed unpaired t test. (**H**) Migration fold change of CDCP1 expressing SCaBER (Ctrl) compared to the CDCP1$^{-/-}$ (KO). Error bars indicate SD. ***$P < 0.001$. Statistical test: two-tailed unpaired t test.

plates and 500 µL of organoids media was added. Organoids were grown for 14 days and pictures were taken. Organoids' growth was defined by measuring height and length with Image J and calculating the approximate surface. Organoids were then collected and fixed in 4% PFA. For the crystal violet proliferation assay, 2,000 cells were seeded per well in a 96-well plate. After overnight incubation, cells were treated and incubated for three to seven days depending on the experiment. All conditions were run in triplicate wells. For staining, cells were fixed with 37% paraformaldehyde for 10 min, then washed with distilled water and stained 0.05% crystal violet for 30 min. Cells were washed twice with distilled water and dried. 0.1% acetic acid was added per well to solubilize the dye. Finally, the absorbance was measured at a wavelength of 570 nm. The mean values of the triplicate wells were divided by a day zero control. Relative optical density (O.D) was normalized respect to the vehicle control.

Westernblot and IHC antibodies. For western blot the following antibodies were used: CDCP1 (#4115, Cell Signaling, Danvers, MA, US), pMEK (#9154S, Cell signaling), MEK (#4694S, Cell signaling), pAKT (#9271 T, Cell signaling), AKT (#2920S, Cell Signaling) pERK (#9102S, Cell Signaling), ERK (#4377, Cell Signaling), GAPDH (#2118, Cell Signaling), β-actin (#A2228, Sigma-Aldrich, St. Louis, MO, US). Some of the membranes used for the western blot were cut prior to hybridization. For IHC analysis, the following antibodies were used: CDCP1 (#4115, rabbit polyclonal, Cell Signaling, 1:50), Ki67 (#MSK018, Zytomed, Berlin, Germany, 1:50), p-Erk1/2 (clone 197G2, rabbit monoclonal, Cell Signaling, 1:50), CK5 (clone XM26, mouse monoclonal, Diagnostic BioSystems®, USA, dilution 1:50), CK14 (clone SP53, rabbit monoclonal, Cell Marque™, USA, dilution 1:40).

Quantitative reverse transcriptase-polymerase chain reaction (qRT-PCR). RNA was isolated with TRIzol method (Invitrogen, Thermo Fisher Scientific, Waltham, MA USA). qRT-PCR was performed using TB Green® Premix Ex Taq™ II (#RR82WR, TaKara, Kusatsu, Japan) on a Quant Studio 5 (applied biosystems, Thermo Fisher Scientific, Wilmington, USA). The primer sequences used were as follow: CDCP1 (Invitrogen Thermo Fisher, forward *TGGTTCCACCCCAGAAATGT*, reverse *GATGATGCACAGACGTTTTAT*), GAPDH (Invitrogen Thermo Fisher Scientific, forward *CTCTGCTCCTCCTGTTCGAC*, reverse *ACGACC AAATCCGTTGACTC*).

CRISPR-CAS9. A functional sgRNA was generated digesting pSpCas9(BB)-2A-Puro (PX459) (#48139, Addgene, Watertown, MA, US) with BbsI-HF (NEB, Ipswich, MA, US) and ligating a double-stranded DNA oligonucleotide which targets the third exon of CDCP1 with T4 DNA ligase (NEB, Ipswich, MA, US). The double-stranded oligonucleotide was obtained by annealing the following single-stranded oligonucleotides: hCDCP1_KO_BS, 5′-AAACccgtggtcaggatcggaac-3′; hCDCP1_KO_TS, 5′-CACCgttccgatcctgaccacgg-3′. After the ligation, px459-CDCP1$^{-/-}$sgRNA plasmid was transfected in the cells using Lipofectamine™ 3000 (Invitrogen, Thermo Fisher Scientific). After 2 days, the transfected clones were selected with a 4-days Puromycin treatment (0.6 µg/mL) and expanded with a polyclonal approach to obtain stable cell lines.

Data availability

The datasets generated and/or analyzed during the current study are available from the corresponding author on reasonable request.

Received: 3 August 2022; Accepted: 16 December 2022
Published online: 02 January 2023

References

1. Witjes, J. A. *et al*. European Association of Urology guidelines on muscle-invasive and metastatic bladder cancer: Summary of the 2020 guidelines. *Eur. Urol.* **79**, 82–104 (2021).
2. Ghatalia, P. & Plimack, E. R. Integration of immunotherapy into the treatment of advanced urothelial carcinoma. *J. Natl. Compr. Cancer Netw.* **18**, 355–361 (2020).
3. Hooper, J. D. *et al.* Subtractive immunization using highly metastatic human tumor cells identifies SIMA135/CDCP1, a 135 kDa cell surface phosphorylated glycoprotein antigen. *Oncogene* **22**, 1783–1794 (2003).
4. Bhatt, A. S., Erdjument-Bromage, H., Tempst, P., Craik, C. S. & Moasser, M. M. Adhesion signaling by a novel mitotic substrate of src kinases. *Oncogene* **24**, 5333–5343 (2005).
5. Takeda, H., Fujimori, Y., Kai, S., Ogawa, H. & Nakano, T. CD318/CUB-domain-containing protein 1 expression on cord blood hematopoietic progenitors. *Exp. Ther. Med.* **1**, 497–501 (2010).
6. Khan, T., Kryza, T., Lyons, N. J., He, Y. & Hooper, J. D. The CDCP1 signaling hub: A target for cancer detection and therapeutic intervention. *Cancer Res.* **81**, 2259–2269 (2021).
7. He, Y. *et al.* Proteolysis-induced N-terminal ectodomain shedding of the integral membrane glycoprotein CUB domain-containing protein 1 (CDCP1) is accompanied by tyrosine phosphorylation of its C-terminal domain and recruitment of Src and PKCdelta. *J. Biol. Chem.* **285**, 26162–26173 (2010).
8. Casar, B. *et al.* In vivo cleaved CDCP1 promotes early tumor dissemination via complexing with activated β1 integrin and induction of FAK/PI3K/Akt motility signaling. *Oncogene* **33**, 255–268 (2014).
9. Spassov, D. S., Baehner, F. L., Wong, C. H., McDonough, S. & Moasser, M. M. The transmembrane src substrate trask is an epithelial protein that signals during anchorage deprivation. *Am. J. Pathol.* **174**, 1756–1765 (2009).
10. Wortmann, A. *et al.* Cellular settings mediating Src substrate switching between focal adhesion kinase tyrosine 861 and CUB-domain-containing protein 1 (CDCP1) tyrosine 734. *J. Biol. Chem.* **286**, 42303–42315 (2011).
11. Alajati, A. *et al.* Interaction of CDCP1 with HER2 enhances HER2-driven tumorigenesis and promotes trastuzumab resistance in breast cancer. *Cell Rep.* **11**, 564–576 (2015).
12. Alajati, A. *et al.* CDCP1 overexpression drives prostate cancer progression and can be targeted in vivo. *J. Clin. Invest.* **130**, 2435–2450 (2020).
13. Alajati, A. *et al.* Mammary tumor formation and metastasis evoked by a HER2 splice variant. *Cancer Res.* **73**, 5320–5327 (2013).

14. Turdo, F. *et al.* CDCP1 is a novel marker of the most aggressive human triple-negative breast cancers. *Oncotarget* **7**, 69649–69665 (2016).
15. Ikeda, J. *et al.* Expression of CUB domain containing protein (CDCP1) is correlated with prognosis and survival of patients with adenocarcinoma of lung. *Cancer Sci.* **100**, 429–433 (2009).
16. Gao, W. *et al.* Isolation and phenotypic characterization of colorectal cancer stem cells with organ-specific metastatic potential. *Gastroenterology* **145**, 636-646.e5 (2013).
17. Harrington, B. S. *et al.* Cell line and patient-derived xenograft models reveal elevated CDCP1 as a target in high-grade serous ovarian cancer. *Br. J. Cancer* **114**, 417–426 (2016).
18. He, Y. *et al.* Elevated CDCP1 predicts poor patient outcome and mediates ovarian clear cell carcinoma by promoting tumor spheroid formation, cell migration and chemoresistance. *Oncogene* **35**, 468–478 (2016).
19. Emerling, B. M. *et al.* Identification of CDCP1 as a hypoxia-inducible factor 2α (HIF-2α) target gene that is associated with survival in clear cell renal cell carcinoma patients. *Proc. Natl. Acad. Sci.* **110**, 3483–3488 (2013).
20. Cao, M. *et al.* HIF-2α regulates CDCP1 to promote PKCδ-mediated migration in hepatocellular carcinoma. *Tumor Biol.* **37**, 1651–1662 (2016).
21. Kryza, T. *et al.* Effective targeting of intact and proteolysed CDCP1 for imaging and treatment of pancreatic ductal adenocarcinoma. *Theranostics* **10**, 4116–4133 (2020).
22. Miyazawa, Y. *et al.* CUB domain-containing protein 1, a prognostic factor for human pancreatic cancers, promotes cell migration and extracellular matrix degradation. *Can. Res.* **70**, 5136–5146 (2010).
23. Bühring, H. *et al.* CDCP1 identifies a broad spectrum of normal and malignant stem/progenitor cell subsets of hematopoietic and nonhematopoietic origin. *Stem Cells* **22**, 334–343 (2004).
24. Heitmann, J. S. *et al.* Identification of CD318 (CDCP1) as novel prognostic marker in AML. *Ann. Hematol.* **99**, 477–486 (2020).
25. Nakashima, K. *et al.* Novel small molecule inhibiting CDCP1-PKCδ pathway reduces tumor metastasis and proliferation. *Cancer Sci* **108**, 1049–1057 (2017).
26. Schäfer, D. *et al.* Identification of CD318, TSPAN8 and CD66c as target candidates for CAR T cell based immunotherapy of pancreatic adenocarcinoma. *Nat. Commun.* **12**, 1453 (2021).
27. Liu, F., Yang, X., Geng, M. & Huang, M. Targeting ERK, an Achilles' Heel of the MAPK pathway, in cancer therapy. *Acta Pharm. Sin. B* **8**, 552–562 (2018).
28. Yang, F. *et al.* Dynamic m6A mRNA methylation reveals the role of METTL3-m6A-CDCP1 signaling axis in chemical carcinogenesis. *Oncogene* **38**, 4755–4772 (2019).
29. Schneider, A.-C. *et al.* Global histone H4K20 trimethylation predicts cancer-specific survival in patients with muscle-invasive bladder cancer. *BJU Int.* **108**, E290-296 (2011).
30. Klümper, N. *et al.* Mediator complex subunit MED1 protein expression is decreased during bladder cancer progression. *Front. Med. (Lausanne)* **4**, 30 (2017).
31. Ying, X. *et al.* Programmable N6-methyladenosine modification of CDCP1 mRNA by RCas9-methyltransferase like 3 conjugates promotes bladder cancer development. *Mol. Cancer* **19**, 169 (2020).
32. Chen, Z. *et al.* Single-cell RNA sequencing highlights the role of inflammatory cancer-associated fibroblasts in bladder urothelial carcinoma. *Nat. Commun.* **11**, 5077 (2020).
33. Drost, J. *et al.* Organoid culture systems for prostate epithelial and cancer tissue. *Nat. Protoc.* **11**, 347–358 (2016).
34. Earl, J. *et al.* The UBC-40 urothelial bladder cancer cell line index: A genomic resource for functional studies. *BMC Genomics* **16**, 403 (2015).
35. Ertl, I. E. *et al.* Molecular and pharmacological bladder cancer therapy screening: Discovery of clofarabine as a highly active compound. *Eur. Urol.* **82**, 261–270 (2022).
36. Law, M. E. *et al.* CUB domain-containing protein 1 and the epidermal growth factor receptor cooperate to induce cell detachment. *Breast Cancer Res.* **18**, 80 (2016).
37. Kamoun, A. *et al.* A consensus molecular classification of muscle-invasive bladder cancer. *Eur. Urol.* **77**, 420–433 (2020).
38. Rebouissou, S. *et al.* EGFR as a potential therapeutic target for a subset of muscle-invasive bladder cancers presenting a basal-like phenotype. *Sci. Transl. Med.* **6**, 244ra91 (2014).
39. Murakami, Y. *et al.* AXL/CDCP1/SRC axis confers acquired resistance to osimertinib in lung cancer. *Sci. Rep.* **12**, 8983 (2022).
40. Dong, Y. *et al.* The cell surface glycoprotein CUB domain-containing protein 1 (CDCP1) contributes to epidermal growth factor receptor-mediated cell migration. *J. Biol. Chem.* **287**, 9792–9803 (2012).
41. He, Y., Harrington, B. S. & Hooper, J. D. New crossroads for potential therapeutic intervention in cancer-intersections between CDCP1, EGFR family members and downstream signaling pathways. *Oncoscience* **3**, 5–8 (2016).
42. Eckstein, M. *et al.* Cytotoxic T-cell-related gene expression signature predicts improved survival in muscle-invasive urothelial bladder cancer patients after radical cystectomy and adjuvant chemotherapy. *J. Immunother. Cancer* **8**, e000162 (2020).

Author contributions

Study concept and design: A.Alajati, M.S.Acquisition of data: M.S., S.F., M.E., O.H., A.S., N.M., D.S.Analysis and interpretation of data: M.S., S.F., M.E., N.K., D.C.Drafting of the manuscript: A.Alajati, M.S., S.F..Critical revision of the manuscript for important intellectual content: A.Alajati, S.H., J.E., M.T., G.K., T.B., A.Alimonti, M.R., M.H.Statistical analysis: M.S., S.F., M.E., N.K., D.C..Administrative, technical, or material support: A.Alajati. Supervision: A.Alajati.

Funding

Open Access funding enabled and organized by Projekt DEAL. M.S. and S.F. are supported by the Universitätsklinikum Bonn (UKB).

Competing interests

The authors declare no competing interests.

Additional information

Supplementary Information The online version contains supplementary material available at https://doi.org/10.1038/s41598-022-26579-z.

Correspondence and requests for materials should be addressed to A.A.

3.3 Publication 3: Adipocyte precursor-derived NRG1 promotes resistance to FGFR inhibition in urothelial carcinoma.

Adipocyte Precursor-Derived NRG1 Promotes Resistance to FGFR Inhibition in Urothelial Carcinoma

Sana Hosni[1], Viola Kilian[1], Niklas Klümper[1,2], Daniela Gabbia[3], Katharina Sieckmann[4], Dillon Corvino[2], Anja Winkler[1], Miriam Saponaro[1], Karin Wörsdörfer[1], Doris Schmidt[1], Oliver Hahn[5,6], Ilaria Zanotto[3], Marina Bertlich[1], Marieta Toma[7], Tobias Bald[2], Markus Eckstein[8], Michael Hölzel[2], Matthias Geyer[9], Manuel Ritter[1], Dagmar Wachten[4], Sara De Martin[3], and Abdullah Alajati[1]

ABSTRACT

Aberrations of the fibroblast growth factor receptor (FGFR) family members are frequently observed in metastatic urothelial cancer (mUC), and blocking the FGF/FGFR signaling axis is used as a targeted therapeutic strategy for treating patients. Erdafitinib is a pan-FGFR inhibitor, which has recently been approved by the FDA for mUC with FGFR2/3 alterations. Although mUC patients show initial response to erdafitinib, acquired resistance rapidly develops. Here, we found that adipocyte precursors promoted resistance to erdafitinib in FGFR-dependent bladder and lung cancer in a paracrine manner. Moreover, neuregulin 1 (NRG1) secreted from adipocyte precursors was a mediator of erdafitinib resistance by activating human epidermal growth factor receptor 3 (ERBB3; also known as HER3) signaling, and knockdown of NRG1 in adipocyte precursors abrogated the conferred paracrine resistance. NRG1 expression was significantly downregulated in terminally differentiated adipocytes compared with their progenitors. Pharmacologic inhibition of the NRG1/HER3 axis using pertuzumab reversed erdafitinib resistance in tumor cells *in vitro* and prolonged survival of mice bearing bladder cancer xenografts *in vivo*. Remarkably, data from single-cell RNA sequencing revealed that NRG1 was enriched in platelet-derived growth factor receptor-A (PDGFRA) expressing inflammatory cancer-associated fibroblasts, which is also expressed on adipocyte precursors. Together, this work reveals a paracrine mechanism of anti-FGFR resistance in bladder cancer, and potentially other cancers, that is amenable to inhibition using available targeted therapies.

Significance: Acquired resistance to FGFR inhibition can be rapidly promoted by paracrine activation of the NRG1/HER3 axis mediated by adipocyte precursors and can be overcome by the combination of pertuzumab and erdafitinib treatment.

See related commentary by Kolonin and Anastassiou, p. 648

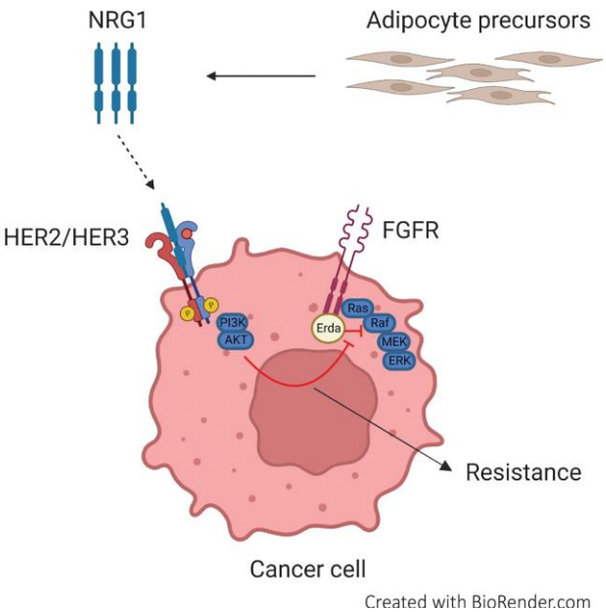

Introduction

For decades, platinum-based combination chemotherapy has been the standard therapy for metastatic urothelial cancer (mUC). However, this treatment is generally not curative and has a limited impact on patient survival. Although the advent of immunotherapy and antibody–drug conjugates has broadened the therapeutic armamentarium for mUC, only a minority of patients respond (1, 2). The fibroblast growth factor receptor (FGFR) family are receptor tyrosine kinases (RTK), which regulate various cellular functions including cell proliferation, survival, differentiation, and migration. Activation of the members of the FGFR family (FGFR1–4) leads to activation of

[1]Department of Urology and Pediatric Urology, University Hospital Bonn (UKB), Bonn, Germany. [2]Institute of Experimental Oncology, University Hospital Bonn (UKB), Bonn, Germany. [3]Department of Pharmaceutical and Pharmacological Sciences, University of Padua, Padua, Italy. [4]Institute of Innate Immunity, Medical Faculty, University of Bonn, Bonn, Germany. [5]Clinic of Urology, University Hospital Göttingen, Göttingen, Germany. [6]Clinic of Urology, University Hospital Würzburg, Würzburg, Germany. [7]Institute of Pathology, University Hospital Bonn (UKB), Bonn, Germany. [8]Institute of Pathology, University Hospital Erlangen, Erlangen-Nuernberg (FAU), Erlangen, Germany. [9]Institute of Structural Biology, Medical Faculty, University of Bonn, Bonn, Germany.

S. Hosni and V. Kilian contributed equally to this article.

Corresponding Author: Abdullah Alajati, Department of Urology and Pediatric Urology, University Hospital Bonn (UKB), Venusberg-Campus 1, Bonn 53127, Germany. E-mail: abdullah.alajati@ukbonn.de

Cancer Res 2024;84:725–40

doi: 10.1158/0008-5472.CAN-23-1398

downstream signaling pathways such as Ras/Raf-MEK-MAPKs and PI3K/AKT (3). Genomic aberrations of FGFR family members are frequently observed in various cancers, most commonly in UC (32% FGFR aberrant; refs. 4–6). Therefore, blocking the FGF/FGFR signaling axis has been developed as a targeted therapeutic strategy in various tumor types including mUC. In 2019, the FDA granted accelerated approval to erdafitinib, a pan-FGFR inhibitor, for patients with FGFR2/3-driven urothelial cancer, based on the BLC2001 study (7, 8). Erdafitinib is a small molecule inhibitor that binds to FGFR and inhibits FGFR autophosphorylation and the resulting downstream signaling (9). Preliminary results from the phase III THOR clinical trial (NCT03390504) suggest significantly improved overall survival and progression-free survival of erdafitinib-treated patients compared with chemotherapy-treated patients (10). Although erdafitinib shows a considerable objective response rate of 40%, the response is not durable in most patients, indicating rapid development of resistance. To date, several efforts have been made to understand the resistance mechanisms to FGFR inhibition, which have primarily focused on tumor cell-intrinsic events (11–14). However, extrinsic factors driven by the tumor microenvironment (TME) play a key role in the development of RTK inhibitors resistance by activating alternative growth-promoting pathways. We hypothesize that the rapid development of erdafitinib resistance is triggered by a prompt protumoral response of the TME. One of the principal components of the TME is the mesenchymal stromal cells (MSC), which are multipotent cells that can differentiate into cancer-associated fibroblasts (CAF), osteocytes, chondrocytes, and adipocytes (15–17). The correlation between obesity and increased cancer progression has been established in multiple cancer types (18). There is increasing evidence suggesting the protumoral role of adipose-derived stem cells (ADSC) or adipocyte precursors in cancer (19). ADSCs are MSCs of adipose tissue and comprise inflammatory, myofibroblastic, and pro-adipogenic subpopulations (19). ADSCs can also promote tumor growth by remodeling the extracellular matrix, promoting angiogenesis, contributing to the recruitment of immunosuppressive cells, and inducing epithelial–mesenchymal transition through paracrine signaling (16, 20–25). Growth arrest and a variety of hormones, for example dexamethasone and insulin, are established means of inducing adipogenic differentiation of adipocyte precursors *in vitro* (26). Despite the abundant presence of tumor-infiltrating adipose tissue in bladder tumors (27, 28), the influence of ADSCs within the TME on the development of erdafitinib resistance has not been explicitly investigated in urothelial cancer. In this study, we sought to investigate whether adipocyte precursors can induce erdafitinib resistance in bladder cancer cell lines, and whether these cells can be specifically targeted by rational combination therapies.

Materials and Methods

Cell culture

All cells were cultured in a humidified 37ºC incubator with 5% CO_2. RT4, T24, TCCSUP, and 3T3-L1 cells were purchased from ATCC. MB49 cell line was purchased from Addexbio, RT112 cell line was purchased from DSMZ (German Collection of Microorganisms and Cell Cultures), and human adipose-derived stem cells (hADSC) were purchased from Lonza. LK2 lung cancer cells were a gift from Dr. Hanibal Bohnenberger (University Hospital G€ottingen). RT4, RT112, T24, TCCSUP, and LK2 cell lines were cultured in RPMI1640 supplemented with 10% FCS, 1% penicillin/streptomycin, and 1% L-glutamine. MB49 cells and 3T3-L1 preadipocytes were cultured in DMEM supplemented with 10% FCS, 1% penicillin/streptomycin (complete DMEM). hADSCs were cultured in hADSCs medium (Lonza) supplemented with 10% FCS, 1% penicillin/streptomycin, and 1% L-glutamine. RT4, RT112, TCCSUP, and T24 are human bladder cancer cell lines. MB49 is a murine bladder cancer cell line. 3T3-L1 are preadipocytes derived from the mouse embryo, which can differentiate into adipocytes under certain conditions (described separately in Materials and Methods). Cells were split twice per week, and regularly checked for *Mycoplasma* contamination by MycoBlue Mycoplasma Detector (NeoBiotech). All cell culture reagents were obtained from Gibco (Thermo Fisher Scientific) unless otherwise specified.

Collection of conditioned media from 3T3-L1 and hADSCs

The 3T3-L1 cells and hADSCs were seeded in a T75 flask and incubated until 70% to 80% confluent (3–4 days). Conditioned media was collected from 3T3-L1 cells and hADSCs, filtered using 0.22 mm filters, aliquoted, and stored at −20ºC.

Crystal violet proliferation assay

Depending on the cell line, 2,500 to 5,000 cells were seeded per well in a 96-well plate. After overnight incubation, cells were treated and incubated for 7 days. All conditions were run in triplicate wells. Treatments were refreshed on day 4. For staining, cells were fixed with 37% paraformaldehyde per well for 10 minutes, then washed with distilled water, and stained 0.05% crystal violet for 30 minutes. Cells were washed twice with distilled water and dried. 0.1% acetic acid was added per well to solubilize the dye. Finally, the absorbance was measured at a wavelength of 570 nm. The mean values of the triplicate wells were divided by a day 0 control. Relative optical density was normalized with respect to the vehicle control.

Concentration of conditioned media

Conditioned media was filtered through Pierce Protein Concentrators PES, 3K MWCO by centrifugation at 2,600 x *g*, at 4ºC, for 1.5 hours. Flow through was collected and tested as the protein-depleted fraction.

Pertuzumab combination treatment with erdafitinib

Cells were pretreated with 10 mg/mL pertuzumab (Perjeta; Roche) in DMEM 1 hour before treatment with erdafitinib (Selleck Chemicals). Erdafitinib treatment was done in media control or conditioned media, with/without pertuzumab. Treatments were refreshed on day 4. Cells were stained with crystal violet on day 7 as described above.

Recombinant NRG1 treatment

A total of 50 ng/mL recombinant Human Heregulin-b1 (Biolegend) in complete DMEM was used to treat the cells. Treatments were refreshed on day 4 by a full media change. Cells were stained with crystal violet on day 7 as described earlier.

Isolation and enrichment of primary murine preadipocytes

Inguinal white adipose tissue was surgically removed from mice, then minced and digested with collagenase II in 0.5% BSA in PBS at 37ºC with agitation. The digestion was quenched by adding AT buffer (0.5% BSA in PBS). Dissociated cells were filtered through a 100 mmol/L filter and centrifuged at 500 x *g* for 10 minutes. The supernatant containing mature adipocytes was aspirated, and the pellet, consisting of the stromal vascular fraction, was resuspended in red blood cell lysis buffer for 2 minutes at room temperature. The reaction was stopped by adding AT buffer and centrifugation at 500 x *g* for 10 minutes. Cells were washed in 2 mL magnetic-activated cell sorting (MACS) buffer (0.5% BSA and 2 mmol/L EDTA in PBS) and labeled with biotin-conjugated antibodies against lineage

markers of endothelial cells (anti-CD31; clone MEC13.3; #102503), immune cells (anti-CD45; clone 30-F11; #103103), and erythrocytes (anti-TER119; clone TER-119; #116203). Cells were then incubated with Streptavidin MicroBeads (Miltenyi, #130–048–101) and subjected to MACS. The lineage depleted cells were harvested and maintained in DMEM/F12, supplemented with 1% GlutaMAX-I, 1% penicillin–streptomycin (all Gibco/Life Technologies), 10% FCS (Biochrom), 33 mmol/L biotin (Sigma), and 17 mmol/L D-pantothenate (Sigma) at 37°C with 5% CO_2. All antibodies were purchased from BioLegend.

Isolation and enrichment of human CAFs

Urothelial carcinoma tumors from four patients were obtained from the University Hospital Bonn under the ethical approval number 363/20. Tumors were minced and digested as described above for the murine adipose tissue. Cells were washed in 2 mL MACS buffer (0.5% BSA and 2 mmol/L EDTA in PBS) and labeled with biotin-conjugated antibodies against lineage markers of endothelial cells (anti-CD31; clone AC128; #130–119–893), immune cells (anti-CD45; clone 5B1; #130–113–116), and epithelial cells [anti-EpCAM (CD326); clone REA764; #130–110–997]. Cells were then incubated with Streptavidin MicroBeads (Miltenyi, #130–048–101) and subjected to MACS. The lineage depleted cells were harvested and maintained in DMEM/F12, supplemented with 1% GlutaMAX-I, 1% penicillin–streptomycin (all Gibco/Life Technologies), 10% FCS (Biochrom), 33 mmol/L biotin (Sigma), and 17 mmol/L D-pantothenate (Sigma) at 37°C with 5% CO_2. Conditioned media (CM) was collected when cells reached confluence of approximately 70%. All antibodies were purchased from BioLegend.

Adipogenic differentiation of primary murine preadipocytes

A total of 200,000 3T3-L1 cells were seeded in complete DMEM per well of a six-well plate and incubated for 2 days to allow them to grow to 100% confluence. Differentiation was induced by 5 mg/mL insulin (Sigma), 1 mmol/L dexamethasone (Sigma), 100 mmol/L 3-isobutyl-1-methylxanthine (IBMX; Sigma), and 1 mmol/L Rosiglitazone (Sigma) in complete DMEM. Following 2 days of induction, adipocytes were maintained in complete DMEM supplemented with 1 mg/mL insulin for five more days, with complete media change every other day.

Adipogenic differentiation of 3T3-L1 cells

A total of 200,000 cells were seeded per well of a six-well plate and incubated for 2 days to allow them to grow to 100% confluence. Differentiation was induced by 0.4 mg/mL insulin, 0.1 mmol/L dexamethasone, and 20 mmol/L 3-isobutyl-1-methylxanthine in complete DMEM. Following 2 days of induction, adipocytes were maintained in complete DMEM supplemented with 1 mg/mL insulin for 6 more days, with media change every other day. Conditioned media was harvested from adipocytes 7 days post-differentiation induction, filtered using 0.22 mm filters, aliquoted, and stored at -20°C.

Western blot analysis

A total of 800,000 cells were seeded per well of a 6-well plate. Following overnight incubation, cells were treated with the indicated treatments and incubated overnight. Cells were washed and lysed using RIPA buffer (Cell Signaling Technology; #9806) freshly supplemented with phenylmethylsulfonyl fluoride (PMSF; Carl Roth; #329–98–6). Protein concentration was determined using the Pierce BCA Protein Assay Kit (Thermo Fisher Scientific; #23225) according to the manufacturer's instructions. Proteins were separated using SDS-PAGE, transferred to nitrocellulose membranes, then blotted with polyclonal anti-ERK1/2 (#9102), anti-pERK1/2 (clone 197G2; #4377), anti-AKT (clone 40D4; #2920), anti-pAKT (clone D9E; #4060), anti-FGFR3 (Santa Cruz Biotechnology; clone B-9; #sc-13121), anti-HER3 (clone D22C5; #12708), anti-pHER3 (clone 21D3; #4791), anti-b-actin (Sigma-Aldrich; clone AC-74; #A2228), polyclonal anti-Heregulin (#2573), polyclonal anti-EGFR (Santa Cruz Biotechnology; #sc-03), anti-pEGFR (clone 1H12, #2236), anti- HER2 (D8F12, #4290), anti-pHER2 (clone 21D3, #2247). All Western blot antibodies were purchased from Cell Signaling Technology unless otherwise specified.

RNA extraction and qRT-PCR

Total RNA extraction was done using TRizol RNA isolation reagent (Invitrogen). RNA concentration was measured using the Thermo Scientific NanoDrop 2000/2000c. Reverse transcription was performed using Prime Script RT Reagent Kit (Takara; #RR064A). RT-PCR mix was prepared using TB Green Premix Ex Taq I (Takara; #RR82WR), and quantified with the QuantStudio 5 RT-PCR System (Applied Biosystems). Primers used: human *NRG1* forward AGAGCCTGTTAAGAAACTCGC, human *NRG1* reverse GTCCACTTCCAATCTGTTAGCA, human *FGFR1* forward AAACCGTATGCCCGTAGCTC, human *FGFR1* reverse AGGTGGCATAACGGACCTTG, human *FGFR2* forward CCTGCGGAGACAGGTAACAG, human *FGFR2* reverse TGCCCAGTGTCAGCTTATCT, human *FGFR3* forward CCCAAATGGGAGCTGTCTCG, human *FGFR3* reverse CCCGGTCCTTGTCAATGCC, human *GAPDH* forward CTCTGCTCCTCCTGTTCGAC, human *GAPDH* reverse ACGACCAAATCCGTTGACTC, murine *Nrg1* forward TTCCCATTCTGGCTTGTCTAGT, murine *Nrg1* reverse CCAGGGTCAAGGTGGGTAG, murine *Fgfr1* forward ACTCTGCGCTGGTTGAAAAAT, murine *Ffgfr1* reverse GGTGGCATAGCGAACCTTGTA, murine *Fgfr2* forward GCTATAAGGTACGAAACCAGCAC, murine *Fgfr2* reverse GGTTGATGGACCCGTATTCATTC, murine *Fgfr3* forward GCCTGCGTGCTAGTGTTCT, murine *Fgfr3* reverse CCTGTACCATCCTTAGCCCAG, murine *Cd36* forward GCAGGTCTATCTACGCTGTGTT, murine *Cd36* reverse GCAAAGGCATTGGCTGGAAG murine *Lpl* forward CATCAACTGGATGGAGGAGGAG, murine *Lpl* reverse GTCAGACTTCCTGCTACGCC, murine *Glut4* forward CATGTCTCGAAGTAGTGTGCAG, murine *Glut4* reverse TGACAGTGACAGCCACAATGATG, murine *Lep* forward CCAGAAAGTCCAGGATGACACC, murine *Lep* reverse GGCGGATACCGACTGCGT, murine *Gapdh* forward AGGTCGGTGTGAACGGATTTG, murine *Gapdh* reverse TGTAGACCATGTAGTTGAGGT. All procedures were performed according to the manufacturer's protocol.

Lentiviral transduction

RT4 cells stably overexpressing NRG1 were generated by lentiviral transduction. Lentivirus was generated in HEK 293T cells through cotransfection of VSV-G, Gag Pol, and pLV[Exp]-Bsd-hPGK>hNRG1 [Vector Builder (NM_001322205.1)] using jetPRIME (Polyplus). RT4 NRG1 cells were selected with 5 mg/mL Blasticidin (Gibco) for 1 week.

3T3-L1 cells and hADSCs stably overexpressing shRNA targeting mNrg1/hNRG1, respectively, were generated by lentiviral transduction. Lentivirus was generated in HEK 293T cells through cotransfection of VSV-G, Gag Pol, and pLV[shRNA]-Puro-U6>mNrg1 [shRNA#1] [Vector Builder (VB230706–1085msf)]/ pLV[shRNA]-Puro-U6>hNRG1[shRNA#2] [Vector Builder (VB230706–1109zqs)] using jetPRIME (Polyplus). 3T3-L1 mNrg1 shRNA cells and hADSCs hNRG1 shRNA cells were selected with 1.6 mg/mL Puromycin (Gibco) for 3 days. Control 3T3-L1 and hADSCs cell lines were transduced

with pLV[shRNA]-Puro-U6>Scramble_shRNA#1 [Vector Builder (VB010000–0005 mme)] and selected as described above.

Phospho-RTK array

A total of 800,000 cells were seeded per well of a 6-well plate. Following overnight incubation, cells were treated with the indicated treatments and incubated overnight. Proteome Profiler Human Phospho-RTK Array Kit (R&D Systems; #ARY001B) was used to perform the array. Mean pixel density was quantified using ImageJ, and the average of duplicate dots per receptor were plotted.

In vivo experiments

All procedures involving animals were conducted in compliance with the 3R principle and the Animal Research: Reporting of In Vivo Experiments (ARRIVE) guidelines, after approval by the Italian Ministry of Health (auth. no. 608/2022-PR). In this study, a xenograft model was set up by subcutaneously injecting RT4-WT or RT4-NRG1 cells (2×10^6 cell/200 mL/mouse) in the flank of CB17-SCID mice (8 ± 3 week of age; Charles River Laboratories). Tumor mass was measured twice a week, and tumor volume was calculated according to the following formula:

$$V(\text{mm}^3) = \frac{\text{length} \times \text{width}^2}{2}$$

Treatment was initiated once the tumor mass was palpable. Mice inoculated with RT4 WT cells were randomized into two experimental groups: control and erdafitinib (5 mg/kg bw by daily gavage). Mice inoculated with RT4-NRG1 cells were randomized into four experimental groups, that is, control, erdafitinib (5 mg/kg bw by daily gavage), pertuzumab (5 mg/kg bw, EV three times a week), combination (erdafitinib 5 mg/kg bw daily gavage þ pertuzumab 5 mg/kg bw three times a week). Mice were sacrificed once tumor measured with caliper reached the volume of about 1,500 mm^2, when a sudden increase of tumor growth was observed, or if the two previous conditions were not reached, at day 37 (final experimental endpoint). Signs of distress, for example, unusual behaviors, excessive weight loss, and hunched posture, were also monitored during treatment. At sacrifice, the tumor was isolated, washed in saline solution, and fixed in a 4% formalin solution. After 24 hours, the tissues were embedded in paraffin blocks for further IHC analysis.

Ki67 IHC

Two to three micrometers of sections were prepared from formalin-fixed, paraffin-embedded tissues. Antigen retrieval was done by microwaving for 10 minutes at 600 W in boiling 10 mmol/L citrate buffer, pH 6.0. 1:200 dilution of mouse anti-Ki67 antibody (Zytomed; MSK018–05) was used for staining. Staining pattern was nuclear. Quantification was done using QuPath Version 0.3.2.

Single-cell RNA sequencing analysis

Single-cell RNA sequencing (scRNA-seq) data of eight bladder cancer samples and three para tumor samples was downloaded from Chen and colleagues (29), using their interactive Shiny R interface. Analysis and dataset processing was performed using Seurat version 4.1.1 running on a mac OS version 12.4 (Monterey). Analysis was performed using standard Seurat dataset processing pipeline. Data were visualized using the Nebulosa (version 1.4.0) and scCustomize (version 0.7.0) packages. The color-blind friendly, perceptually uniform and ordered "batlow" color pallet was used via the R package scico (version 1.3.0). The publication ready figure was arranged and formatted using Adobe Illustrator version 27. Data availability: Publicly available scRNA-seq data were obtained from Chen and colleagues (29). Code availability: Code to reproduce scRNA-seq data can be found at https://github.com/BaldLab.

The Cancer Genome Atlas data analysis

Log_2-transformed RSD (RNA-Seq by Expectation Maximization) RNA-sequencing data (RNA-Seq v2) of PDGFRA, MMP3, DPP4, and NRG1 generated by The Cancer Genome Atlas (TCGA) Research Network (http://cancergenome.nih.gov/) were downloaded from the UCSC Xena browser (http://xena.ucsc.edu) for $n = 408$ urothelial bladder carcinoma (BLCA). Correlation analysis were based on the median expression of NRG1 among the samples.

NRG1 IHC

Two to three micrometers of sections were prepared from formalin-fixed, paraffin-embedded tissues. The sections were mounted on adhesion microscope slides (TOMO). Dewaxing (EZ Prep #950–102), heat pretreatment (Ultra CC1 buffer at pH 8; #950–224), and further steps were performed in the Ventana BenchMark Ultra (Roche) according to the manufacturer's instructions. All reagents were purchased from Ventana Medical Systems unless otherwise specified. Staining was done using 1:100 dilution of the monoclonal anti-NRG1 antibody (Thermo Fisher Scientific; clone 7D5; #MA5–12986). OptiView DAB Detection Kit (#760–700) was used for detection. A cutoff *H*-score of 150 was applied for NRG1 cytoplasmic intensity on tumor cells, whereas cytoplasmic staining intensity was classified as low and high on stromal NRG1 intensity.

Statistical analysis

GraphPad Prism 8 was used for statistical analysis. For comparisons between two independent variables, unpaired *t* test was performed. For comparisons among more than two independent variable, two-way ANOVA was performed. At least three biological replicates of all *in vitro* experiments were performed. Log-rank (Mantel-0-Cox) test was used for statistical analysis of survival data. In all figures, mean ± SD was reported. 4 to 9 mice were treated for *in vivo* experiments. Not significant (n.s.), $P < 0.05$ (*), $P < 0.01$ (**), $P < 0.001$ (***), and $P < 0.0001$ (****).

Data availability statement

The scRNA-seq data analyzed in this paper are available from the Sequence Read Archive (SRA) at PRJNA662018 (https://www.ncbi.nlm.nih.gov/bioproject/?term¼PRJNA662018). The RNA-seq data generated by the TCGA for urothelial BLCA that was analyzed in this study are available in the Genomic Data Commons Data Portal (https://portal.gdc.cancer.gov/). All other raw data generated in this study are available upon request from the corresponding author.

Results

Adipocyte precursors promote resistance to erdafitinib in bladder cancer cell lines

To test the susceptibility to growth inhibition by erdafitinib treatment, several bladder cancer cell lines (human RT4, RT112, TCCSUP, T24, and the murine MB49) were screened for their *FGFR2* and *FGFR3* mRNA expression. qRT-PCR analysis showed that RT4 and RT112 cell lines express high levels of *FGFR3* and moderate levels of *FGFR2*, whereas all other tested cell lines express scant levels of *FGFR2/3* (Supplementary Fig. S1A). Because RT4 and RT112 cell lines are known to be FGFR3-dependent (30–32), FGFR3 expression was also analyzed at the protein level. Western blot analysis confirmed the

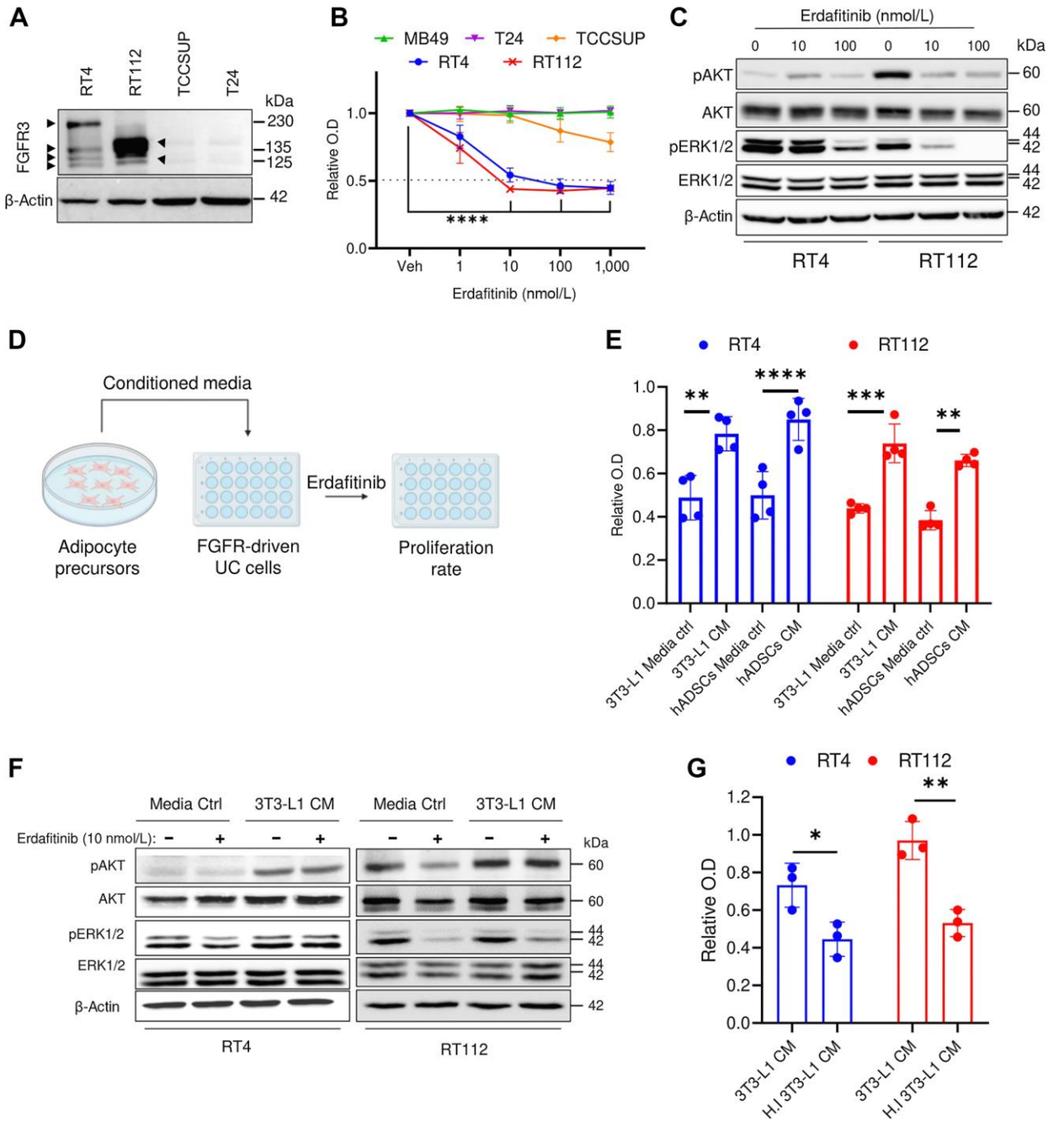

Figure 1.

Adipocyte precursors promote resistance against erdafitinib in bladder cancer cell lines. A, Western blot analysis of FGFR3 in four bladder cancer cell lines: RT4, RT112, TSCCUP, and T24. b-Actin served as a loading control. B, Proliferation analysis of five bladder cancer cell lines RT4, RT112, TSCCUP, T24, and MB49 treated with vehicle (Veh) or erdafitinib (1, 10, 100, 1,000 nmol/L). Crystal violet staining was done on day 7. Three biological replicates were performed. Data are represented as mean ± SD. C, Western blot analysis of pAKT and pERK1/2 in RT4 and RT112 cells treated with DMSO (Veh) or erdafitinib (10 and 100 nmol/L) for 16 hours. b-Actin served as a loading control. D, Schematic diagram of the proliferation assay performed to investigate the effect of CM of different stromal cells on erdafitinib response. E, Proliferation analysis of RT4 and RT112 cells treated with 10 nmol/L erdafitinib in media control (ctrl) or CM of 3T3-L1 cells or hADSC. Crystal violet staining was performed on day 7. Data are normalized to cells treated with vehicle. Four biological replicates were performed. Data are represented as mean ± SD. F, Western blot analysis of pAKT and pERK1/2 in RT4 and RT112 cells treated with 10 nmol/L erdafitinib in media control or CM of 3T3-L1 cells. b-Actin served as a loading control. G, Proliferation analysis of RT4 cells and RT112 cells treated with 10 nmol/L erdafitinib in CM of 3T3-L1 cells or heat-inactivated (HI) CM of 3T3-L1. Data were normalized to cells treated with vehicle. Crystal violet staining was performed on day 7. Three biological replicates were performed. Data are represented as mean ± SD. Two-way ANOVA was used for statistical analysis. *, $P < 0.05$; **, $P < 0.01$; ***, $P < 0.001$; ****, $P < 0.0001$.

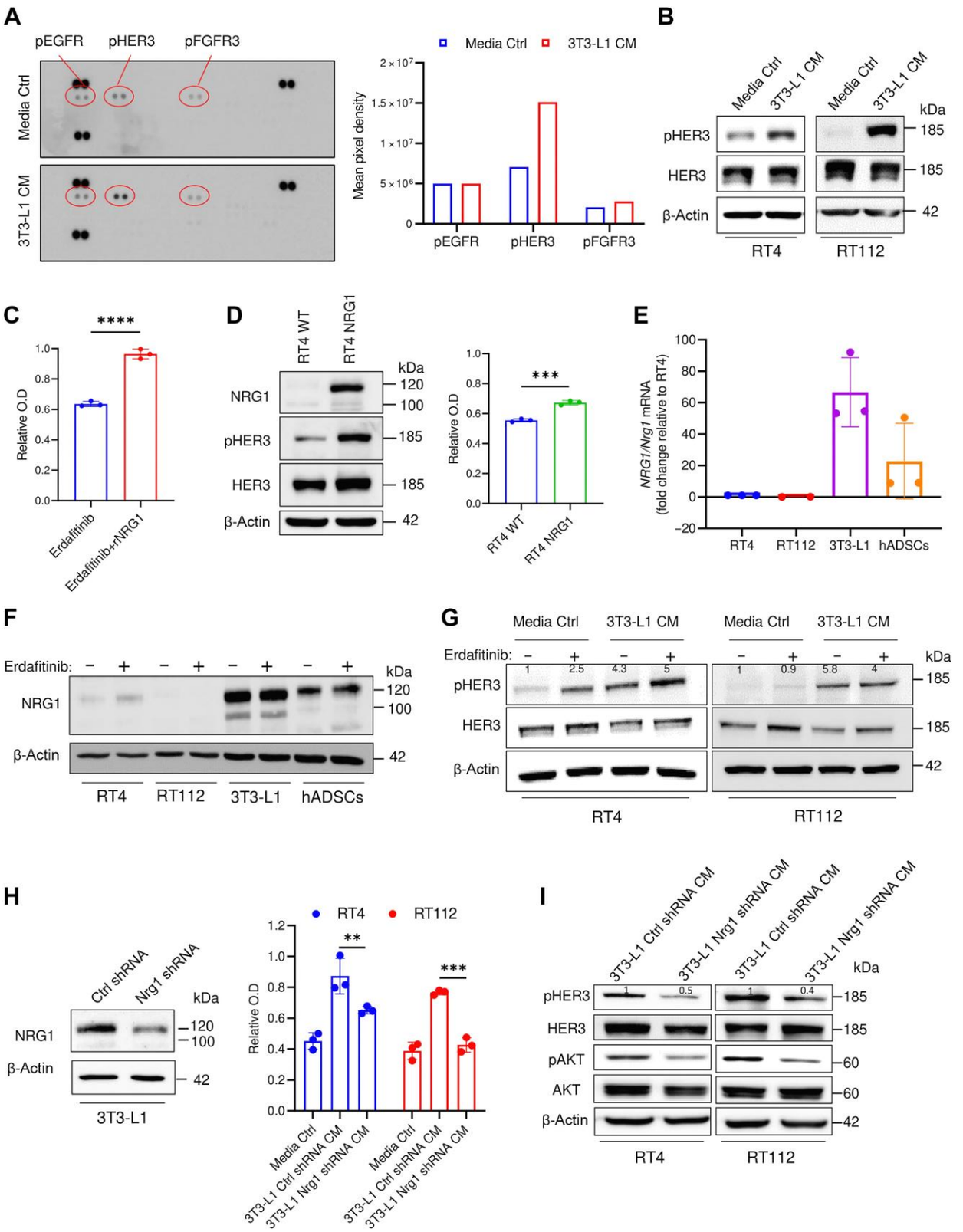
A
pEGFR
pHER3
pFGFR3
Media Ctrl
3T3-L1 CM
Media Ctrl
3T3-L1 CM
Mean pixel density
pEGFR
pHER3
pFGFR3
B
Media Ctrl
3T3-L1 CM
Media Ctrl
3T3-L1 CM
kDa
pHER3
HER3
β-Actin
185
185
42
RT4
RT112
C
****
Relative O.D
Erdafitinib
Erdafitinib+rNRG1
D
RT4 WT
RT4 NRG1
kDa
NRG1
pHER3
HER3
β-Actin
120
100
185
185
42
***
Relative O.D
RT4 WT
RT4 NRG1
E
NRG1/Nrg1 mRNA
(fold change relative to RT4)
RT4
RT112
3T3-L1
hADSCs
F
Erdafitinib:
kDa
NRG1
β-Actin
120
100
42
RT4
RT112
3T3-L1
hADSCs
G
Media Ctrl
3T3-L1 CM
Media Ctrl
3T3-L1 CM
Erdafitinib:
kDa
pHER3
HER3
β-Actin
1
2.5
4.3
5
1
0.9
5.8
4
185
185
42
RT4
RT112
H
Ctrl shRNA
Nrg1 shRNA
kDa
NRG1
β-Actin
120
100
42
3T3-L1
RT4
RT112
**
***
Relative O.D
Media Ctrl
3T3-L1 Ctrl shRNA CM
3T3-L1 Nrg1 shRNA CM
Media Ctrl
3T3-L1 Ctrl shRNA CM
3T3-L1 Nrg1 shRNA CM
I
3T3-L1 Ctrl shRNA CM
3T3-L1 Nrg1 shRNA CM
3T3-L1 Ctrl shRNA CM
3T3-L1 Nrg1 shRNA CM
kDa
pHER3
HER3
pAKT
AKT
β-Actin
1
0.5
1
0.4
185
185
60
60
42
RT4
RT112

expression of FGFR3 in RT4 and RT112 cell lines (Fig. 1A), which was detected as multiple bands indicative of FGFR3–Transforming Acidic Coiled-Coil Containing Protein 3 (TACC3) fusions at different breakpoints (33, 34). FGFR3–TACC3 fusions lead to constitutive phosphorylation of the FGFR3 tyrosine kinase residues, promoting aberrant FGFR3 activation and consequent growth induction (35). FGFR3–TACC3 fusions have been clinically associated with a greater sensitivity to FGFR3 inhibitors (36, 37). Proliferation analysis demonstrated that MB49, TCCSUP, and T24 are not susceptible to erdafitinib treatment, whereas RT4 and RT112 respond with an IC_{50} of 10 nmol/L (Fig. 1B), as reported previously (14). To assess an on-target effect at the molecular level, RT4 and RT112 cells were treated with vehicle, 10 or 100 nmol/L erdafitinib. As expected, Western blot analysis showed a dose-dependent inactivation of ERK1/2 in RT4 and RT112 cells (Fig. 1C), whereas AKT was only inactivated in RT112 (Fig. 1C; ref. 9). On the basis of the recent reports describing the protumoral role of adipocyte precursors in several cancers (16, 20–23), we aimed to investigate the potential paracrine effect of adipocyte precursors on erdafitinib susceptibility (Fig 1D). CM of adipocyte precursor cell lines, 3T3-L1 cells and hADSCs, conferred significant resistance against erdafitinib in RT4 and RT112 cells, shown by unrepressed proliferation (Fig. 1E). To note, CM of 3T3-L1 cells collected without serum conferred equivalent resistance to that collected with serum, which indicates that the resistance factor is not stimulated by serum (Supplementary Fig. S1B). Importantly, 3T3-L1 cells were refractory to erdafitinib treatment, even at a concentration of 1,000 nmol/L (Supplementary Fig. S1C). At the molecular level, AKT pathway was activated in RT4 and RT112 cells grown in CM of 3T3-L1 cells compared with media control under erdafitinib treatment (Fig. 1F). Of note, deactivation of ERK1/2 in response to erdafitinib treatment was still observed when RT112 cells were treated in 3T3-L1 CM (Fig. 1F), suggesting that AKT activation may serve as a compensatory growth-promoting pathway in the case of ERK1/2 inhibition. We postulated that the resistance-promoting effect of adipocyte precursors' CM on cancer cells during anti-FGFR treatment could occur through three possible mechanisms: metabolites, vesicles that carry genetic material, or proteins such as growth factors secreted by adipocyte precursor cells. To test this hypothesis, conditioned media was heat-inactivated at 95ºC for 10 minutes. Indeed, heat inactivation abolished the ability of adipocyte precursors' CM to rescue proliferation during erdafitinib treatment, suggesting that the soluble factors responsible for conferring resistance are proteins (Fig. 1G). To confirm this, CM from 3T3-L1 cells was filtered through a protein-binding column and the flowthrough (protein-depleted fraction) was collected. The flowthrough did not confer any resistance to erdafitinib, confirming that the factor responsible for the observed resistance is a protein (Supplementary Fig. S1D). Taken together, these data show that adipocyte precursors can confer anti-FGFR3 resistance in bladder cancer via soluble proteins in a paracrine manner.

NRG1 is secreted from adipocyte precursors and induces erdafitinib resistance in bladder cancer cells by activating HER3 signaling

To screen for the mediator responsible for the observed erdafitinib resistance, we performed a phosphorylated-receptor tyrosine kinase (phospho-RTK) array analysis on RT4 cells cultured in conditioned media of 3T3-L1 cells or media control. The phospho-RTK array revealed phosphorylated human epidermal growth factor receptor 3 (pHER3) as the only activated RTK in the conditioned media treatment compared to the media control (Fig. 2A). In parallel, Western blot analysis confirmed the activation of pHER3 in RT4 and RT112 cells when cultured with 3T3-L1 cells and hADSCs CM (Fig. 2B; Supplementary Fig. S2A). Because the phospho-RTK array was conducted on human RT4 cells stimulated with murine 3T3-L1 CM (Fig. 2A), we sought to investigate potential species-related differences in modulating RTKs. To address this, an additional phospho-RTK was performed on RT4 cells treated with CM of hADSCs or media control. In line with the previous results (Fig. 2A), this phospho-RTK revealed that pHER3 is the only upregulated kinase in the CM treatment compared to media control (Supplementary Fig. S2B), suggesting no bias related to species-mismatch. Because neuregulin 1 (NRG1) is the best characterized and principal ligand of HER3 (38), we investigated whether recombinant NRG1 (rNRG1) can recapitulate the resistance conferred by the CM of adipocyte precursors. Notably, rNRG1 induced significant resistance against erdafitinib in RT4 cells (Fig. 2C). To confirm this phenotype in an additional model, we stably overexpressed NRG1 in RT4 cells (RT4 NRG1), where HER3 activation was shown (Fig. 2D; Supplementary Fig. S2C). In line with our previous results, RT4 NRG1 cells are resistant against erdafitinib compared with the wild-type cells (Fig. 2D). Further, qRT-PCR analysis using *NRG1*/*Nrg1*-specific primers showed that 3T3-L1 and hADSCs express high levels of *Nrg1*, whereas RT4 and RT112 cells barely express *NRG1* (Fig. 2E). To gain further insights on the dynamics of NRG1 expression upon FGFR3 inhibition, we analyzed the protein levels of NRG1 in bladder cancer cell lines and adipocyte precursors treated with erdafitinib or vehicle control. Consistent with the *NRG1*/*Nrg1* mRNA expression (Fig. 2E), NRG1 protein levels were highest in both adipocyte precursor cell lines compared with the

Figure 2.

NRG1 is secreted from preadipocytes and induces erdafitinib resistance in RT4 and RT112 bladder cancer cells by activating HER3. A, Left, RTK array on RT4 cells cultured in media control (ctrl) or CM of 3T3-L1 cells for 16 hours. Right, quantification of mean pixel density of the RTK array shown on the left. Data are represented as mean of the duplicate dots per kinase. B, Western blot analysis of pHER3 in RT4 and RT112 cells cultured in media control or CM of 3T3-L1 cells for 16 hours. b-Actin served as a loading control. C, Proliferation analysis of RT4 cells treated with 10 nmol/L erdafitinib in DMEM, with or without 50 ng/mL recombinant NRG1. Crystal violet staining was performed on day 7. Data were normalized to cells treated with vehicle. Data are represented as mean ± SD. Three biological replicates were performed. Unpaired *t* test was used for statistical analysis. D, Left, Western blot analysis of baseline NRG1 and pHER3 in RT4 WT cells and NRG1-overexpressing RT4 (RT4 NRG1) cells. b-Actin served as a loading control. Right, proliferation analysis of RT4 WT cells and RT4 NRG1 cells treated with 10 nmol/L erdafitinib in DMEM. Crystal violet staining was performed on day 7. Data are normalized to cells treated with vehicle. Data are represented as mean ± SD. Three biological replicates were performed. Unpaired *t* test was used for statistical analysis. E, qRT-PCR analysis of baseline *NRG1* expression in RT4, RT112, 3T3-L1, and hADSC cells. Two to three biological replicates were performed. Expression levels are normalized to *GAPDH*. Data are represented as mean ± SD. F, Western blot analysis of NRG1 in RT4, RT112, 3T3-L1, and hADSC cells treated for 16 hours in 10 nmol/L erdafitinib or vehicle control. b-Actin served as a loading control. G, Western blot analysis of pHER3 in RT4 and RT112 cells treated for 16 hours with 10 nmol/L erdafitinib or vehicle control in media control or 3T3-L1 CM. b-Actin served as a loading control. H, Left, Western blot analysis of NRG1 in 3T3-L1 cells transduced with lentivirus encoding control shRNA or Nrg1 shRNA. b-Actin served as a loading control. Right, proliferation analysis of RT4 and RT112 cells treated with 10 nmol/L erdafitinib in media control or CM of 3T3-L1 ctrl/Nrg1 shRNA cells. Crystal violet staining was performed on day 7. Data were normalized to cells treated with vehicle. Three biological replicates were performed. Data are represented as mean ± SD. Two-way ANOVA was used for statistical analysis. I, Western blot analysis of pHER3 and pAKT in RT4 and RT112 cells treated with CM of 3T3-L1 ctrl/Nrg1 shRNA cells for 16 hours. b-Actin served as a loading control. **, $P < 0.01$; ***, $P < 0.001$; ****, $P < 0.0001$.

bladder cancer cell lines (Fig. 2F). Although the *NRG1*/NRG1 mRNA and protein levels remained unchanged upon erdafitinib treatment in adipocyte precursors, they slightly increased upon erdafitinib treatment in RT4 cells (Fig. 2F; Supplementary Fig. S2D) as reported previously (11, 12, 14). Nevertheless, the mRNA and protein levels of *NRG1*/NRG1 in erdafitinib-treated RT4 cells remain negligible compared with those in adipocyte precursors, supporting a paracrine mechanism of resistance to anti-FGFR inhibition, mediated by NRG1. Further Western blot analysis of pHER3 demonstrated clear upregulation of pHER3 in RT4 and RT112 cells cultured in 3T3-L1 CM, with and without erdafitinib treatment, compared with media control (Fig. 2G). Although pHER3 was upregulated upon erdafitinib treatment in media control in RT4 cells, pHER3 expression upon erdafitinib treatment in CM was higher (Fig. 2G). To investigate whether NRG1 is the principal mediator of resistance in the CM of adipocyte precursors, Nrg1/NRG1 shRNA was stably expressed by means of lentiviral transduction in 3T3-L1 cells and hADSCs, respectively. Western blot analysis of NRG1 revealed a robust knockdown of NRG1 in 3T3-L1 Nrg1 shRNA cells (Fig. 2H), and a complete knockdown of NRG1 in hADSCs NRG1 shRNA (Supplementary Fig. S2E). Unlike CM of 3T3-L1 cells and hADSCs expressing control shRNA, CM of Nrg1/NRG1 shRNA cells failed to confer comparable resistance to erdafitinib in RT4 and RT112 cells (Fig. 2H; Supplementary Fig. S2E). Of note, CM of 3T3-L1 Nrg1 shRNA cells conferred slight resistance in RT4 cells, which could be attributed due to the incomplete knockdown of Nrg1 in 3T3-L1 cells (Fig. 2H), and to the intrinsic upregulation of NRG1 in RT4 cells upon erdafitinib treatment (Fig. 2F and G). To verify the effect of Nrg1/NRG1 knockdown on downstream signaling, further Western blot analysis of RT4 and RT112 cells treated with CM of 3T3-L1 cells and hADSCs expressing control or Nrg1/NRG1 shRNA was performed. This Western blot revealed a downregulation of pHER3 and pAKT upon treatment with CM of Nrg1/NRG1 shRNA cells compared with CM of control shRNA cells (Fig. 2I; Supplementary Fig. S2F). Moreover, to confirm the observed HER3 and AKT regulation by CM of 3T3-L1 cells in species-matched cells, murine MB49 cells were treated with media control, or CM of 3T3-L1 cells expressing control or Nrg1 shRNA. Western blot analysis of these cells showed upregulation of pHER3 and pAKT upon treatment with CM of 3T3-L1 control shRNA cells compared with media control, and downregulation of pHER3 and pAKT upon treatment with CM of 3T3-L1 Nrg1 shRNA cells compared with CM of 3T3-L1 control shRNA cells (Supplementary Fig. S2G). This corroborates the previously observed regulation of pHER3 and pAKT upon CM treatment in human RT4 and RT112 cells, and implies the lack of disparity due to species-mismatch. Because HER3 lacks kinase activity, it is known to heterodimerize with HER2 or EGFR upon ligand binding (39). Therefore, we analyzed pHER2 and pEGFR upon conditioning RT4 and RT112 cells with 3T3-L1 CM by Western blot analysis (Supplementary Fig. S2H). This analysis showed downregulation of pHER2 in CM treated cells compared with media control treated cells, and a lack of pEGFR expression in both conditions, suggesting the dimerization of HER3 with HER2 upon HER3 activation by NRG1. To sum, these results suggest that NRG1 is secreted into the CM of 3T3-L1 cells and hADSCs, and mediates resistance against erdafitinib by activating the HER3/HER2 pathway.

NRG1-mediated resistance against erdafitinib is restricted to preadipocytes

The 3T3-L1 cell line is widely used in adiposity research and is an adipocyte precursor cell line that can, under specific conditions, differentiate into adipocytes (26). To test whether NRG1 secretion is restricted to preadipocytes, we applied a differentiation protocol to generate adipocytes from 3T3-L1 cells (26). The production of lipid droplets (Fig. 3A), and the upregulation of the main adipocytic markers such as cluster of differentiation 36 (*Cd36*), Leptin (*Lep*), solute carrier family 2 (facilitated glucose transporter), member 4 (*Glut4*), and lipoprotein lipase (*Lpl*; refs. 40–43) confirmed the differentiation process (Supplementary Fig. S3). Remarkably, CM from differentiated adipocytes (7 days post-differentiation) failed to rescue the growth inhibition in RT4 cells treated with erdafitinib, compared with the media control (Fig. 3B), implying that the resistance phenotype is restricted to adipocyte precursor-derived NRG1. Importantly, *Nrg1* mRNA levels were greatly reduced in terminally differentiated adipocytes when compared with 3T3-L1 progenitor cells (Fig. 3C). In line with the mRNA levels of *Nrg1*, Western blot analysis of NRG1 revealed gradual downregulation of protein expression during adipogenic differentiation (Fig. 3D). Primary preadipocytes from murine white adipose tissue were isolated to validate the dynamic expression of *Nrg1* (Fig. 3E). Indeed, *Nrg1* mRNA expression was significantly downregulated after adipogenic differentiation of primary preadipocytes (Fig. 3F), confirming the dynamic expression observed upon differentiation of 3T3-L1 cells (Fig. 3C and D). Moreover, 3T3-L1-derived adipocytes' CM failed to activate HER3 and AKT in RT4 and RT112 cells (Fig. 3G). Taken together, these results highlight the restriction of NRG1 expression in preadipocytes, and the impact of this dynamic expression on resistance.

Pertuzumab reverses NRG1-mediated resistance against erdafitinib

Having established the paracrine NRG1/HER3 signaling as a driver of rapid resistance to FGFR inhibition, we next explored the inhibitory effect of this signaling pathway *in vitro* and *in vivo*. We first treated RT4 and RT112 cell lines cultured in adipocyte precursors CM with erdafitinib alone or in combination with a HER2/HER3 dimerization-inhibitory antibody, pertuzumab (44, 45). A negligible growth inhibition on proliferation was observed in RT4 and RT112 cells cultured in adipocytes precursors' CM and treated with pertuzumab as single agent (Fig. 4A). However, cotreatment with erdafitinib and pertuzumab significantly reversed the resistance mediated by adipocyte precursors' CM (Fig. 4A). To investigate whether pertuzumab leads to reversal of resistance or resensitization, RT4 and RT112 cells were temporally treated with erdafitinib in media ctrl or 3T3-L1 CM for 3 days, and pertuzumab was added (or not added) on the third day of treatment. This proliferation analysis revealed a marked growth arrest in the cells that were treated with the combination treatment of erdafitinib and pertuzumab in 3T3-L1 CM, compared with those that were only treated with erdafitinib in 3T3-L1 CM. These results imply that pertuzumab leads to the reversal of resistance to erdafitinib conferred by 3T3-L1 CM, rather than resensitization (Supplementary Fig. S4A). Accordingly, combination treatment of erdafitinib and pertuzumab abolished activation of AKT and HER3 in cells cultured in CM of 3T3-L1 (Fig. 4B). We then evaluated the antitumoral effect of the combined treatment using a xenograft mouse model of RT4 and RT4 NRG1 cells (Fig. 4C). In line with the *in vitro* results, erdafitinib treatment demonstrated potent and sustained antitumor activity, indicated by prolonged survival of RT4 tumor-harboring mice and diminished tumoral Ki-67 expression (Fig. 4D and E). Thereafter, we carried out an *in vivo* approach to assess the combinational effect of both erdafitinib and pertuzumab on RT4 NRG1 xenografts. Interestingly, erdafitinib induced only insignificant prolongation of survival

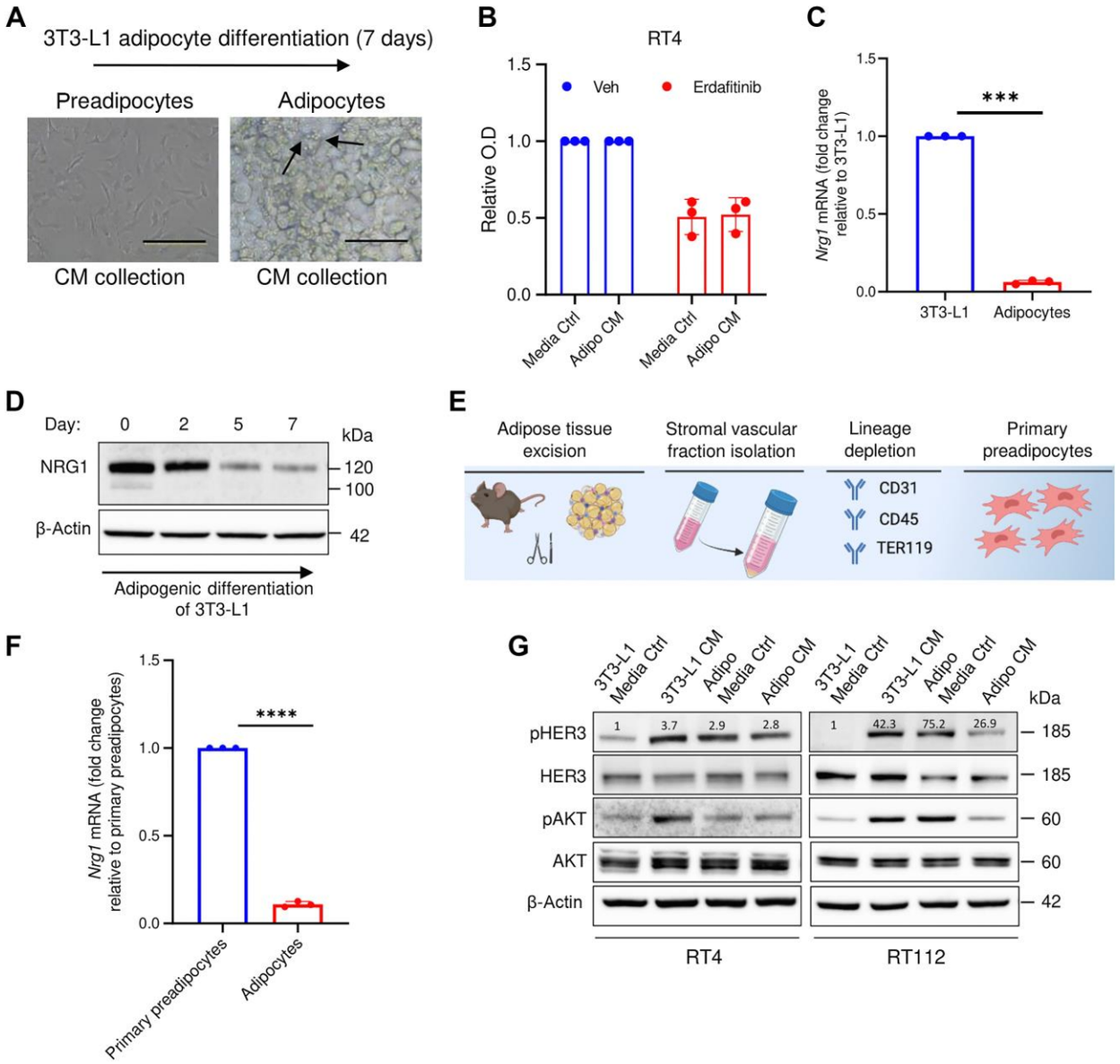

Figure 3.

NRG1-mediated resistance against erdafitinib is restricted to preadipocytes. A, Representative images showing the adipogenic differentiation of 3T3-L1 cells (preadipocytes) to differentiated adipocytes. The differentiation process was carried out for 7 days. Arrows, formation of lipid droplets in adipocytes. B, Proliferation analysis of RT4 cells treated with 10 nmol/L erdafitinib in media control (ctrl) or CM of adipocytes collected after 7 days of differentiation. Crystal violet staining was performed on day 7. Data were normalized to cells treated with vehicle. Three biological replicates were performed. Data are represented as mean ± SD. C, qRT-PCR analysis of baseline *NRG1* expression in 3T3-L1 cells and 3T3-L1-derived adipocytes. Three biological replicates were performed. Expression levels are normalized to *GAPDH*. Data are represented as mean ± SD. D, Western blot analysis of NRG1 in 3T3-L1 under adipogenic differentiation. b-Actin served as a loading control. E, Schematic illustration of the process of isolating primary preadipocytes from mice. F, qRT-PCR analysis of baseline *NRG1* expression in primary preadipocytes and primary preadipocyte-derived adipocytes. Three biological replicates were performed. Expression levels are normalized to *GAPDH*. Data are represented as mean ± SD. G, Western blot analysis of pHER3 and pAKT in RT4 and RT112 cells treated with CM of 3T3-L1 cells or 3T3-L1-derived adipocytes, or the respective media control. b-Actin served as a loading control. Unpaired *t* test was used for statistical analysis. ***, $P < 0.001$; ****, $P < 0.0001$. (E, Created with BioRender.com.)

and Ki-67 reduction in RT4 NRG1 xenografts, confirming that NRG1/HER3 signaling confers resistance to anti-FGFR3 treatment *in vivo* (Fig. 4F and G; Supplementary Fig. S4B). Similar to erdafitinib treatment as a single agent, pertuzumab monotreatment showed minor antitumoral effect on RT4 NRG1 xenografts (Fig. 4F and G; Supplementary Fig. S4B). Importantly, RT4 NRG1 xenografts treated with combination of erdafitinib and pertuzumab showed increased overall survival of mice as indicated by Kaplan–Meier cumulative survival curve (Fig. 4F), and reduced Ki-67 staining, and tumor volume (Fig. 4G; Supplementary Fig. S4B). These data demonstrate

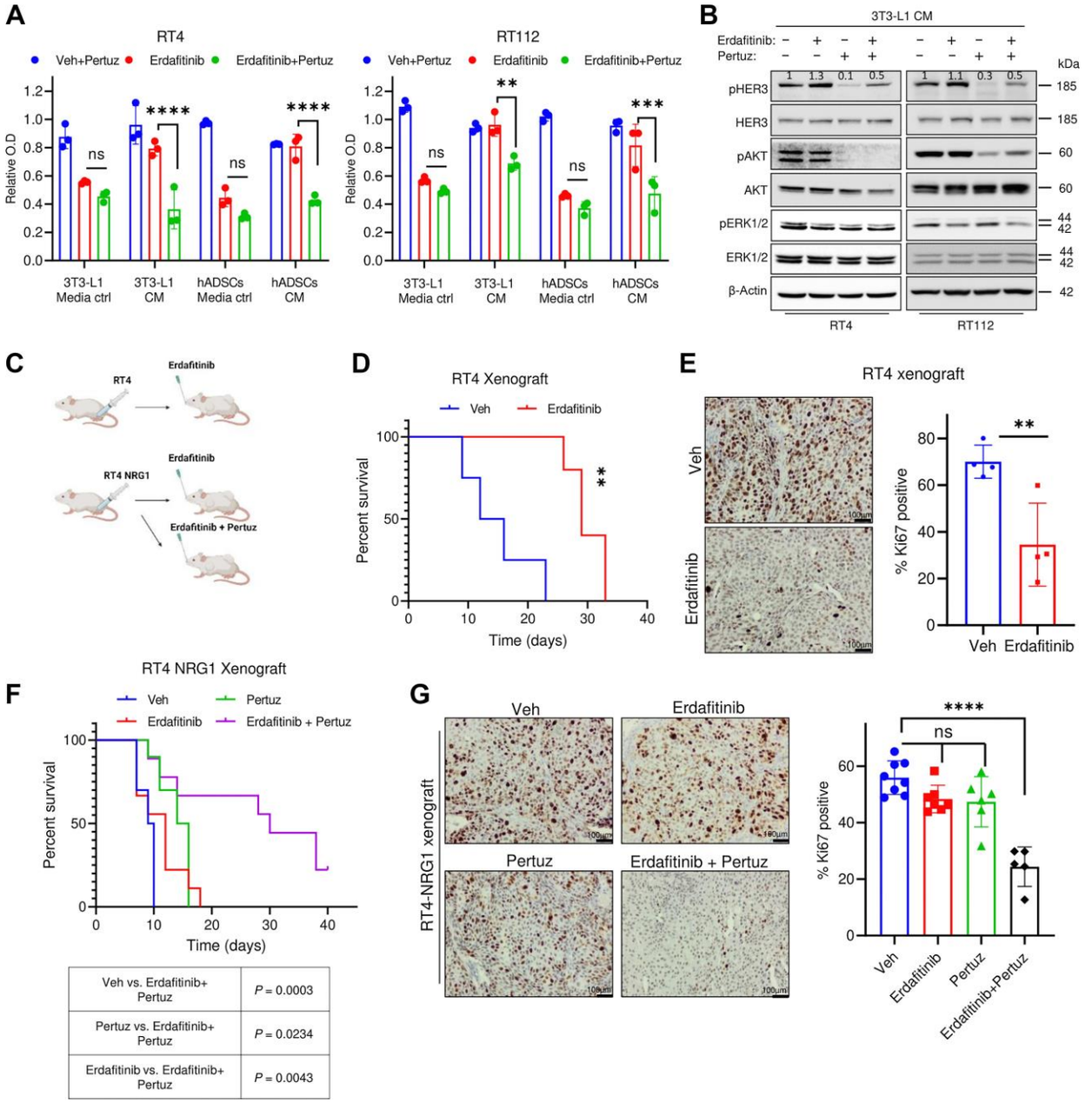

Figure 4.

Pertuzumab reverses NRG1-mediated resistance against erdafitinib. A, Proliferation analysis of RT4 and RT112 treated with 10 mg/mL pertuzumab (Pertuz) and vehicle control (Veh), 10 nmol/L erdafitinib, or erdafitinib and pertuzumab. Cells were treated in media control (ctrl) or CM of 3T3-L1 cells or hADSCs. Crystal violet staining was done on day 7. Data are normalized to cells treated with vehicle. Three biological replicates were performed. Data are represented as mean ± SD. Two-way ANOVA was used for statistical analysis. B, Western blot analysis of pHER3, pAKT, pERK1/2 in RT4 and RT112 treated with 10 mg/mL pertuzumab and vehicle control (Veh), 10 nmol/L erdafitinib, or erdafitinib and pertuzumab in 3T3-L1 CM. b-Actin served as a loading control. C, Schematic diagram of *in vivo* model performed by injecting RT4 or RT4 NRG1 cells in CB17-SCID mice. D, Kaplan–Meier survival curve of RT4-tumor bearing CB17-SCID mice treated with vehicle or 5 mg/kg erdafitinib. Four mice were tested per group in D and E. Log-rank (Mantel–Cox) test was used for statistical analysis. E, Left, IHC staining of Ki67 on RT4 xenografts treated as in D. Right, quantification of IHC staining of Ki67. Unpaired *t* test was used for statistical analysis. F, Kaplan–Meier survival curve of RT4 NRG1 tumor-bearing CB17-SCID mice treated with vehicle, 5 mg/kg erdafitinib, 5 mg/kg pertuzumab, or combinational treatment. The number of mice tested per group was: 9 mice in the erdafitinib and the combination treatment groups, 10 mice in the vehicle and pertuzumab treatment groups. Log-rank (Mantel–Cox) test was used for statistical analysis. G, Left, IHC staining of Ki67 on RT4 NRG1 xenografts treated as in F. Right, quantification of IHC staining of Ki67. The number of xenografts (each from a different mouse) analyzed per group is 8 in the vehicle group, 7 in the erdafitinib group, 6 in the pertuzumab group, and 5 in the combination treatment group. One-way ANOVA was used for statistical analysis. **, $P < 0.01$; ***, $P < 0.001$; ****, $P < 0.0001$; n.s., not significant. (C, Created with BioRender.com.)

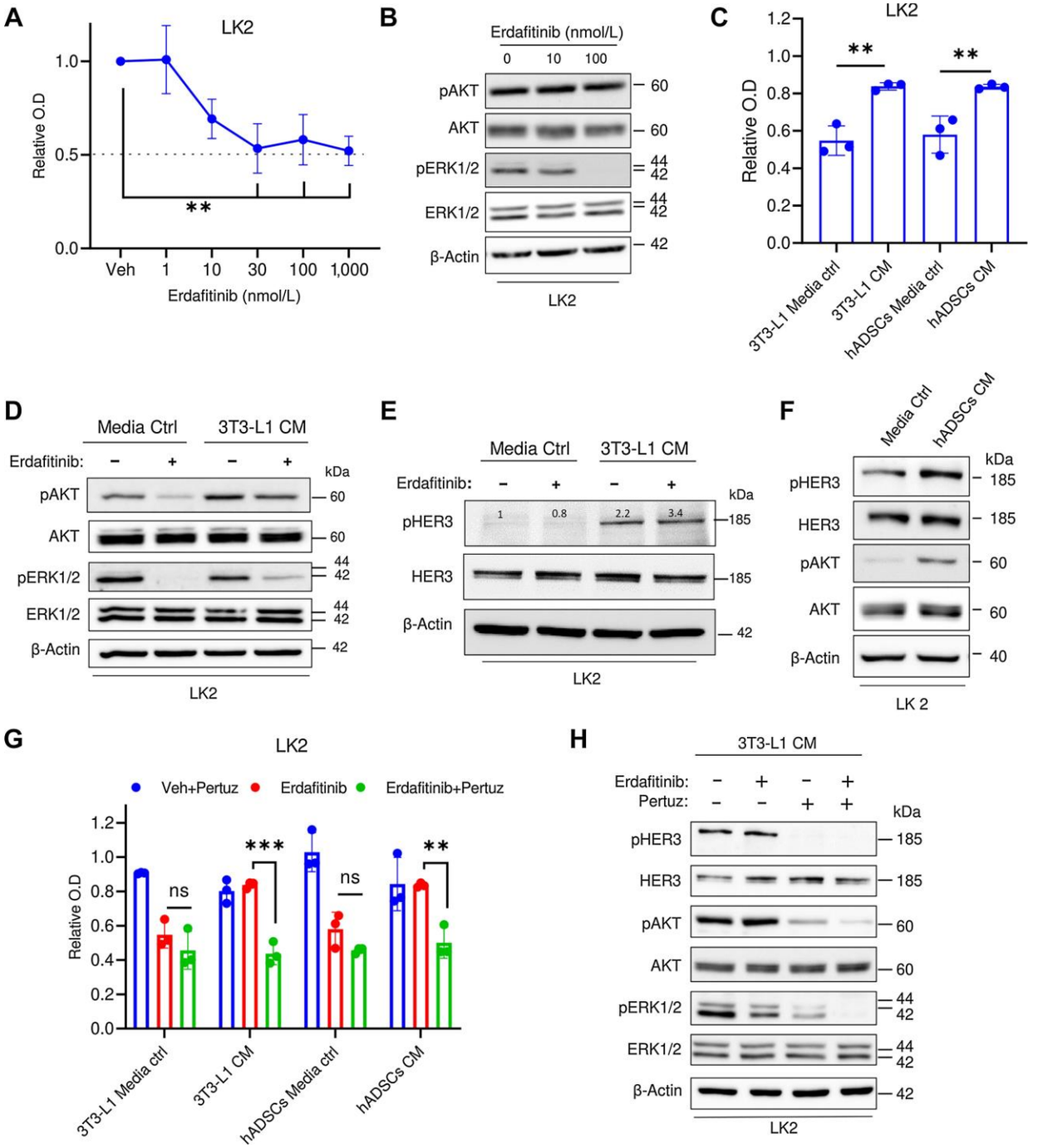

Figure 5.

NRG1 mediates resistance against erdafitinib in lung carcinoma cell line LK2. A, Proliferation analysis of LK2 cells treated with vehicle (Veh) or erdafitinib (1, 10, 30, 100, and 1,000 nmol/L). Crystal violet staining was done on day 7. Three biological replicates were performed. Data are represented as mean ± SD. One-way ANOVA was used for statistical analysis. B, Western blot analysis of pAKT and pERK12/ in LK2 cells treated with vehicle control, 10 or 100 nmol/L Erda for 16 hours. b-Actin served as a loading control. C, Proliferation analysis of LK2 cells treated with 30 nmol/L erdafitinib in media control (ctrl) or CM of 3T3-L1 cells or hADSCs. Crystal violet staining was done on day 7. Data are normalized to cells treated with vehicle. Three biological replicates were performed. Data are represented as mean ± SD. One-way ANOVA was used for statistical analysis. D, Western blot analysis of pAKT and pERK1/2 in LK2 cells treated with vehicle control, or 100 nmol/L Erda in media control or CM of 3T3-L1 cells for 16 hours. b-Actin served as a loading control. E, Western blot analysis of pHER3 in LK2 cells treated with vehicle control, or 100 nmol/L Erda in media control or CM of 3T3-L1 cells for 16 hours. b-Actin served as a loading control. F, Western blot analysis of pHER3 and pAKT in LK2 cells treated with media control or CM of hADSCs for 16 hours. b-Actin served as a loading control. G, Proliferation analysis of LK2 cells treated with 10 mg/mL pertuzumab (Pertuz) and vehicle control (Veh), 10 nmol/L Erda, or Erda and pertuzumab. Cells were treated in media control or CM of 3T3-L1 cells or hADSCs. Crystal violet staining was done on day 7. Data were normalized to cells treated with vehicle. Three biological replicates were performed. Data are represented as mean ± SD. Two-way ANOVA was used for statistical analysis. H, Western blot analysis of pHER3, pAKT, and pERK1/2 in LK2 cells treated with vehicle, 10 mg/mL pertuzumab, 100 nmol/L Erda, or Erda and pertuzumab. Cells were treated in CM of 3T3-L1 cells. b-Actin served as a loading control. **, $P < 0.01$; ***, $P < 0.001$; n.s., not significant.

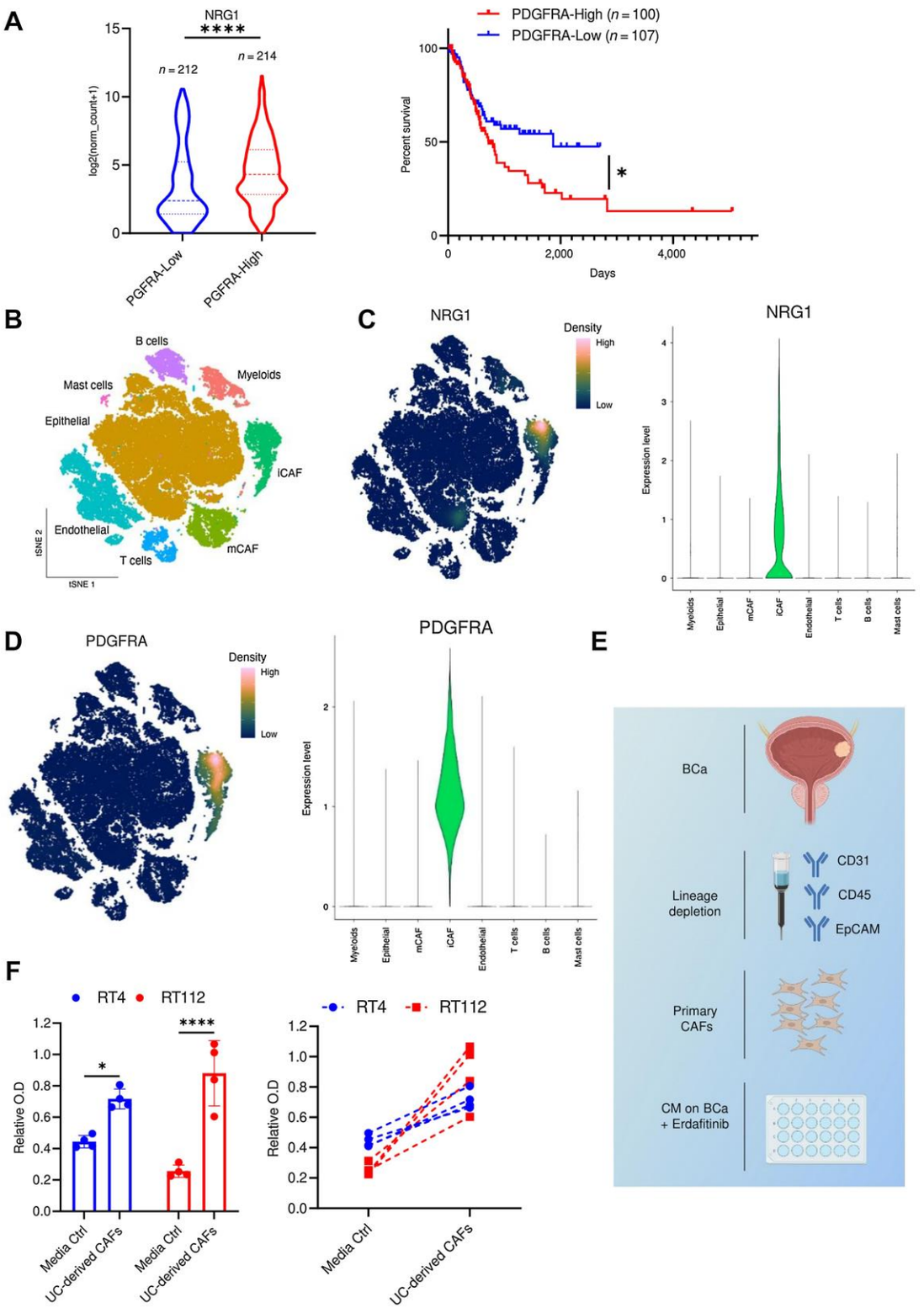
A
NRG1
****
n = 212
n = 214
log2(norm_count+1)
PGFRA-Low
PGFRA-High
PDGFRA-High (n = 100)
PDGFRA-Low (n = 107)
Percent survival
Days
B
B cells
Mast cells
Myeloids
Epithelial
iCAF
Endothelial
mCAF
T cells
tSNE 2
tSNE 1
C
NRG1
Density
High
Low
Expression level
Myeloids
Epithelial
mCAF
iCAF
Endothelial
T cells
B cells
Mast cells
D
PDGFRA
Density
High
Low
E
BCa
Lineage depletion
CD31
CD45
EpCAM
Primary CAFs
CM on BCa + Erdafitinib
F
RT4
RT112
Relative O.D
Media Ctrl
UC-derived CAFs

that NRG1 mediates resistance to erdafitinib *in vitro* and *in vivo*, and can potentially be exploited for therapeutic targeting using clinically approved inhibitors of the NRG1/HER3 signaling axis, such as pertuzumab.

NRG1 mediates resistance against erdafitinib in FGFR1-dependent lung carcinoma

Because FGFRs are altered in other tumor types like lung cancer, we investigated whether the observed NRG1-driven resistance mechanism can be of clinical relevance in other tumor entities. Here we utilized the non–small cell lung carcinoma (NSCLC) cell line, LK2, that is FGFR1-driven (46). First, we confirmed the overexpression of FGFR1 mRNA in this cell line (Supplementary Fig. S5). Proliferation analysis revealed significant growth inhibition by erdafitinib (Fig. 5A), and Western blot analysis showed inactivation of ERK1/2 in LK2 cells (Fig. 5B). Similar to bladder cancer cell lines, CM of 3T3-L1 cells and hADSCs, conferred significant resistance against erdafitinib-mediated growth inhibition in LK2 cell line (Fig. 5C). At the molecular level, the HER3/AKT axis was activated in LK2 cells grown in CM of 3T3-L1 cells compared with media control with or without erdafitinib treatment (Fig 5D and E). Of note, similar to RT112 cells, deactivation of ERK1/2 in response to erdafitinib treatment was still observed in LK2 cells treated in CM of 3T3-L1 cells (Fig. 5D). Similarly, HER3 and AKT were also upregulated upon treatment of LK2 cells in hADSCs CM compared with media control (Fig. 5F). We next tested the inhibitory effect of erdafitinib in combination with pertuzumab in LK2 cell line. Although a minor proliferation inhibition effect was observed in LK2 cells cultured in adipocytes precursors' CM and treated with erdafitinib or pertuzumab as single agents, combinational treatment of both drugs significantly reversed the resistance phenotype mediated by adipocyte precursors' CM (Fig. 5G). In line with our results in bladder cancer cell lines, cotreatment of erdafitinib and pertuzumab abolished the activation of HER3 and AKT in LK2 cells cultured in 3T3-L1 CM (Fig 5H). Together, our results demonstrate that the activation of NRG1/HER3 axis induces erdafitinib resistance in FGFR1-dependent NSCLC, which may imply potential clinical relevance in other FGFR-driven tumor entities.

NRG1 expression correlates with preadipocytic markers and is predominantly expressed in inflammatory CAFs in human bladder carcinoma

The platelet-derived growth factor receptor-A (PDGFRA) is one of the most established markers of mesenchymal cells, and is differentially expressed on adipocyte precursors but not on mature adipocytes (47, 48). To assess whether NRG1 expression correlates with PDGFRA expression in urothelial cancer, we analyzed RNA-seq data from TCGA BLCA cohort. This analysis revealed that NRG1 expression is significantly higher in patients that have high PDGFRA expression (PDHFRA-High) compared with those with low expression (PDGFRA-Low; Fig. 6A). Interestingly, higher PDGFRA expression correlated with significantly lower survival (Fig. 6A). To assess the clinical relevance of NRG1 in urothelial cancer, we performed IHC staining of NRG1 on a cohort of 154 paraffin-embedded human muscle-invasive urothelial bladder cancer (MIBC) samples (49, 50). We found that both tumors and stroma showed expression of NRG1 (Supplementary Fig. S6A). Interestingly, stromal NRG1 expression levels increased with tumor stage (Supplementary Fig. S6B; Table 1). To gain further insights into the clinical relevance of NRG1-expressing mesenchymal cells in urothelial cancer, we accessed a publicly available scRNA-seq data set of urothelial bladder (29). As evident in the tSNE overview of sequenced cells, the authors of the dataset have identified two CAF subsets; myo-CAFs (mCAF) and inflammatory CAFs (iCAF; Fig. 6B). NRG1 was predominantly expressed within the iCAF subset (Fig. 6C). Importantly, the expression pattern of NRG1 clearly correlated with the expression of PDGFRA, a marker of iCAFs (29) and adipocyte precursors (Fig. 6D; refs. 47, 48). NRG1 expression also correlated with preadipocyte markers, MMP3 and DPP4 (Supplementary Figs. S6C and S6D), which are known to be differentially expressed in preadipocytes but not in differentiated adipocytes (51–53). In line with this, NRG1 expression significantly correlated with the expression of MMP3 and DPP4 in the TCGA BLCA cohort (Supplementary Fig. S6E). To add more rigor to our findings, we utilized an additional scRNA-seq study that described four subclusters (C1–C4) of CAFs in bladder cancer (54). In this study, subcluster three (C3) showed high expression levels of NRG1, MMP3, and PDGFRA. Interestingly, the gene signature of C3 was clearly enriched in the iCAF population presented in Chen and colleagues (Supplementary Fig. S6F). In addition, Luo and colleagues (55) revealed that "adipogenic CAFs" (CAF_{adi}) were delineated in the same activation trajectory as iCAFs, which was identified as CAF_{state3}. CAF_{adi} were described to be expressing PDGFRA, TWIST2, TCF21, CFD, and CREB3L1, which were also enriched in the NRG1-expressing iCAF population presented in Chen and colleagues (Supplementary Fig. S6G; ref. 29). Moreover, the expression of several ADSC markers described in Zhu and colleagues (53), was also enriched in the iCAF population and most of them correlated with NRG1 expression (Table 2). To investigate the effect of primary CAFs derived from urothelial bladder, we isolated CAFs by depleting the dissociated UC tumors of CD31, CD45, and EpCAM-expressing cells by MACS (Fig. 6E). CM from urothelial bladder-derived CAFs conferred significant resistance to erdafitinib treatment in RT4 and RT112 cells (Fig. 6F). Taken together, these

Figure 6.

NRG1 expression correlates with preadipocytic markers and is predominantly expressed in inflammatory CAFs in human bladder carcinoma. A, Data obtained from the TCGA BLCA data set, *N* ¼ 426 samples. Left, expression levels of NRG1 in bladder cancer stratified based on PDGFRA expression. The low and high cutoffs were determined based on the median expression levels of PDGFRA among the samples. Ten samples did not have the expression level provided and therefore could not be included. Two-tailed unpaired *t* test was used for statistical analysis. Right, Kaplan–Meier survival analysis of patients with bladder cancer stratified based on the quartile expression of PDGFRA (PDGFRA-High, upper quartile; PDGFRA-Low, lower quartile). Statistical test: log-rank (Mantel–Cox) test. B, tSNE plot of single cells from bladder cancer and paratumor mucosa samples taken from Chen and collegues (29). Plot is colored by major cell types of the tumor microenvironment in bladder cancer. mCAF, myo-cancer–associated fibroblast. C, Imputed gene expression of NRG1 displayed as a function of expression density (left) or in a violin plot (right). D, Imputed gene expression of PDGFRA displayed as a function of expression density (left) or in a violin plot (right). E, Schematic diagram of isolation of CAFs from human bladder cancer (BCa) by MACS. Bladder cancer cell lines were treated with erdafitinib in CM from these CAFs. F, Proliferation analysis of RT4 and RT112 cells treated with 10 nmol/L erdafitinib in media control (ctrl) or CM of CAFs. Crystal violet staining was done on day 7. Data are plotted in a scatter bar graph (left) and in an aligned graph showing matched values of the CM from the same tumor (right). Data were normalized to cells treated with vehicle. Four biological replicates were performed. Data are represented as mean ± SD. Two-way ANOVA was used for statistical analysis. *, $P < 0.05$; ****, $P < 0.0001$; n.s., not significant. (E, Created with BioRender.com.)

Table 1. NRG1 expression in different MIBC stages.

	pT2	pT3	pT4	Total
NRG1 TC high/stroma high	5	23	7	35
NRG1 TC high/stroma low	14	12	5	31
NRG1 TC low/stroma high	5	21	16	42
NRG1 TC low/stroma low	20	18	8	46
Total:	44	74	36	154

results highlight the clinical relevance of CAFs in mediating erdafitinib resistance in bladder tumors.

Discussion

It is well established that resistance to RTK inhibitors commonly occurs through feedback activation of additional signaling pathways. Indeed, cancer cell-intrinsic activation of HER2/HER3 (11, 12, 14) and EGFR (13) has been previously reported as resistance determinants to FGFR inhibitors; BGJ398 (14), AZD4547 (12), and PD173074 (13). These reports have documented autocrine resistance mechanisms that develop in response to FGFR inhibition and do not consider the contribution of the TME. In the last decade, research has shed light on the association of the TME in cancer progression and therapy resistance (56–58). In this study, we investigated the effect of the crosstalk between mesenchymal cells and FGFR-driven UC and NSCLC cells in the response to erdafitinib. In summary, our results demonstrated that the CM of adipocyte precursors (3T3-L1 cells and hADSCs) confer resistance to erdafitinib in three FGFR-dependent cell lines (RT4, RT112, and LK2 cells). NRG1 secreted from adipocyte precursor cell lines was identified as a mediator of paracrine resistance against erdafitinib by activating the HER3 pathway. Interestingly, the pharmacologic blockade of the NRG1/HER3 axis using pertuzumab resensitized cancer cells to erdafitinib *in vitro* and *in vivo*. Importantly, primary preadipocytes isolated form bladder cancer tumors recapitulated the resistance to erdafitinib conferred by the adipocyte precursor cell lines. To our knowledge, the role of adipocyte precursors in treatment resistance in urothelial bladder is largely unknown and only few reports suggest their involvement in chemotherapy resistance in ovarian (23), breast (22), and pancreatic (16) cancers. Here, our study reveals the role of adipocyte precursors in promoting erdafitinib treatment resistance in urothelial bladder. The dynamics of NRG1 expression in adipocyte precursors was also demonstrated in our study. Our results showed that the expression of NRG1 is downregulated in terminally differentiated adipocytes at both RNA and protein levels compared with their progenitors. In line with this, we observed that CM of differentiated adipocytes failed to confer resistance to erdafitinib. In contrast, one report showed that CM of 3T3-L1 adipocytes and not that of parental preadipocytes conferred resistance to lapatinib in HER2þ breast cancer cells (59). However, this study did not identify the specific factor(s) responsible for this phenotype, nor did it reveal the modulation of downstream signaling proteins in response to the adipocytes' CM treatment. This impedes the constructive comparison of results. Nevertheless, we believe that the discrepancy in results could be related to the type of drug and cancer investigated (context-dependent).

Table 2. Enrichment of ADSCs' markers in iCAFs.

	iCAF (Chen et al., 2022)	NRG1 overlap
DCN	Yes	Yes
LUM	Yes	Yes
APOD	Yes	Partially
CFD	Yes	Yes
MGP	Yes	No
SERPINF1	Yes	Yes
DPT	Yes	No
COL1A2	Yes	Yes
COL6A3	Yes	Yes
CXCL12	Yes	Partially
SRPX	Yes	Yes
MMP2	Yes	Yes
CCDC80	Yes	Partially

Interestingly, secreted NRG1 has been reported to be implicated in paracrine anti-androgen resistance in prostate cancer (60, 61). Although Gil and colleagues (60) revealed that NRG1 derived from murine bone marrow–derived macrophages and myeloid-derived suppressor cells promotes prostate cancer growth, Zhang and colleagues (61) showed that CAFs secrete NRG1, which drives resistance against anti-androgen treatment in prostate cancer. Thus, our work corroborates the findings of these studies in urothelial cancer, albeit involving a specific subtype of fibroblasts, adipocyte precursors, and a novel drug, erdafitinib. FGFR3 alterations are present in 5% to 20% of muscle-invasive bladder cancer cases, and are particularly prevalent in the luminal-papillary molecular subtype (40% FGFR3-mutated; refs. 5, 6, 62). However, our data suggest that stroma-rich tumors, which mainly display luminal tumor cell differentiation (63), are less likely to respond to erdafitinib as a single-agent therapy. Importantly, HER3 is also enriched in the luminal subtype of bladder cancer (64, 65). Therefore, the enrichment of NRG1-secreting stroma in the TME could be a negative predictive biomarker for erdafitinib single-agent therapy. These tumors may be the prime candidates for our proposed combination therapy of erdafitinib and pertuzumab (66). Moreover, because obesity results in a higher frequency of ADSCs, and an altered ADSC biology towards increased protumorigenic signaling (67, 68), our proposed combination therapy could be even more relevant in obese patients. Further investigations through biomarker-driven clinical trials is necessary to confirm these hypotheses.

Our results demonstrated that the NRG1/HER3 axis also induces erdafitinib resistance to the NSCLC cell line, LK2, that is FGFR1-driven (46). These indicate that our identified TME-driven resistance mechanism can be of clinical relevance in other tumor entities, where FGFR1–4 inhibitors are used/in clinical investigation, for example, cholangiocarcinoma (NCT04083976; ref. 69).

In conclusion, this study provides preclinical evidence confirming the efficacy of cotargeting the FGFR1–4 and NRG1/HER3 pathways to overcome resistance to erdafitinib in FGFR-dependent tumors.

Authors' Disclosures

S. Hosni reports grants from Deutsche Forschungsgemeinschaft (DFG; German research society) during the conduct of the study. V. Kilian reports grants from BONFOR F€orderungsprogramm during the conduct of the study. N. Klu€mper reports personal fees from Astellas, Novartis, Ipsen, Photocure, MSD, and Eisai outside the submitted work. K. Sieckmann reports personal fees from Studienstiftung des Deutschen Volkes during the conduct of the study. O. Hahn reports grants from Janssen-Cilag and DFG, and personal fees and nonfinancial support from Bristol-Myers Squibb, AstraZeneca, Bayer, Medac, Astellas, and Merck Sharp & Dohme outside the submitted work. M. Bertlich reports grants from DFG during the conduct of the study and grants from Wolfgang.Dieckmann-Stiftung outside the submitted

work. M. Eckstein reports grants and personal fees from AstraZeneca, Janssen, Owkin, and Gilead; personal fees from MSD and Diaceutics outside the submitted work. M. H€olzel reports grants from DFG during the conduct of the study; grants and personal fees from TME Pharma AG; and personal fees from Novartis and BMS outside the submitted work. D. Wachten reports grants from DFG during the conduct of the study. A. Alajati reports grants from DFG during the conduct of the study. No disclosures were reported by the other authors.

Authors' Contributions

S. Hosni: Conceptualization, validation, investigation, writing–original draft, writing–review and editing. V. Kilian: Data curation. N. Klu€mper: Conceptualization. D. Gabbia: Data curation, formal analysis. K. Sieckmann: Investigation. D. Corvino: Formal analysis. A. Winkler: Methodology. M. Saponaro: Formal analysis, validation, investigation. K. Wo€rsdo€rfer: Investigation. D. Schmidt: Methodology. O. Hahn: Investigation. I. Zanotto: Methodology. M. Bertlich: Methodology. M. Toma: Investigation. T. Bald: Supervision. M. Eckstein: Methodology. M. Ho€lzel: Supervision. M. Geyer: Supervision. M. Ritter: Funding acquisition. D. Wachten: Supervision. S. De Martin: Validation. A. Alajati: Conceptualization, supervision, funding acquisition, writing–original draft, writing–review and editing.

Acknowledgments

S. Hosni was supported by the Deutsche Forschungsgemeinschaft (DFG; SPP2084)-AL 2692/1. V. Kilian was funded by the Sci-Med stipend (application no.: 2021–4-12). Marina Bertlich was funded by DFG (DFG SPP 2048). Research in the lab of D. Wachten was funded by DFG: SFB 1454 – Project-ID 432325352, TRR333/1 – Project-ID 450149205, FOR5547 – Project-ID 503306912, WA 3382/8–1 – Project-ID 513767027, under Germany's Excellence Strategy – EXC2151 – Project-ID 390873048. K. Sieckmann was supported by a fellowship from the DFG. T. Bald is supported by the DFG under Germany's Excellence Strategy – EXC2151–390873048. M. H€olzel was supported by the DFG under Germany's Excellence Strategy–EXC2151–390873048. Research in the lab of A. Alajati was funded by DFG (SPP2084)-AL 2692/1.

Note

Supplementary data for this article are available at Cancer Research Online (http://cancerres.aacrjournals.org/).

Received May 10, 2023; revised September 12, 2023; accepted December 21, 2023; published first January 4, 2024.

References

1. Sharma P, Callahan MK, Bono P, Kim J, Spiliopoulou P, Calvo E, et al. Nivolumab monotherapy in recurrent metastatic urothelial carcinoma (CheckMate 032): a multicentre, open-label, two-stage, multi-arm, phase 1/2 trial. Lancet Oncol 2016;17:1590–8.
2. Powles T, Rosenberg JE, Sonpavde GP, Loriot Y, Dur,an I, Lee JL, et al. Enfortumab vedotin in previously treated advanced urothelial carcinoma. N Engl J Med 2021;384:1125–35.
3. Krook MA, Reeser JW, Ernst G, Barker H, Wilberding M, Li G, et al. Fibroblast growth factor receptors in cancer: genetic alterations, diagnostics, therapeutic targets and mechanisms of resistance. Br J Cancer 2021;124:880–92.
4. Helsten T, Elkin S, Arthur E, Tomson BN, Carter J, Kurzrock R. The FGFR landscape in cancer: analysis of 4,853 tumors by next-generation sequencing. Clin Cancer Res 2016;22:259–67.
5. Kamoun A, de Reyni'es A, Allory Y, Sj€odahl G, Robertson AG, Seiler R, et al. A consensus molecular classification of muscle-invasive bladder cancer. Eur Urol 2020;77:420–33.
6. van Rhijn BWG, Mertens LS, Mayr R, Bostrom PJ, Real FX, Zwarthoff EC, et al. FGFR3 mutation status and FGFR3 expression in a large bladder cancer cohort treated by radical cystectomy: implications for anti-FGFR3 treatment?†. Eur Urol 2020;78:682–7.
7. Loriot Y, Necchi A, Park SH, Garcia-Donas J, Huddart R, Burgess E, et al. Erdafitinib in locally advanced or metastatic urothelial carcinoma. N Engl J Med 2019;381:338–48.
8. Zheng X, Wang H, Deng J, Yao M, Zou X, Zhang F, et al. Safety and efficacy of the pan-FGFR inhibitor erdafitinib in advanced urothelial carcinoma and other solid tumors: a systematic review and meta-analysis. Front Oncol 2023;12:907377.
9. Perera TPS, Jovcheva E, Mevellec L, Vialard J, De Lange D, Verhulst T, et al. Discovery and pharmacological characterization of JNJ-42756493 (Erdafitinib), a functionally selective small-molecule FGFR family inhibitor. Mol Cancer Ther 2017;16:1010–20.
10. Loriot Y, Matsubara N, Park SH, Huddart RA, Burgess EF, Houede N, et al. Phase 3 THOR study: Results of erdafitinib (erda) versus chemotherapy (chemo) in patients (pts) with advanced or metastatic urothelial cancer (mUC) with select fibroblast growth factor receptor alterations (*FGFRalt*). J Clin Oncol 2023;41 (17_suppl):LBA4619.
11. Wang J, Mikse O, Liao RG, Li Y, Tan L, Janne PA, et al. Ligand-associated ERBB2/3 activation confers acquired resistance to FGFR inhibition in FGFR3-dependent cancer cells. Oncogene 2014;34:2167–77.
12. Wang L, VSuVsti,c T, Leite de Oliveira R, Lieftink C, Halonen P, van de Ven M, et al. A functional genetic screen identifies the phosphoinositide 3-kinase pathway as a determinant of resistance to fibroblast growth factor receptor inhibitors in FGFR mutant urothelial cell carcinoma. Eur Urol 2017;71:858–62.
13. Herrera-Abreu MT, Pearson A, Campbell J, Shnyder SD, Knowles MA, Ashworth A, et al. Parallel RNA interference screens identify EGFR activation as an escape mechanism in *FGFR3* -mutant cancer. Cancer Discov 2013; 3:1058–71.
14. Weickhardt AJ, Lau DK, Hodgson-Garms M, Lavis A, Jenkins LJ, Vukelic N, et al. Dual targeting of FGFR3 and ERBB3 enhances the efficacy of FGFR inhibitors in FGFR3 fusion-driven bladder cancer. BMC Cancer 2022;22: 478.
15. Liu T, Han C, Wang S, Fang P, Ma Z, Xu L, et al. Cancer-associated fibroblasts: an emerging target of anti-cancer immunotherapy. J Hematol OncolJ Hematol Oncol 2019;12:86.
16. Miyazaki Y, Oda T, Inagaki Y, Kushige H, Saito Y, Mori N, et al. Adipose-derived mesenchymal stem cells differentiate into heterogeneous cancer-associated fibroblasts in a stroma-rich xenograft model. Sci Rep 2021;11: 4690.
17. Atiya H, Frisbie L, Pressimone C, Coffman L. Mesenchymal stem cells in the tumor microenvironment. Adv Exp Med Biol 2020;1234:31–42.
18. Quail DF, Dannenberg AJ. The obese adipose tissue microenvironment in cancer development and progression. Nat Rev Endocrinol 2019;15:139–54.
19. Saha A, Kolonin MG, DiGiovanni J. Obesity and prostate cancer - microenvironmental roles of adipose tissue. Nat Rev Urol 2023;20:579–96.
20. Maj M, Kokocha A, Bajek A, Drewa T. The interplay between adipose-derived stem cells and bladder cancer cells. Sci Rep 2018;8:15118.
21. Fajka-Boja R, Szebeni GJ, Hunyadi-Guly,as E›, Pusk,as LG, Katona RL. Polyploid adipose stem cells shift the balance of IGF1/IGFBP2 to promote the growth of breast cancer. Front Oncol 2020;10:157.
22. Lu Y, Yang Y, Liu Y, Hao Y, Zhang Y, Hu Y, et al. Upregulation of PAG1/Cbp contributes to adipose-derived mesenchymal stem cells promoted tumor progression and chemoresistance in breast cancer. Biochem Biophys Res Commun 2017;494:719–27.
23. Koren Carmi Y, Khamaisi H, Adawi R, Noyman E, Gopas J, Mahajna J. Secreted soluble factors from tumor-activated mesenchymal stromal cells confer platinum chemoresistance to ovarian cancer cells. Int J Mol Sci 2023;24:7730.
24. Zhang T, Tseng C, Zhang Y, Sirin O, Corn PG, Li-Ning-Tapia EM, et al. CXCL1 mediates obesity-associated adipose stromal cell trafficking and function in the tumour microenvironment. Nat Commun 2016;7:11674.
25. Zhang Y, Daquinag A, Traktuev DO, Amaya-Manzanares F, Simmons PJ, March KL, et al. White adipose tissue cells are recruited by experimental tumors and promote cancer progression in mouse models. Cancer Res 2009;69:5259–66.
26. Zebisch K, Voigt V, Wabitsch M, Brandsch M. Protocol for effective differentiation of 3T3-L1 cells to adipocytes. Anal Biochem 2012;425:88–90.
27. Cheng L, Montironi R, Davidson DD, Lopez-Beltran A. Staging and reporting of urothelial carcinoma of the urinary bladder. Mod Pathol Off J U S Can Acad Pathol Inc 2009;22 Suppl 2:S70–95.
28. Philip AT, Amin MB, Tamboli P, Lee TJ, Hill CE, Ro JY. Intravesical adipose tissue: a quantitative study of its presence and location with implications for therapy and prognosis. Am J Surg Pathol 2000;24:1286–90.

29. Chen Z, Zhou L, Liu L, Hou Y, Xiong M, Yang Y, et al. Single-cell RNA sequencing highlights the role of inflammatory cancer-associated fibroblasts in bladder urothelial carcinoma. Nat Commun 2020;11:5077.
30. Lamont FR, Tomlinson DC, Cooper PA, Shnyder SD, Chester JD, Knowles MA. Small molecule FGF receptor inhibitors block FGFR-dependent urothelial carcinoma growth in vitro and in vivo. Br J Cancer 2010;104:75–82.
31. Tomlinson DC, Hurst CD, Knowles MA. Knockdown by shRNA identifies S249C mutant FGFR3 as a potential therapeutic target in bladder cancer. Oncogene 2007;26:5889–99.
32. Earl J, Rico D, Carrillo-de-Santa-Pau E, Rodríguez-Santiago B, M,endez-Pertuz M, Auer H, et al. The UBC-40 urothelial bladder cancer cell line index: a genomic resource for functional studies. BMC Genomics [Electronic Resource] 2015;16:403.
33. Williams SV, Hurst CD, Knowles MA. Oncogenic FGFR3 gene fusions in bladder cancer. Hum Mol Genet 2012;22:795–803.
34. Mahe M, Dufour F, Neyret-Kahn H, Moreno-Vega A, Beraud C, Shi M, et al. An FGFR 3/MYC positive feedback loop provides new opportunities for targeted therapies in bladder cancers. EMBO Mol Med 2018;10:e8163.
35. Costa R, Carneiro BA, Taxter T, Tavora FA, Kalyan A, Pai SA, et al. *FGFR3-TACC3* fusion in solid tumors: mini review. Oncotarget 2016;7:55924–38.
36. Nassar AH, Lundgren K, Pomerantz M, Van Allen E, Harshman L, Choudhury AD, et al. Enrichment of FGFR3-TACC3 fusions in patients with bladder cancer who are young, asian, or have never smoked. JCO Precis Oncol 2018:1–11.
37. Tabernero J, Bahleda R, Dienstmann R, Infante JR, Mita A, Italiano A, et al. Phase I dose-escalation study of JNJ-42756493, an oral pan–fibroblast growth factor receptor inhibitor, in patients with advanced solid tumors. J Clin Oncol 2015;33: 3401–8.
38. Ieguchi K, Fujita M, Ma Z, Davari P, Taniguchi Y, Sekiguchi K, et al. Direct binding of the EGF-like domain of neuregulin-1 to integrins (avb3 and a6b4) is involved in neuregulin-1/ErbB signaling. J Biol Chem 2010;285:31388–98.
39. Lyu H, Han A, Polsdofer E, Liu S, Liu B. Understanding the biology of HER3 receptor as a therapeutic target in human cancer. Acta Pharm Sin B 2018;8:503–10.
40. Christiaens V, Van Hul M, Lijnen HR, Scroyen I. CD36 promotes adipocyte differentiation and adipogenesis. Biochim Biophys Acta BBA - Gen Subj 2012; 1820:949–56.
41. Bengestrate L, Virtue S, Campbell M, Vidal-Puig A, Hadaschik D, Hahn P, et al. Genome-wide profiling of MicroRNAs in adipose mesenchymal stem cell differentiation and mouse models of obesity. Navarro A., editor. PLoS One 2011;6:e21305.
42. Dalen KT, Ulven SM, Bamberg K, Gustafsson JÅ, Nebb HI. Expression of the insulin-responsive glucose transporter GLUT4 in adipocytes is dependent on liver X receptor a. J Biol Chem 2003;278:48283–91.
43. Gonzales AM, Orlando RA. Role of adipocyte-derived lipoprotein lipase in adipocyte hypertrophy. Nutr Metab 2007;4:22.
44. Agus DB, Akita RW, Fox WD, Lewis GD, Higgins B, Pisacane PI, et al. Targeting ligand-activated ErbB2 signaling inhibits breast and prostate tumor growth. Cancer Cell 2002;2:127–37.
45. Franklin MC, Carey KD, Vajdos FF, Leahy DJ, de Vos AM, Sliwkowski MX. Insights into ErbB signaling from the structure of the ErbB2-pertuzumab complex. Cancer Cell 2004;5:317–28.
46. Hibi M, Kaneda H, Tanizaki J, Sakai K, Togashi Y, Terashima M, et al. *FGFR* gene alterations in lung squamous cell carcinoma are potential targets for the multi-kinase inhibitor nintedanib. Cancer Sci 2016;107:1667–76.
47. Berry R, Jeffery E, Rodeheffer MS. Weighing in on adipocyte precursors. Cell Metab 2014;19:8–20.
48. Lee YH, Petkova AP, Mottillo EP, GJG. In Vivo identification of bipotential adipocyte progenitors recruited by b3-adrenoceptor activation and high-fat feeding. Cell Metab 2012;15:480–91.
49. Eckstein M, Strissel P, Strick R, Weyerer V, Wirtz R, Pfannstiel C, et al. Cytotoxic T-cell-related gene expression signature predicts improved survival in muscle-invasive urothelial bladder cancer patients after radical cystectomy and adjuvant chemotherapy. J Immunother Cancer 2020;8:e000162.
50. Saponaro M, Flottmann S, Eckstein M, Hommerding O, Klu€mper N, Corvino D, et al. CDCP1 expression is frequently increased in aggressive urothelial carcinoma and promotes urothelial tumor progression. Sci Rep 2023;13:73.
51. Alexander CM, Selvarajan S, Mudgett J, Werb Z. Stromelysin-1 regulates adipogenesis during mammary gland involution. J Cell Biol 2001;152:693–703.
52. Chowdhury HH, Velebit J, Radi,c N, FranVciVc V, Kreft M, Zorec R. Hypoxia alters the expression of dipeptidyl peptidase 4 and induces developmental remodeling of human preadipocytes. J Diabetes Res 2016;2016:1–9.
53. Zhu K, Cai L, Cui C, de Los Toyos JR, Anastassiou D. Single-cell analysis reveals the pan-cancer invasiveness-associated transition of adipose-derived stromal cells into COL11A1-expressing cancer-associated fibroblasts. PLoS Comput Biol 2021;17:e1009228.
54. Ma Z, Li X, Mao Y, Wei C, Huang Z, Li G, et al. Interferon-dependent SLC14A1þ cancer-associated fibroblasts promote cancer stemness via WNT5A in bladder cancer. Cancer Cell 2022;40:1550–65.
55. Luo H, Xia X, Huang LB, An H, Cao M, Kim GD, et al. Pan-cancer single-cell analysis reveals the heterogeneity and plasticity of cancer-associated fibroblasts in the tumor microenvironment. Nat Commun 2022;13:6619.
56. Mink SR, Vashistha S, Zhang W, Hodge A, Agus DB, Jain A. Cancer-associated fibroblasts derived from EGFR-TKI–resistant tumors reverse EGFR pathway inhibition by EGFR-TKIs. Mol Cancer Res 2010;8:809–20.
57. Wang W, Li Q, Yamada T, Matsumoto K, Matsumoto I, Oda M, et al. Crosstalk to stromal fibroblasts induces resistance of lung cancer to epidermal growth factor receptor tyrosine kinase inhibitors. Clin Cancer Res 2009;15:6630–8.
58. Wu F, Yang J, Liu J, Wang Y, Mu J, Zeng Q, et al. Signaling pathways in cancer-associated fibroblasts and targeted therapy for cancer. Signal Transduct Target Ther 2021;6:218.
59. Geneste A, Duong MN, Molina L, Conilh L, Beaumel S, Cleret A, et al. Adipocyte-conditioned medium induces resistance of breast cancer cells to lapatinib. BMC Pharmacol Toxicol 2020;21:61.
60. Gil V, Miranda S, Riisnaes R, Gurel B, D'Ambrosio M, Vasciaveo A, et al. HER3 is an actionable target in advanced prostate cancer. Cancer Res 2021;81:6207–18.
61. Zhang Z, Karthaus WR, Lee YS, Gao VR, Wu C, Russo JW, et al. Tumor microenvironment-derived NRG1 promotes antiandrogen resistance in prostate cancer. Cancer Cell 2020;38:279–96.
62. The Cancer Genome Atlas Research Network. Comprehensive molecular characterization of urothelial bladder carcinoma. Nature 2014;507:315–22.
63. Cox A, Klu€mper N, Stein J, Sikic D, Breyer J, Bolenz C, et al. Molecular urothelial tumor cell subtypes remain stable during metastatic evolution. Eur Urol 2023; S0302283823026982.
64. Choi W, Porten S, Kim S, Willis D, Plimack ER, Hoffman-Censits J, et al. Identification of distinct basal and luminal subtypes of muscle-invasive bladder cancer with different sensitivities to frontline chemotherapy. Cancer Cell 2014; 25:152–65.
65. Czerniak B, Dinney C, McConkey D. Origins of bladder cancer. Annu Rev Pathol Mech Dis 2016;11:149–74.
66. Guardia C, Bianchini G, Arpí-LLuci'a O, Menendez S, Casadevall D, Galbardi B, et al. Preclinical and clinical characterization of fibroblast-derived neuregulin-1 on trastuzumab and pertuzumab activity in HER2-positive breast cancer. Clin Cancer Res 2021;27:5096–108.
67. Bunnell BA, Martin EC, Matossian MD, Brock CK, Nguyen K, Collins-Burow B, et al. The effect of obesity on adipose-derived stromal cells and adipose tissue and their impact on cancer. Cancer Metastasis Rev 2022;41:549–73.
68. Strong AL, Pei DT, Hurst CG, Gimble JM, Burow ME, Bunnell BA. Obesity enhances the conversion of adipose-derived stromal/stem cells into carcinoma-associated fibroblast leading to cancer cell proliferation and progression to an invasive phenotype. Stem Cells Int 2017;2017:1–11.
69. Goyal L, Meric-Bernstam F, Hollebecque A, Valle JW, Morizane C, Karasic TB, et al. Futibatinib for *FGFR2* -rearranged intrahepatic cholangiocarcinoma. N Engl J Med 2023;388:228–39.

4. Discussion with references

4.1 Expression of ARv's is associated with upregulated DNA repair genes

In the first paper, 273 tissue samples from 167 patients with different PCa stages, 10 benign prostatic hyperplasia patients, and 7 healthy participants (control) were used for mRNA expression analysis by nCounter platform (NanoString technologies) (Tolkach et al., 2022). The CodeSet gene panels were comprised of five panels; full-length AR and its variants, DNA repair genes, AR transcriptional targets, proliferation genes, and "other" genes. The results revealed that the mRNA expression of AR-Vs (AR-V1, AR-V3, AR-V7, AR-V9) increases after receiving ADT (in ADT and CRPC groups), and is absent from normal and benign tissue samples. While few studies report low expression of AR-V7 mRNA in the benign prostate (Gjyrezi et al., 2021; Hörnberg et al., 2011), most studies demonstrate that AR-V7 protein expression is only induced after ADT, which is usually used to treat high-risk PCa (Sharp et al., 2018; Sprenger and Plymate, 2014). Our paper also showed that AR-V expression is significantly correlated with Ki-67 expression in ADT and CRPC, indicating higher proliferation. In CRPC, the DNA-repair score and AR targets score significantly correlated with AR-V expression. A closer analysis of individual DNA repair genes revealed significant upregulation of BRCA1, RAD21, RAD51AP1, ATR, and CHEK1; and non-significant upregulation of RAD54L, EXO1, and XRCC4 in AR-V positive CRPC. To validate these findings *in-vitro*, we generated LNCaP cells overexpressing AR-V7 (LNCaP/V7), since it is the most common AR-V (Tolkach et al., 2022; Zhang et al., 2020), to model AR-V positive CRPC. We also generated LNCaP cells overexpressing full-length AR (LNCaP/AR) to model AR-V negative CRPC. To evaluate DNA repair, both cell lines were irradiated and assayed for γH2A.X foci at different timepoints. LNCaP/V7 exhibited significantly less foci 24 hours after irradiation, compared to LNCaP/AR, indicating accelerated DNA repair. DNA repair genes BRCA1, CHEK1, EXO1, RAD54L, and XRCC2 were upregulated in LNCaP/V7 compared to LNCaP/AR six-hours after irradiation, corroborating the findings in AR-V positive CRPC clinical samples. The accelerated DNA repair associated with AR-V7 expression was further corroborated *in-vitro* by another study (Haoge Luo et al., 2022; Yin et

al., 2017). Considering the enhanced DNA repair and resistance to antiandrogens mediated by AR-Vs (Cao et al., 2014; Li et al., 2013; Tolkach et al., 2022), their expression in advanced PCa may render the combination of ADT and PARP inhibitors or irradiation ineffective (Haoge Luo et al., 2022; Yin et al., 2017). Therefore AR-V testing maybe helpful in assigning alternative therapies that may enhance the prognosis of CRPC patients.

4.2 CDCP1 is upregulated in UC and negatively correlates with overall survival

In the second paper (Saponaro et al., 2023), CDCP1 expression was evaluated in two independent UC TMA cohorts. The first TMA consists of 136 UC samples at different tumor stages (T1-T4), and 31 benign (control) samples (Klümper et al., 2017; Schneider et al., 2011). The second TMA consists of 184 MIBC samples (Eckstein et al., 2020). Analysis of the first TMA showed that CDCP1 expression is negative or weak in control samples, and is enhanced in cancer samples, particularly in the MIBC stages (T2-T4), in agreement with a previous study (Yang et al., 2019). CDCP1 expression significantly correlated with worse overall survival in both TMAs. Analysis of the second TMA and the BCa dataset of the cancer genome atlas (TCGA) revealed that CDCP1 is specifically enriched in the basal/squamous subtype of MIBC. Basal/squamous MIBC is an aggressive disease, and the median overall survival in patients is the second shortest after neuroendocrine MIBC (1.2 years) (Kamoun et al., 2020), indicating the importance of characterizing potential drug targets. Interestingly, a paper published shortly after ours has corroborated the enrichment of CDCP1 in basal/squamous MIBC, and demonstrated the efficacy of CDCP1-trageted radiotherapy *in-vivo* (Chopra et al., 2023). Other papers have also shown the anti-tumor activity of targeting CDCP1 with antibody-drug conjugates and radiolabeled antibodies in pancreatic, kidney, ovarian, colorectal, and prostate cancers (Khan et al., 2022; Lim et al., 2022; Moroz et al., 2020; Zhao et al., 2022). Basal/squamous MIBC is known to express high levels of EGFR and EGF (Kamoun et al., 2020; Rebouissou et al., 2014). Some studies have shown that EGFR stimulation induces CDCP1 upregulation (Dong et al., 2012), and CDCP1 directly interacts with EGFR (Law et al., 2016), implying a strong rational for testing combination therapies targeting CDCP1 and EGFR in basal/squamous MIBC (Murakami et al., 2022). On

the functional level, CDCP1 expression in murine bladder organoids promoted growth and proliferation, indicated by larger organoid size and higher Ki-67 expression compared to controls. CDCP1 knockout in SCaBER cells led to reduced proliferation, migration, and oncogenic signaling (AKT and MEK/ERK1/2) activation. Together, these results suggest the role of CDCP1 in promoting bladder cancer progression and aggressiveness.

4.3 Paracrine resistance to Erdafitinib can be conferred by soluble NRG1

The clinical availability of targeted therapy, such as immune checkpoint inhibitors, TKIs, and antibody-drug conjugates, has improved the prognosis of UC patients that progress on/after chemotherapy (Loriot et al., 2023; Rosenberg et al., 2023; Sharma et al., 2016). The clinical significance of Erdafitinib in FGFR-dependent luminal papillary MIBC lies in the fact that most of these tumors are devoid of immune cells (“cold” tumors) (Kamoun et al., 2020), and poorly respond to immunotherapy (Benjamin et al., 2022; Siefker-Radtke and Curti, 2018). However, a knowledge gap remains in characterizing response biomarkers and resistance mechanisms to efficiently assign specific combination therapies to each cancer patient. Although certain FGFR mutations and translocations are well-established biomarkers of Erdafitinib response before treatment onset, the short progression-free survival indicates the utmost need of identifying targetable resistance mechanisms (Bahleda et al., 2019; Gong et al., 2024; Loriot et al., 2023, 2019).

Growing evidence suggests the role of ADSCs in promoting cancer progression, invasiveness, and resistance to chemotherapy (Fajka-Boja et al., 2020; Lu et al., 2017; Maj et al., 2018; Miyazaki et al., 2021). In the third paper, we sought to investigate the effect of secreted factors from ADSCs and 3T3-L1 pre-adipocytes on Erdafitinib response in FGFR-dependent cell lines (Hosni et al., 2024). Our results showed that Erdafitinib inhibits cell growth and ERK1/2 activation in three FGFR-dependent cell lines (RT4, RT112, and LK2) at nanomolar concentrations, as reported (Perera et al., 2017). RT4 and RT112 are luminal BCa cell lines harboring FGFR3–Transforming Acidic Coiled-Coil Containing Protein 3 (TACC3) fusions (Warrick et al., 2016; Williams et al., 2012). LK2 is a lung squamous cell carcinoma cell line expressing FGFR1 copy number gain (Hibi et al., 2016). Erdafitinib treatment in

conditioned media (CM) of ADSCs and 3T3-L1 cells conferred resistance to cell death compared to treatment in normal media. Molecular analyses revealed that CM induced AKT and HER3 activation in the three FGFR-dependent cell lines. Multiple experimental models revealed secreted NRG1, the best characterized ligand of HER3 (Ieguchi et al., 2010), as a mediator of resistance in the CM. Gene silencing of NRG1/*Nrg1* in ADSCs and 3T3-L1 cells abrogated the resistance conferred by the CM of wildtype cells. NRG1 stable overexpression in RT4 cells led to Erdafitinib resistance compared to wildtype cells *in-vitro* and *in-vivo*. Pertuzumab, a monoclonal antibody that inhibits HER2/HER3 dimerization (Franklin et al., 2004), reversed the CM-mediated resistance to Erdafitinib *in-vitro* and *in-vivo*. As a clinically approved drug for cancer treatment (Howie et al., 2019), Pertuzumab offers an easy to implement rational combination therapy with Erdafitinib in FGFR-altered UC. Our results also demonstrated that combination of Pertuzumab and Erdafitinib reversed the CM-mediated resistance in LK2 cells. This finding may pave the way for a novel combination therapy, aiming at prolonging the progression-free survival in various FGFR-dependent cancers where Erdafitinib was shown to have antitumor activity (Pant et al., 2023). All in all, our study elucidates a novel paracrine resistance mechanism mediated by NRG1, and warrants further clinical testing of stromal NRG1 as a biomarker for the combination of Pertuzumab with Erdafitinib.

4.3.1 NRG1 is expressed in pre-adipocytes and PDGFRA-positive CAFs in BCa

In the second part of our paper, NRG1 expression was shown to be downregulated in differentiated 3T3-L1-derived adipocytes compared to progenitor 3T3-L1 cells, and the adipocytes' CM did not confer Erdafitinib resistance (Hosni et al., 2024). To gain insights into the clinical relevance of NRG1 in patient BCa samples, we analyzed the TCGA bladder cancer cohort. We found significant positive correlations between NRG1 and mesenchymal markers that are downregulated after terminal differentiation of pre-adipocytes; platelet-derived growth factor receptor-A (PDGFRA), Matrix Metallopeptidase 3 (MMP3) and dipeptidyl peptidase 4 (DPP4) (Alexander et al., 2001; Berry et al., 2014; Chowdhury et al., 2016; Lee et al., 2012). The enrichment of NRG1 in PDGFRA-expressing CAFs in BCa was

demonstrated by analyzing a published single-cell RNA sequencing of BCa (Chen et al., 2020), where NRG1 and PDGFRA were shown to be enriched in inflammatory CAFs (iCAFs). Two additional gene signatures of NRG1-expressing CAFs (Ma et al., 2022) and adipogenic CAFs (Han Luo et al., 2022) were also enriched in the iCAF population (Chen et al., 2020). Moreover, CM from CAFs derived from UC tumor samples recapitulated the Erdafitinib resistance conferred by CM of 3T3-L1 and ADSCs in RT4 and RT112 cell lines. These findings indicate that NRG1-expressing CAFs are present in human bladder tumors; and support further characterization of these CAFs, to explore additional biomarkers and targets for overcoming the acquisition of Erdafitinib resistance. A recent commentary on our paper has supported our findings in (Hosni et al., 2024), and mentioned that the gene signature of NRG1-expressing CAFs is also expressed by fibro-adipogenic progenitors found in adipose tissue of cancer-free individuals; suggesting their recruitment form the adipose tissue to the tumor sites (Kolonin and Anastassiou, 2024). Last but not least, because ADSCs in obese patients are found at a higher frequency and express CAF markers (Bunnell et al., 2022; Strong et al., 2017), it would be worthy to evaluate obesity as an indication for combination of Erdafitinib with Pertuzumab.

4.4 References

Alexander, C.M., Selvarajan, S., Mudgett, J., Werb, Z., 2001. Stromelysin-1 Regulates Adipogenesis during Mammary Gland Involution. J. Cell Biol. 152, 693–703. https://doi.org/10.1083/jcb.152.4.693

Bahleda, R., Italiano, A., Hierro, C., Mita, A., Cervantes, A., Chan, N., Awad, M., Calvo, E., Moreno, V., Govindan, R., Spira, A., Gonzalez, M., Zhong, B., Santiago-Walker, A., Poggesi, I., Parekh, T., Xie, H., Infante, J., Tabernero, J., 2019. Multicenter Phase I Study of Erdafitinib (JNJ-42756493), Oral Pan-Fibroblast Growth Factor Receptor Inhibitor, in Patients with Advanced or Refractory Solid Tumors. Clin. Cancer Res. 25, 4888–4897. https://doi.org/10.1158/1078-0432.CCR-18-3334

Benjamin, D.J., Mar, N., Rezazadeh Kalebasty, A., 2022. Immunotherapy With Checkpoint Inhibitors in FGFR-Altered Urothelial Carcinoma. Clin. Med. Insights Oncol. 16, 117955492211262. https://doi.org/10.1177/11795549221126252

Berry, R., Jeffery, E., Rodeheffer, M.S., 2014. Weighing in on Adipocyte Precursors. Cell Metab. 19, 8–20. https://doi.org/10.1016/j.cmet.2013.10.003

Bunnell, B.A., Martin, E.C., Matossian, M.D., Brock, C.K., Nguyen, K., Collins-Burow, B., Burow, M.E., 2022. The effect of obesity on adipose-derived stromal cells and adipose

tissue and their impact on cancer. Cancer Metastasis Rev. 41, 549–573. https://doi.org/10.1007/s10555-022-10063-1

Cao, B., Qi, Y., Zhang, G., Xu, D., Zhan, Y., Alvarez, X., Guo, Z., Fu, X., Plymate, S.R., Sartor, O., Zhang, H., Dong, Y., 2014. Androgen receptor splice variants activating the full-length receptor in mediating resistance to androgen-directed therapy. Oncotarget 5, 1646–1656. https://doi.org/10.18632/oncotarget.1802

Chen, Z., Zhou, L., Liu, L., Hou, Y., Xiong, M., Yang, Y., Hu, J., Chen, K., 2020. Single-cell RNA sequencing highlights the role of inflammatory cancer-associated fibroblasts in bladder urothelial carcinoma. Nat. Commun. 11, 5077. https://doi.org/10.1038/s41467-020-18916-5

Chopra, S., Trepka, K., Sakhamuri, S., Carretero-González, A., Zhu, J., Egusa, E., Zhou, J., Leung, K., Zhao, N., Hooshdaran, N., Feng, F.Y., Wells, J.A., Chou, J., Evans, M.J., 2023. Theranostic Targeting of CUB Domain–Containing Protein 1 (CDCP1) in Multiple Subtypes of Bladder Cancer. Clin. Cancer Res. 29, 1232–1242. https://doi.org/10.1158/1078-0432.CCR-22-1973

Chowdhury, H.H., Velebit, J., Radić, N., Frančič, V., Kreft, M., Zorec, R., 2016. Hypoxia Alters the Expression of Dipeptidyl Peptidase 4 and Induces Developmental Remodeling of Human Preadipocytes. J. Diabetes Res. 2016, 1–9. https://doi.org/10.1155/2016/7481470

Dong, Y., He, Y., de Boer, L., Stack, M.S., Lumley, J.W., Clements, J.A., Hooper, J.D., 2012. The Cell Surface Glycoprotein CUB Domain-containing Protein 1 (CDCP1) Contributes to Epidermal Growth Factor Receptor-mediated Cell Migration. J. Biol. Chem. 287, 9792–9803. https://doi.org/10.1074/jbc.M111.335448

Eckstein, M., Strissel, P., Strick, R., Weyerer, V., Wirtz, R., Pfannstiel, C., Wullweber, A., Lange, F., Erben, P., Stoehr, R., Bertz, S., Geppert, C.I., Fuhrich, N., Taubert, H., Wach, S., Breyer, J., Otto, W., Burger, M., Bolenz, C., Keck, B., Wullich, B., Hartmann, A., Sikic, D., BRIDGE Consortium e.V., Mannheim, Germany, 2020. Cytotoxic T-cell-related gene expression signature predicts improved survival in muscle-invasive urothelial bladder cancer patients after radical cystectomy and adjuvant chemotherapy. J. Immunother. Cancer 8, e000162. https://doi.org/10.1136/jitc-2019-000162

Fajka-Boja, R., Szebeni, G.J., Hunyadi-Gulyás, É., Puskás, L.G., Katona, R.L., 2020. Polyploid Adipose Stem Cells Shift the Balance of IGF1/IGFBP2 to Promote the Growth of Breast Cancer. Front. Oncol. 10, 157. https://doi.org/10.3389/fonc.2020.00157

Franklin, M.C., Carey, K.D., Vajdos, F.F., Leahy, D.J., de Vos, A.M., Sliwkowski, M.X., 2004. Insights into ErbB signaling from the structure of the ErbB2-pertuzumab complex. Cancer Cell 5, 317–328. https://doi.org/10.1016/S1535-6108(04)00083-2

Gjyrezi, A., Galletti, G., Zhang, J., Worroll, D., Sigouros, M., Kim, S., Cooley, V., Ballman, K.V., Ocean, A.J., Shah, M.A., Scandura, J.M., Sboner, A., Nanus, D.M., Beltran, H., Tagawa, S., Giannakakou, P., 2021. Androgen receptor variant shows heterogeneous expression in prostate cancer according to differentiation stage. Commun. Biol. 4, 785. https://doi.org/10.1038/s42003-021-02321-9

Gong, J., Mita, A.C., Wei, Z., Cheng, H.H., Mitchell, E.P., Wright, J.J., Ivy, S.P., Wang, V., Gray, R.C., McShane, L.M., Rubinstein, L.V., Patton, D.R., Williams, P.M., Hamilton, S.R., Tricoli, J.V., Conley, B.A., Arteaga, C.L., Harris, L.N., O'Dwyer, P.J., Chen, A.P., Flaherty, K.T., 2024. Phase II Study of Erdafitinib in Patients With Tumors With Fibroblast Growth Factor Receptor Mutations or Fusions: Results From the NCI-MATCH ECOG-ACRIN Trial (EAY131) Subprotocol K2. JCO Precis. Oncol. e2300407. https://doi.org/10.1200/PO.23.00407

Hibi, M., Kaneda, H., Tanizaki, J., Sakai, K., Togashi, Y., Terashima, M., De Velasco, M.A., Fujita, Y., Banno, E., Nakamura, Y., Takeda, M., Ito, A., Mitsudomi, T., Nakagawa, K., Okamoto, I., Nishio, K., 2016. *FGFR* gene alterations in lung squamous cell carcinoma are potential targets for the multikinase inhibitor nintedanib. Cancer Sci. 107, 1667–1676. https://doi.org/10.1111/cas.13071

Hörnberg, E., Ylitalo, E.B., Crnalic, S., Antti, H., Stattin, P., Widmark, A., Bergh, A., Wikström, P., 2011. Expression of Androgen Receptor Splice Variants in Prostate Cancer Bone Metastases is Associated with Castration-Resistance and Short Survival. PLoS ONE 6, e19059. https://doi.org/10.1371/journal.pone.0019059

Hosni, S., Kilian, V., Klümper, N., Gabbia, D., Sieckmann, K., Corvino, D., Winkler, A., Saponaro, M., Woersdoerfer, K., Schmidt, D., Hahn, O., Zanotto, I., Bertlich, M., Toma, M., Bald, T., Eckstein, M., Hölzel, M., Geyer, M., Ritter, M., Wachten, D., De Martin, S., Alajati, A., 2024. Adipocyte precursor-derived NRG1 promotes resistance to FGFR inhibition in urothelial carcinoma. Cancer Res. https://doi.org/10.1158/0008-5472.CAN-23-1398

Howie, L.J., Scher, N.S., Amiri-Kordestani, L., Zhang, L., King-Kallimanis, B.L., Choudhry, Y., Schroeder, J., Goldberg, K.B., Kluetz, P.G., Ibrahim, A., Sridhara, R., Blumenthal, G.M., Pazdur, R., Beaver, J.A., 2019. FDA Approval Summary: Pertuzumab for Adjuvant Treatment of HER2-Positive Early Breast Cancer. Clin. Cancer Res. 25, 2949–2955. https://doi.org/10.1158/1078-0432.CCR-18-3003

Ieguchi, K., Fujita, M., Ma, Z., Davari, P., Taniguchi, Y., Sekiguchi, K., Wang, B., Takada, Y.K., Takada, Y., 2010. Direct Binding of the EGF-like Domain of Neuregulin-1 to Integrins (αvβ3 and α6β4) Is Involved in Neuregulin-1/ErbB Signaling. J. Biol. Chem. 285, 31388–31398. https://doi.org/10.1074/jbc.M110.113878

Kamoun, A., de Reyniès, A., Allory, Y., Sjödahl, G., Robertson, A.G., Seiler, R., Hoadley, K.A., Groeneveld, C.S., Al-Ahmadie, H., Choi, W., Castro, M.A.A., Fontugne, J., Eriksson, P., Mo, Q., Kardos, J., Zlotta, A., Hartmann, A., Dinney, C.P., Bellmunt, J., Powles, T., Malats, N., Chan, K.S., Kim, W.Y., McConkey, D.J., Black, P.C., Dyrskjøt, L., Höglund, M., Lerner, S.P., Real, F.X., Radvanyi, F., Aine, M., Al-Ahmadie, H., Allory, Y., Bellmunt, J., Bernard-Pierrot, I., Black, P.C., Castro, M.A.A., Chan, K.S., Choi, W., Czerniak, B., Dinney, C.P., Dyrskjøt, L., Eriksson, P., Fontugne, J., Gibb, E.A., Groeneveld, C.S., Hartmann, A., Hoadley, K.A., Höglund, M., Kamoun, A., Kardos, J., Kim, J., Kim, W.Y., Kwiatkowski, D.J., Lebret, T., Lerner, S.P., Liedberg, F., Malats, N., McConkey, D.J., Mo, Q., Powles, T., Radvanyi, F., Real, F.X., de Reyniès, A., Robertson, A.G., Siefker-Radtke, A., Sirab, N., Seiler, R., Sjödahl, G., Taber, A., Weinstein, J., Zlotta, A., 2020. A Consensus Molecular Classification of Muscle-invasive Bladder Cancer. Eur. Urol. 77, 420–433. https://doi.org/10.1016/j.eururo.2019.09.006

Khan, T., Lyons, N.J., Gough, M., Kwah, K.K.X., Cuda, T.J., Snell, C.E., Tse, B.W., Sokolowski, K.A., Pearce, L.A., Adams, T.E., Rose, S.E., Puttick, S., Pajic, M., Adams, M.N., He, Y., Hooper, J.D., Kryza, T., 2022. CUB Domain-Containing Protein 1 (CDCP1) is a rational target for the development of imaging tracers and antibody-drug conjugates for cancer detection and therapy. Theranostics 12, 6915–6930. https://doi.org/10.7150/thno.78171

Klümper, N., Syring, I., Vogel, W., Schmidt, D., Müller, S.C., Ellinger, J., Adler, D., Brägelmann, J., Perner, S., 2017. Mediator Complex Subunit MED1 Protein Expression Is Decreased during Bladder Cancer Progression. Front. Med. 4, 30. https://doi.org/10.3389/fmed.2017.00030

Kolonin, M.G., Anastassiou, D., 2024. Adipose Stromal Cell–Derived Cancer-Associated Fibroblasts Suppress FGFR Inhibitor Efficacy. Cancer Res. 84, 648–649. https://doi.org/10.1158/0008-5472.CAN-23-3904

Law, M.E., Ferreira, R.B., Davis, B.J., Higgins, P.J., Kim, J.-S., Castellano, R.K., Chen, S., Luesch, H., Law, B.K., 2016. CUB domain-containing protein 1 and the epidermal growth factor receptor cooperate to induce cell detachment. Breast Cancer Res. 18, 80. https://doi.org/10.1186/s13058-016-0741-1

Lee, Y.-H., Petkova, A.P., Mottillo, E.P., Granneman, J.G., 2012. In Vivo Identification of Bipotential Adipocyte Progenitors Recruited by β3-Adrenoceptor Activation and High-Fat Feeding. Cell Metab. 15, 480–491. https://doi.org/10.1016/j.cmet.2012.03.009

Li, Y., Chan, S.C., Brand, L.J., Hwang, T.H., Silverstein, K.A.T., Dehm, S.M., 2013. Androgen Receptor Splice Variants Mediate Enzalutamide Resistance in Castration-Resistant Prostate Cancer Cell Lines. Cancer Res. 73, 483–489. https://doi.org/10.1158/0008-5472.CAN-12-3630

Lim, S.A., Zhou, J., Martinko, A.J., Wang, Y.-H., Filippova, E.V., Steri, V., Wang, D., Remesh, S.G., Liu, J., Hann, B., Kossiakoff, A.A., Evans, M.J., Leung, K.K., Wells, J.A., 2022. Targeting a proteolytic neoepitope on CUB domain containing protein 1 (CDCP1) for RAS-driven cancers. J. Clin. Invest. 132, e154604. https://doi.org/10.1172/JCI154604

Loriot, Y., Matsubara, N., Park, S.H., Huddart, R.A., Burgess, E.F., Houede, N., Banek, S., Laguerre, B., Guadalupi, V., Ku, J.H., Triantos, S., Akapame, S., Deprince, K., Mukhopadhyay, S., Siefker-Radtke, A.O., 2023. Phase 3 THOR study: Results of erdafitinib (erda) versus chemotherapy (chemo) in patients (pts) with advanced or metastatic urothelial cancer (mUC) with select fibroblast growth factor receptor alterations (*FGFRalt*). J. Clin. Oncol. 41, LBA4619–LBA4619. https://doi.org/10.1200/JCO.2023.41.17_suppl.LBA4619

Loriot, Y., Necchi, A., Park, S.H., Garcia-Donas, J., Huddart, R., Burgess, E., Fleming, M., Rezazadeh, A., Mellado, B., Varlamov, S., Joshi, M., Duran, I., Tagawa, S.T., Zakharia, Y., Zhong, B., Stuyckens, K., Santiago-Walker, A., De Porre, P., O'Hagan, A., Avadhani, A., Siefker-Radtke, A.O., 2019. Erdafitinib in Locally Advanced or Metastatic Urothelial Carcinoma. N. Engl. J. Med. 381, 338–348. https://doi.org/10.1056/NEJMoa1817323

Lu, Y., Yang, Y., Liu, Yan, Hao, Y., Zhang, Y., Hu, Y., Jiang, L., Gong, Y., Wu, K., Liu, Yingbin, 2017. Upregulation of PAG1/Cbp contributes to adipose-derived mesenchymal stem

cells promoted tumor progression and chemoresistance in breast cancer. Biochem. Biophys. Res. Commun. 494, 719–727. https://doi.org/10.1016/j.bbrc.2017.10.118

Luo, Haoge, Liu, Y., Li, Y., Zhang, C., Yu, B., Shao, C., 2022. Androgen receptor splicing variant 7 (ARv7) promotes DNA damage response in prostate cancer cells. FASEB J. 36, e22495. https://doi.org/10.1096/fj.202200190R

Luo, Han, Xia, X., Huang, L.-B., An, H., Cao, M., Kim, G.D., Chen, H.-N., Zhang, W.-H., Shu, Y., Kong, X., Ren, Z., Li, P.-H., Liu, Yang, Tang, H., Sun, R., Li, C., Bai, B., Jia, W., Liu, Yi, Zhang, W., Yang, L., Peng, Y., Dai, L., Hu, H., Jiang, Y., Hu, Y., Zhu, J., Jiang, H., Li, Z., Caulin, C., Park, J., Xu, H., 2022. Pan-cancer single-cell analysis reveals the heterogeneity and plasticity of cancer-associated fibroblasts in the tumor microenvironment. Nat. Commun. 13, 6619. https://doi.org/10.1038/s41467-022-34395-2

Ma, Z., Li, X., Mao, Y., Wei, C., Huang, Z., Li, G., Yin, J., Liang, X., Liu, Z., 2022. Interferon-dependent SLC14A1+ cancer-associated fibroblasts promote cancer stemness via WNT5A in bladder cancer. Cancer Cell 40, 1550-1565.e7. https://doi.org/10.1016/j.ccell.2022.11.005

Maj, M., Kokocha, A., Bajek, A., Drewa, T., 2018. The interplay between adipose-derived stem cells and bladder cancer cells. Sci. Rep. 8, 15118. https://doi.org/10.1038/s41598-018-33397-9

Miyazaki, Y., Oda, T., Inagaki, Y., Kushige, H., Saito, Y., Mori, N., Takayama, Y., Kumagai, Y., Mitsuyama, T., Kida, Y.S., 2021. Adipose-derived mesenchymal stem cells differentiate into heterogeneous cancer-associated fibroblasts in a stroma-rich xenograft model. Sci. Rep. 11, 4690. https://doi.org/10.1038/s41598-021-84058-3

Moroz, A., Wang, Y.-H., Sharib, J.M., Wei, J., Zhao, N., Huang, Y., Chen, Z., Martinko, A.J., Zhuo, J., Lim, S.A., Zhang, L.H., Seo, Y., Carlin, S., Leung, K.K., Collisson, E.A., Kirkwood, K.S., Wells, J.A., Evans, M.J., 2020. Theranostic Targeting of CUB Domain Containing Protein 1 (CDCP1) in Pancreatic Cancer. Clin. Cancer Res. 26, 3608–3615. https://doi.org/10.1158/1078-0432.CCR-20-0268

Murakami, Y., Kusakabe, D., Watari, K., Kawahara, A., Azuma, K., Akiba, J., Taniguchi, M., Kuwano, M., Ono, M., 2022. AXL/CDCP1/SRC axis confers acquired resistance to osimertinib in lung cancer. Sci. Rep. 12, 8983. https://doi.org/10.1038/s41598-022-12995-8

Pant, S., Schuler, M., Iyer, Gopa, Witt, O., Doi, T., Qin, S., Tabernero, J., Reardon, D.A., Massard, C., Minchom, A., Lugowska, I., Carranza, O., Arnold, D., Gutierrez, M., Winter, H., Stuyckens, K., Crow, L., Najmi, S., Hammond, C., Thomas, S., Santiago-Walker, A., Triantos, S., Sweiti, H., Loriot, Y., Carranza, O., Greco, M.A., Coward, J., Joshua, A., Karapetis, C., Hart, C., Zhang, A., Prenen, H., Goeminne, J.-C., Machiels, J.-P., Rottey, S., Corassa, M., Molin, G.Z.D., Tiscoski, K., Jardim, D.L.F., Mak, M., Fu, W., Yao, H., Huang, J., Jiang, H., Qin, S., Chen, B., Yan, D., Yang, Y., Loriot, Y., Le Tourneau, C., Penel, N., Salas, S., Blay, J.-Y., Brachet, P.-E., Durando, X., Emambux, S., Ravaud, A., Folprecht, G., Arnold, D., Schuler, M., Ahrens, M., Golf, A., Haag, G.M., Lordick, F., Desuki, A., Cazzaniga, M., Ciardiello, F., Milella, M., Koyama, T., Hirooka, Y., Okamoto, W., Aogi, K., Kuboki, Y., Lee, J., Kim, S.-B., Ahn, M.-J., Chang, J.H., Kim, Y.-M., Nam, D.-H., Park, J.-S., Lugowska, I., Paz-Ares, L., Moreno, V., Cervantes, A.,

Calvo, M., Falcon, A., Gonzalez, A., Tabernero, J., Martinez Bueno, A., García-Corbacho, J., Longo, F., Yen, C.-J., Chen, J.-S., Hou, M.-F., Chao, Y., Rau, K.-M., Chiu, T.-J., Feng, Y.-H., Hsu, C.-H., Huang, W.-T., Lai, K.-M., Yeh, S., Palmer, D., Minchom, A., Winter, H., Welsh, L., Plummer, R., Iyer, Gopakumar, Gutierrez, M., Bilen, M., Arrowsmith, E., Pant, S., Spigel, D.R., Zandberg, D.P., Doroshow, D., Lu-Emerson, C., Moezi, M., Paulson, S., Reardon, D., Ward, P., Chaves, J., Grigg, C., Hussein, A., Manda, S., Monticelli, M., Qamar, R., Richey, S.L., Tamura, D., Wilks, S., 2023. Erdafitinib in patients with advanced solid tumours with FGFR alterations (RAGNAR): an international, single-arm, phase 2 study. Lancet Oncol. 24, 925–935. https://doi.org/10.1016/S1470-2045(23)00275-9

Perera, T.P.S., Jovcheva, E., Mevellec, L., Vialard, J., De Lange, D., Verhulst, T., Paulussen, C., Van De Ven, K., King, P., Freyne, E., Rees, D.C., Squires, M., Saxty, G., Page, M., Murray, C.W., Gilissen, R., Ward, G., Thompson, N.T., Newell, D.R., Cheng, N., Xie, L., Yang, J., Platero, S.J., Karkera, J.D., Moy, C., Angibaud, P., Laquerre, S., Lorenzi, M.V., 2017. Discovery and Pharmacological Characterization of JNJ-42756493 (Erdafitinib), a Functionally Selective Small-Molecule FGFR Family Inhibitor. Mol. Cancer Ther. 16, 1010–1020. https://doi.org/10.1158/1535-7163.MCT-16-0589

Rebouissou, S., Bernard-Pierrot, I., de Reyniès, A., Lepage, M.-L., Krucker, C., Chapeaublanc, E., Hérault, A., Kamoun, A., Caillault, A., Letouzé, E., Elarouci, N., Neuzillet, Y., Denoux, Y., Molinié, V., Vordos, D., Laplanche, A., Maillé, P., Soyeux, P., Ofualuka, K., Reyal, F., Biton, A., Sibony, M., Paoletti, X., Southgate, J., Benhamou, S., Lebret, T., Allory, Y., Radvanyi, F., 2014. EGFR as a potential therapeutic target for a subset of muscle-invasive bladder cancers presenting a basal-like phenotype. Sci. Transl. Med. 6. https://doi.org/10.1126/scitranslmed.3008970

Rosenberg, J.E., Powles, T., Sonpavde, G.P., Loriot, Y., Duran, I., Lee, J.-L., Matsubara, N., Vulsteke, C., Castellano, D., Mamtani, R., Wu, C., Matsangou, M., Campbell, M., Petrylak, D.P., 2023. EV-301 long-term outcomes: 24-month findings from the phase III trial of enfortumab vedotin versus chemotherapy in patients with previously treated advanced urothelial carcinoma. Ann. Oncol. 34, 1047–1054. https://doi.org/10.1016/j.annonc.2023.08.016

Saponaro, M., Flottmann, S., Eckstein, M., Hommerding, O., Klümper, N., Corvino, D., Hosni, S., Schmidt, A., Mönig, N., Schmidt, D., Ellinger, J., Toma, M., Kristiansen, G., Bald, T., Alimonti, A., Ritter, M., Hölzel, M., Alajati, A., 2023. CDCP1 expression is frequently increased in aggressive urothelial carcinoma and promotes urothelial tumor progression. Sci. Rep. 13, 73. https://doi.org/10.1038/s41598-022-26579-z

Schneider, A.-C., Heukamp, L.C., Rogenhofer, S., Fechner, G., Bastian, P.J., von Ruecker, A., Müller, S.C., Ellinger, J., 2011. Global histone H4K20 trimethylation predicts cancer-specific survival in patients with muscle-invasive bladder cancer: *GLOBAL HISTONE H4K20 TRIMETHYLATION PREDICTS CSS IN PATIENTS WITH MIBC*. BJU Int. 108, E290–E296. https://doi.org/10.1111/j.1464-410X.2011.10203.x

Sharma, P., Callahan, M.K., Bono, P., Kim, J., Spiliopoulou, P., Calvo, E., Pillai, R.N., Ott, P.A., de Braud, F., Morse, M., Le, D.T., Jaeger, D., Chan, E., Harbison, C., Lin, C.-S., Tschaika, M., Azrilevich, A., Rosenberg, J.E., 2016. Nivolumab monotherapy in recurrent metastatic urothelial carcinoma (CheckMate 032): a multicentre, open-label,

two-stage, multi-arm, phase 1/2 trial. Lancet Oncol. 17, 1590–1598. https://doi.org/10.1016/S1470-2045(16)30496-X

Sharp, A., Coleman, I., Yuan, W., Sprenger, C., Dolling, D., Rodrigues, D.N., Russo, J.W., Figueiredo, I., Bertan, C., Seed, G., Riisnaes, R., Uo, T., Neeb, A., Welti, J., Morrissey, C., Carreira, S., Luo, J., Nelson, P.S., Balk, S.P., True, L.D., de Bono, J.S., Plymate, S.R., 2018. Androgen receptor splice variant-7 expression emerges with castration resistance in prostate cancer. J. Clin. Invest. 129, 192–208. https://doi.org/10.1172/JCI122819

Siefker-Radtke, A., Curti, B., 2018. Immunotherapy in metastatic urothelial carcinoma: focus on immune checkpoint inhibition. Nat. Rev. Urol. 15, 112–124. https://doi.org/10.1038/nrurol.2017.190

Sprenger, C.C.T., Plymate, S.R., 2014. The Link Between Androgen Receptor Splice Variants and Castration-Resistant Prostate Cancer. Horm. Cancer 5, 207–217. https://doi.org/10.1007/s12672-014-0177-y

Strong, A.L., Pei, D.T., Hurst, C.G., Gimble, J.M., Burow, M.E., Bunnell, B.A., 2017. Obesity Enhances the Conversion of Adipose-Derived Stromal/Stem Cells into Carcinoma-Associated Fibroblast Leading to Cancer Cell Proliferation and Progression to an Invasive Phenotype. Stem Cells Int. 2017, 1–11. https://doi.org/10.1155/2017/9216502

Tolkach, Y., Kremer, A., Lotz, G., Schmid, M., Mayr, T., Förster, S., Garbe, S., Hosni, S., Cronauer, M.V., Kocsmár, I., Kocsmár, É., Riesz, P., Alajati, A., Ritter, M., Ellinger, J., Ohlmann, C.-H., Kristiansen, G., 2022. Androgen Receptor Splice Variants Contribute to the Upregulation of DNA Repair in Prostate Cancer. Cancers 14, 4441. https://doi.org/10.3390/cancers14184441

Warrick, J.I., Walter, V., Yamashita, H., Chung, E., Shuman, L., Amponsa, V.O., Zheng, Z., Chan, W., Whitcomb, T.L., Yue, F., Iyyanki, T., Kawasawa, Y.I., Kaag, M., Guo, W., Raman, J.D., Park, J.-S., DeGraff, D.J., 2016. FOXA1, GATA3 and PPARɣ Cooperate to Drive Luminal Subtype in Bladder Cancer: A Molecular Analysis of Established Human Cell Lines. Sci. Rep. 6, 38531. https://doi.org/10.1038/srep38531

Williams, S.V., Hurst, C.D., Knowles, M.A., 2012. Oncogenic FGFR3 gene fusions in bladder cancer. Hum. Mol. Genet. 22, 795–803. https://doi.org/10.1093/hmg/dds486

Yang, F., Jin, H., Que, B., Chao, Y., Zhang, H., Ying, X., Zhou, Z., Yuan, Z., Su, J., Wu, B., Zhang, W., Qi, D., Chen, D., Min, W., Lin, S., Ji, W., 2019. Dynamic m6A mRNA methylation reveals the role of METTL3-m6A-CDCP1 signaling axis in chemical carcinogenesis. Oncogene 38, 4755–4772. https://doi.org/10.1038/s41388-019-0755-0

Yin, Y., Li, R., Xu, K., Ding, Sentai, Li, J., Baek, G., Ramanand, S.G., Ding, Sam, Liu, Z., Gao, Y., Kanchwala, M.S., Li, X., Hutchinson, R., Liu, X., Woldu, S.L., Xing, C., Desai, N.B., Feng, F.Y., Burma, S., de Bono, J.S., Dehm, S.M., Mani, R.S., Chen, B.P.C., Raj, G.V., 2017. Androgen Receptor Variants Mediate DNA Repair after Prostate Cancer Irradiation. Cancer Res. 77, 4745–4754. https://doi.org/10.1158/0008-5472.CAN-17-0164

Zhang, T., Karsh, L.I., Nissenblatt, M.J., Canfield, S.E., 2020. Androgen Receptor Splice Variant, AR-V7, as a Biomarker of Resistance to Androgen Axis-Targeted Therapies in

Advanced Prostate Cancer. Clin. Genitourin. Cancer 18, 1–10. https://doi.org/10.1016/j.clgc.2019.09.015

Zhao, N., Chopra, S., Trepka, K., Wang, Y.-H., Sakhamuri, S., Hooshdaran, N., Kim, H., Zhou, J., Lim, S.A., Leung, K.K., Egusa, E.A., Zhu, J., Zhang, L., Foye, A., Sriram, R., Chan, E., Seo, Y., Feng, F.Y., Small, E.J., Chou, J., Wells, J.A., Aggarwal, R., Evans, M.J., 2022. CUB Domain-Containing Protein 1 (CDCP1) Is a Target for Radioligand Therapy in Castration-Resistant Prostate Cancer, including PSMA Null Disease. Clin. Cancer Res. 28, 3066–3075. https://doi.org/10.1158/1078-0432.CCR-21-3858

5. Acknowledgements

I would like to thank my supervisors Dr. Abdullah Alajati and Prof. Dr. Manuel Ritter for offering me the opportunity to conduct my PhD in their lab, and for guiding me throughout the journey. I would also like to acknowledge our lab technicians Doris Schmidt, Anja Winkler, and Karin Wörsdörfer for their technical support. Additionally, I'm grateful for my colleagues Miriam Saponaro, Viola Kilian, and Dr. Niklas Klümper for their cooperation and advice. I would also like to acknowledge Dr. Sarah Förster for her collaboration. I would also like to thank all members of my doctoral committee; Prof. Dr. Manuel Ritter, Prof. Dr. Michael Hölzel, Prof. Dr. Sven Perner, and Prof. Dr. Marieta Toma for their time and support. Last but not least, I would like to specially thank my family for their unconditional support.